

Alma Mater Studiorum – Università di Bologna

DOTTORATO DI RICERCA IN
Ingegneria Civile, Chimica, Ambientale e dei Materiali

Ciclo XXIX

Settore Concorsuale di afferenza: 09/D2

Settore Scientifico disciplinare: ING-IND/24

**MASS TRANSPORT AND STRESS FIELD IN POLYMER-SOLUTE SYSTEMS:
ANALYSIS AND SOLUTIONS OF COUPLED PROBLEMS**

Presentata da: **Dott.ssa Elisa Pavesi**

Coordinatore Dottorato

Chiar.mo Prof.
Luca Vittuari

Relatore

Chiar.mo Prof.
Ferruccio Doghieri

Esame finale anno 2017

TABLE OF CONTENTS

ABSTRACT	1
INTRODUCTION	3
THERMODYNAMIC AND MECHANICAL MODELS	6
2.1 Sanchez and Lacombe Model	8
2.1.1 Pure Fluids	8
2.1.2 Mixtures	10
2.1.3 Characteristic parameters	12
2.1.4 Solubility	14
2.2 PC-SAFT	16
2.2.1 Pure Fluids	16
2.2.1.1 Pure-component parameter	18
2.2.1.1.1 Non-associating components	18
2.2.1.1.2 Associating components	18
2.2.2 Mixtures	18
2.2.3 Solubility	19
2.3 NELF Model	21
2.4 Affine network theory	26
2.5 Calculation tools	28
IN-PLANE STRESS MEASUREMENT	29
3.1 Bending Beam	30
3.1.1 Choice of support material	30
3.1.2 Preparation of the sample	31
3.1.3 Bending measure	31
3.1.4 Polymer thickness and mechanical properties	32
3.2 Stress state	33
3.3 Materials & Methods	36
3.3.1 General apparatus description	36
3.3.2 Material	39
3.3.3 Apparatus set-up	40
3.3.3.1 Sorption of solutes by grease vacuum	40
3.3.3.2 Leakages inside the sample compartment	40

3.3.3.3	Weakness in the bending beam.....	41
3.3.4	Equation of state calculation for analysis of bending beam data.....	46
3.3.5	Quartz Crystal Microbalance	47
3.5	Experimental Test.....	50
3.5.1	Polymer thickness VS Bending signal.....	50
3.5.2	Static VS Dynamic configuration	50
3.5.3	Experiments in flow	51
3.6	Data Analysis	54
3.6.1	n-pentane.....	54
3.6.2	Toluene.....	57
3.7	Conclusions.....	61
	ORGANIC SOLVENT NANOFILTRATION	62
4.1	Definition	63
4.2	Theory background	65
4.2.1	Membrane performance	65
4.2.2	Young's modulus	65
4.2.3	Sorption.....	67
4.3	Materials and Methods.....	68
4.3.1	Materials.....	68
4.3.2	Experimental Procedure.....	69
4.3.2.1	OSN experimental setup and procedure.....	69
4.3.2.2	Young's modulus measurement.....	70
4.3.2.3	Sorption measurement.....	72
4.4	Experimental Results	74
4.4.1	Performance characterization.....	74
4.4.1.1	Toluene-Hexane mixture.....	75
4.4.1.2	Hexane-Ethanol mixture	78
4.4.2	Young's modulus measurements	81
4.4.3	Sorption measurements	83
4.5	Modeling	85
4.5.1	Transport Modeling.....	85
4.5.1.1	Solution-Diffusion Model based on Fick's law	86
4.5.1.1.1	Fick's law analysis for binary mixtures	87
4.5.1.2	Solution-Diffusion Model based on Maxwell-Stefan equation	88

4.5.1.2.1 Maxwell-Stefan equation for binary mixtures	89
4.5.2 Mixtures thermodynamics.....	90
4.5.3 Mechanics: Crosslink Degree	91
4.5.4 Mixtures Thermodynamics and Mechanics	92
4.5.4.1 k_{ij} from sorption experiments	93
4.5.4.2 k_{ij} fixed equal to zero.....	94
4.5.5 Diffusion Coefficient or Conductance	94
4.5.5.1 Pure component.....	94
4.5.5.1.1 k_{ij} from experiments.....	95
4.5.5.1.2 k_{ij} fixed equal to zero.....	95
4.5.5.2 Binary mixtures.....	97
4.5.5.3 Ternary mixtures	99
4.5.6 Calculation tools	99
4.6 Results.....	101
4.6.1 Toluene-Hexane Mixtures.....	101
4.6.2 Hexane-Ethanol mixture	104
4.7 Conclusions.....	108
CONCLUSIONS	110
APPENDIX A: PERFORMANCE CHARACTERIZATION	112
APPENDIX B: FICK'S LAW ANALYSIS FOR TERNARY MIXTURES	118
APPENDIX C: MAXWELL-STEFAN EQUATION FOR TERNARY MIXTURES.....	120
APPENDIX D: MODELING PREDICTION.....	123
Bibliography.....	129

ABSTRACT

This work focuses on the analysis of transport phenomena in solid polymer-solute systems and it specifically addresses problems in which a mutual influence exists between mass transport and stress development in polymers. Indeed, in several different applications of polymeric materials, from structural elements to sensors, coating film, membrane for gas separation and drug release devices, deformation associated to sorption or desorption of low molecular weight components affects boundary conditions of relevance to stress distribution in the material. On the other side, constraints to sample deformation affects thermodynamic properties which have major influence on mass transport in and through polymers. Modeling analysis of above conditions requires the use of accurate constitutive equations for both thermodynamic and transport properties which express the influence of shape and volume deformation, as well as of penetrant concentration, on both stress and chemical potential. Several efforts have been done in the past to build a frame which could host proper constitutive equations but the complexity of the matter did not allow so far to recognize an approach which is comprehensive enough to give a satisfactory representation of the mentioned coupling effects. In turn, set up of constitutive model requires specific quantitative information which are not covered by typical characterization, such as stress effect on solute chemical potential or concentration effect on elastic and shear modulus. From this picture the need emerges also for the development of experimental techniques which specifically address the quantitative evaluation of these cross effects. Far from proposing a comprehensive approach to the representation the coupling problem described above, this work aims at contributing to the development of specific tools for both its modeling and experimental characterization. Toward this objective, two specific themes have been selected, which refer to the cases of different mechanical properties for the polymeric materials. The first problem refers to the design of an apparatus which allows to measure in-plane stresses that arises and relaxes in polymer coating of commercial polystyrene, around room conditions, below the glass transition temperature (T_g) as result of vapor sorption/desorption processes. The in-plane stress is measured using bending beam cantilever technique for which an apparatus was specifically designed and set up in this work. The experiments were performed at different temperatures in the range from 30 to 50°C, using different fugacity of n-pentane inside the system. In-plane stress in PS coating was measured for the case of experiments in which solute fugacity is changed according to prescribed laws. From the stress state, knowing the material properties, the estimation was finally attempted of change in the system volume during the sorption/desorption process and results have been compared with data registered under the same conditions for mass uptake in the system from gravimetric measurements. The second problem selected refers to the analysis of the effect of elastic mechanical characteristics on separation performances for dense polymeric membrane for organic solvent nanofiltration. In this view, two different commercial PDMS-based membranes were characterized and based on the experimental results a model was developed to provide a thermodynamic and mechanical frame for the representation of flux and rejection for the case

of different solutes and solvent mixtures. Permeation rates and solute rejection were thus investigated in details for two different PDMS-based membranes, through an extensive experimental campaign. The characterization was done using different n-alkane solutes with variable chain length, corresponding to molecular weight in the range from 170 to 310 kg/kmol and several solvents with different properties (toluene, n-hexane, ethanol and butanol) and the results are interpreted in terms of the solution-diffusion model. Crucial to the analysis of both first and second problem is the use of constitutive equation for free energy of the system which is suitable to describe contribution from network elasticity (for the case of crosslinked OSN membranes) or from out-of-equilibrium conditions below the glass transition temperature (glassy states for thermoplastic-penetrant systems). Because of the relevance of this problem, emphasis is given in this work to the elaboration of equation-of-state in the field of lattice fluid or tangent-hard-spheres-chain theories which could be implemented with terms suitable for the representation of the effect of mechanical constraint to the system as well as of the constitutive properties for stress-strain relationships.

Chapter 1

INTRODUCTION

Products made out of polymeric materials interact with fluid phases in a much more relevant and complex way with respect to goods built from other solid materials, in view of their amorphous nature, compressibility and free volume. In this respect it could be mentioned, for example, that the ability of polymers of absorbing gases and vapor components from the surroundings is not shared with materials they compete with in structural applications and this endows them with rather peculiar characteristics [1]. In turn, sorption of low molecular weight components in polymeric materials significantly affects properties of the latter, including those which preside over their rheological and mechanical behavior. Mechanism by which this influence is exerted deserves to be examined closely, as it is indeed conveyed primarily, although not exclusively, by the volume changes induced by mass sorption. It can be immediately recognized that the displacement of the elements of the polymeric sample which is produced by volume variation may dramatically intersect the mechanical problem of stress development [2]. On the other hand, constraints to shape and volume deformation of the materials has a major influence on both solubility and diffusivity of solutes. The coupling between mechanical and mass transport problems in polymeric materials thus emerges naturally in a number of applications, representing both a challenge for properties characterization and modeling and an opportunity to design processes and products with new and specific features. Effects of the coupling indicated above is evident, for example, in those applications in which pipe made of polymeric materials are used to host flow of organic components. In automotive applications, dilation of polymer pipe walls associated to corresponding sorption of fuel or lubricant components may compromise the sealing effect in pipe junctions [3]. The combined effect of mass transport and stress development is responsible of the so called “explosive decompression”, which occurs in the polymeric layer of the wall of a pipe in which a high pressure gaseous stream flows, when the pipe is suddenly depressurized. Under those conditions the gas absorbed into the polymer may produce cracks in the layer as a consequence of the nucleation and growth of gaseous phase domains and of the mechanical answer of polymer elements [4]. In a different field of application, it may be observed that the structure of cells in a polymer foam produced by means of a physical blowing agent through a heating or a depressurization process is essentially determined by the coupled phenomena of stress development and mass diffusion of the agent across the cell walls. On the other hand, non-uniform stress field induced by mass transport can be responsible of anomalous diffusion kinetics which, in turn, can be exploited, for example, to produce new devices for controlled release. Similarly, design and production of new sensing devices for vapor and gaseous components to be used in industrial or environmental applications may take advantage of the reciprocal influence between stress/deformation state and solubility properties which are expressed by polymeric materials. Several attempts have

been done in the last decades to provide solutions for coupled mechanical-diffusion problems which were based on a solid background for what refers to thermodynamics and continuum mechanics frame [5]. However, in view of the complexity of the problem, solution provided for the representation of thermodynamic and transport properties are either too difficult to implement in the absence of detailed data from non-standard characterization protocols, or empirical in characters and not easy to extend out of the field in which they have been developed. For polymeric materials specific difficulties arises in the representation of relations between mechanical and thermodynamic properties when the case of non-equilibrium states need to be considered, as for conditions below the glass transition temperature [6]. One more peculiar feature of long chain molecule species with respect to relation between stress and vapor solubility is in the possibility to separately tailor properties such as volume compressibility and tensile characteristics working on distinct factors like chain segment interaction energy and degree of crosslinking. This work aims at contributing to understanding and representation of the coupling between mechanical and mass transport processes in polymeric materials, specifically addressing both the problem of complex relaxation in polymeric materials below the glass transition temperature and that of interaction between sorption and mechanical deformation in crosslinked rubbers. Far from the idea of developing a comprehensive approach for all possible interaction between mechanical and sorption problems in polymeric materials, the work offers separate analyses of specific coupled problems, illustrating the use of rigorous approach to the representation of thermodynamic properties and of the effect of both mechanical and composition variables on the relevant characteristics of solute/polymer mixtures of interest. Specific problems in focus in this work are rather different in nature, field and objectives, although the modeling tools which have been used to approach their analysis have a common basis. The first problem addressed is the development of experimental techniques and proper modeling tools for the analysis of structural relaxation of glassy polymers as induced by vapor sorption. The first aim identified is the set-up of convenient experimental protocols to monitor both stress evolution and apparent solubility change in polymeric samples stressed by prescribed variation of vapor fugacity under assigned mechanical constraint. To this goal, already established techniques have been revised and existing apparatuses have been revamped to insure the same conditions for the polymer sample are reached in different tests devoted to the measurement of stress or solubility data and to optimize the characteristic of the experimental tests to emphasize the role of structural relaxation on both mechanical and mass transport properties. The second problem considered in this work addressed the experimental characterization and modeling of the performance of rubbery membranes for organic solvent nanofiltration (OSN), for which both affinity and resistance to solvent component are of relevance. The experimental characterization of membrane performances, in terms of permeability and rejection for the case of different solvent mixtures and solutes were first collected for two similar membranes and the results have been discussed in terms of both their mechanical and thermodynamic properties. While problems addressed and approaches considered for their discussion are rather different, modeling tools used to represent mechanical and thermodynamic properties have the same origin. Indeed, they all belong to the class of Equations of State and have been modified and specialized to account for the effect of non-equilibrium conditions, for the case of glassy polymers, or for that of elastic term from

crosslinks which provide the material with the necessary resistance to solvents, for the case of rubbery OSN membrane. In view of their crucial role in the development of modeling tools for the analysis of both glassy and rubbery state of polymeric materials of interest in this work, the presentation of EoS models for the description of mixing properties in solute-polymer systems is given first in this report. The separate discussions of the specific topics addressed in this work are given in the sections which follows. Conclusions from the different analysis are also given separately, considering they aim at representing first steps in a complex path toward the comprehensive representation of the link between stress development and mass transport in polymeric materials.

Chapter 2

THERMODYNAMIC AND MECHANICAL MODELS

The prediction or correlation of thermodynamic properties and phase equilibria with equations of state remains an important goal to describe different processes. Although the use of equations of state has for a long time been restricted to systems of simple fluids, there is an increasing demand for models that are also suitable for complex and macromolecular compounds. The most apparent progress toward equations of state with such capabilities was made by applying principles of statistical mechanics. Some early models derived from statistical mechanics assumed molecules to be arranged in a lattice [7] [8], whereas many of the more recent theories picture molecules to be moving freely in continuous space. Wei and Sadus [9] developed a detailed review of different lines followed to describe the molecule distribution in different theories. During the past few years, many studies assumed nonspherical molecules to be chains of freely jointed spherical segments. Despite its simplicity, this molecular model accounts for size and shape effects of molecules and has successfully been applied to simple species as well as large polymeric fluids and their mixtures. In 1988, Chapman et al [10] [11], developed a perturbed theory that assumes molecule to be chain of connected spherical segments. The basic idea of the perturbation theory is to divide the interactions of molecules in a repulsive and attractive part of the potential. Perturbed-chain statistical associating fluid theory (PC-SAFT) enter in this last one classification [12].

The lattice theories are based on the application of the statistic thermodynamic to derive the partition function $Z = Z(p, T)$ and differ as Z is described. From partition function the Gibbs free energy G and other thermodynamics properties are derived. According to statistical mechanic, general expressions for Z and G are:

$$Z(p, T) = \sum_V \sum_E \Omega(E, V, N) \left(\frac{E+pV}{kT} \right) \quad (2.1)$$

$$G = -kT \ln Z(p, T) \quad (2.2)$$

Where $\Omega(E, V, N)$ is the number of possible configuration for a system characterized by:

- Number of molecules N ;
- Configuration energy of molecules E ;
- Volume of molecules V .

The critical point for every lattice theory is therefore in $\Omega(E, V, N)$, and in particular in the ways in which the molecules are located.

Considering a general molecule represented by flexible chain of r segments, the partition function Z is influenced by the internal motions of single molecules and by the interactions between different segments. These interactions are responsible for pVT properties.

The description of the intermolecular potential and the lattice differentiate the various theories, of which the most famous and used is the Flory Huggins theory [13] [14] [15] [16]. It is considered a repulsive potential at rigid spheres, a simple cubic type cell geometry and compressibility and thermal expansion of the system attributable to changes in the cell volume.

In Eq. 2.3 Flory Huggins mixing free energy for mixture of solute (specie A) and polymer (species B) is represented, from which solute chemical potential and, ultimately, solubility can be calculated:

$$G_{mix} = RT(n_A \ln \phi_A + n_A \phi_B \chi) \quad (2.3)$$

where n_i and ϕ_i are number of moles and volume fraction of specie i respectively, while χ is a model parameter for interaction energy

The limits of the above free energy expression are due to the fact that it is referred to:

- incompressible network;
- absence of mixing volume.

Perturbation theory molecules are conceived to be chains composed by spherical segments. According to this theory, the interaction of molecules is divided into a repulsive and attractive part of the potential.

2.1 Sanchez and Lacombe Model

Latest *Lattice Fluid* models were suggested by Panayiotou and Vera [17] [18] and by Sanchez and Lacombe [7] [8] [19] [20]. The *Lattice Fluid* theory developed by Sanchez and Lacombe is similar to the lattice theory suggested by Flory Huggins. The new model has the advantage of considering the compressibility of the fluid mixture and offer the possibility of estimating the specific volume of equilibrium.

2.1.1 Pure Fluids

Through this model [7] the space is assimilated to a three-dimension lattice consisting of identical cells, each confined with other z cells. The molecules are represented by flexible chains of r segments, each occupying a single cell for a total of r cells per molecule. Two adjacent segments in the molecule occupy two adjacent cells in the network. The compressibility of the substances is insured by the presence inside the lattice of non-occupied cells N_0 .

To determine the partition function Z , the numbers of configurations which assumes a system composed by N molecules, each occupying r contiguous cells and N_0 empty cells. The problem solution is found based on the Guggenheim's approximation:

- 1) random mixing of all the molecules among themselves and with empty sites;
- 2) when two cells of the lattice are not occupied from the same segment, the probability to be vacant or occupied are independent for the two points (*mean field approximation*)

The number of possible configuration Ω seems to be dependent from:

- Number of empty cell N_0
- Number of occupied cell Nr
- Coordination number z

$$\Omega = (N_0, Nr, z) \quad (2.4)$$

The lattice energy E is calculated considering the interaction energy between the empty cell and the molecule segment equal to zero. The principle of additivity is valid between two empty cells. The total energy will be the sum of energetic contributes extended to all pairs of nearest neighbors:

$$E = E(N_0, Nr, z, \varepsilon_{ij}) \quad (2.5)$$

where $\varepsilon_{ij} = \varepsilon_{ji}$ is the interaction energy between i -th and j -th segments that are not united by primary bonds.

Flory's approximation will be important afterwards and it considers that the coordination number z tends to infinity.

In the total volume definition, two terms will appear:

- Free volume V_0 corresponding to N_0 cells;
- Volume V corresponding to Nr occupied cells.

$$V_{tot} = V_0 + V \quad (2.6)$$

Assuming the volume of the cell (v^*) constant and independent from the temperature:

$$V = V(N_0, Nr, v^*) \quad (2.7)$$

Because the functions E , Ω and V are dependent from concentration and characteristic parameters, the double summation on E and V presents in the partition function (Eq. 2.1) can be correctly substitute with a single summation on N_0 :

$$Z(p, T) = \sum_V \sum_E \Omega(E, V, N) \left(-\frac{E+pV}{kT} \right) = \sum_{N_0=0}^{\infty} \Omega \left(-\frac{E+pV}{kT} \right) \quad (2.8)$$

Divided the Gibb's free energy expression (Eq. 2.2) by the characteristic parameter product ($Nr\varepsilon^*$), a dimensionless equation is obtained:

$$\frac{G}{Nr\varepsilon^*} = \tilde{G} = -\tilde{\rho} + \frac{\tilde{p}}{\tilde{\rho}} + \tilde{T} \left[\frac{1-\tilde{\rho}}{\tilde{\rho}} \ln(1-\tilde{\rho}) + \frac{1}{r} \ln \left(\frac{\tilde{\rho}}{\omega} \right) \right] \quad (2.9)$$

$$\varepsilon^* = \frac{z\varepsilon_{ij}}{2} \quad (2.10)$$

$$\begin{aligned} \tilde{T} &= \frac{T}{T^*}, & T^* &= \frac{\varepsilon^*}{k} \\ \tilde{p} &= \frac{p}{p^*}, & p^* &= \frac{\varepsilon^*}{v^*} \\ \tilde{\rho} &= \frac{V^*}{V}, & V^* &= N(rv^*) \end{aligned} \quad (2.11)$$

ω is the number of possible configuration for a single segment (*close-packed*).

Minimizing the reduced free energy \tilde{G} compared to the reduced volume $\tilde{v} = \frac{1}{\tilde{\rho}}$ and fixed reduced pressure and temperature constants, the equation of state able to describe the equilibrium volume is derived:

$$\left. \frac{\partial \tilde{G}}{\partial \tilde{v}} \right|_{\tilde{T}, \tilde{p}} = \left. \frac{\partial \tilde{G}}{\partial (1/\tilde{\rho})} \right|_{\tilde{T}, \tilde{p}} = 0 \quad (2.12)$$

$$\tilde{\rho}^2 + \tilde{\rho} + \tilde{T} \left[\ln(1 - \tilde{\rho}) + \left(1 - \frac{1}{r}\right) \tilde{\rho} \right] = 0 \quad (2.13)$$

2.1.2 Mixtures

The treatment carried out previously for pure fluids can be extended to the mixtures [19].

Each component inside the mixture occupies $N_i r_i$ cells in the lattice and to each i -th segment is possible to associated an energetic contribute ε_{ij}^* due to the interaction with a j -th segment. In this way the composition is expressed as a occupied sites from the molecule related to the total ones occupied:

$$Nr = \sum_i N_i r_i \quad (2.14)$$

$$\Phi_i = \frac{N_i r_i}{Nr} \quad (2.15)$$

The characteristic energy associated to the mixture is defined starting from single components:

$$\varepsilon^* = \sum_i \Phi_i \varepsilon_{ij}^* - kT \sum_i \sum_j \Phi_i \Phi_j \chi_{ij} \quad (2.16)$$

$$\chi_{ij} = \frac{(\varepsilon_{ij}^* + \varepsilon_{jj} - 2\varepsilon_{ij}^*)}{kT} \quad (2.17)$$

$\varepsilon_{ij}^*, \varepsilon_{jj}$ are the interaction energy between similar segments and ε_{ij}^* is a binary interaction parameter that is equal to:

$$\varepsilon_{ij}^* = \sqrt{\varepsilon_{ii}^* \varepsilon_{jj}^*} \quad (2.18)$$

Two hypothesis has to be inserted to describe the mixture volume:

- 1) The close-packed volume in each species is preserved;

$$r_i^0 v_i^* = r_i v^* \quad (2.19)$$

- 2) The total number of binary interactions in the mixture is equal to the pure component interaction sum.

$$\left(\frac{Z}{2}\right) \sum r_i^0 N_i = \left(\frac{Z}{2}\right) \sum r_i N_i = \left(\frac{Z}{2}\right) rN \quad (2.20)$$

These two hypothesis ensure the additivity of *close-packed* volume:

$$r = \frac{1}{N} \sum_j r_j^0 N_j \quad (2.21)$$

$$\phi_i^0 = \frac{r_j^0 N_j}{\sum_j r_j^0 N_j} = \frac{r_j^0 N_j}{rN} \quad (2.22)$$

$$v^* = \sum_i \phi_i^0 v_i^* \quad (2.23)$$

The quantity with the apex 0 are referred to pure state while those without apex are referred to the mixtures.

The expression of the partition function Z and of Gibb's free energy are not change than to the pure fluid case.

$$\Omega = \Omega(N_0, N_i r_i, z) \quad i = 1 \dots N \quad (2.24)$$

$$E = E(N_0, N_i r_i, z, \varepsilon^*) \quad i = 1 \dots N \quad (2.25)$$

$$V = V(N_0, N_i r_i, v^*) \quad i = 1 \dots N \quad (2.26)$$

As is the previous chapter a dimensionless expression of Gibb's free energy is obtained:

$$\tilde{G} = -\tilde{\rho} + \frac{\tilde{p}}{\tilde{\rho}} + \tilde{T} \left[\frac{1-\tilde{\rho}}{\tilde{\rho}} \ln(1-\tilde{\rho}) + \frac{1}{r} \ln\left(\frac{\tilde{\rho}}{\omega}\right) + \sum_i \frac{\phi_i}{r_i} \ln\left(\frac{\phi_i}{\omega_i}\right) \right] \quad (2.27)$$

The equation of state is then obtained minimizing the energy related to the reduced volume at constant pressure and temperature is equal to Eq. 2.13.

$$\left. \frac{\partial \tilde{G}}{\partial \tilde{v}} \right|_{\tilde{T}, \tilde{p}} = \left. \frac{\partial \tilde{G}}{\partial (1/\tilde{\rho})} \right|_{\tilde{T}, \tilde{p}} = 0 \quad (2.28)$$

$$\tilde{\rho}^2 + \tilde{\rho} + \tilde{T} \left[\ln(1-\tilde{\rho}) + \left(1 - \frac{1}{r}\right) \tilde{\rho} \right] = 0 \quad (2.29)$$

2.1.3 Characteristic parameters

The previous paragraph shows that in the *Lattice Fluid* theory each fluid is characterized by three molecular parameters ε^* , v^* and r or by three parameters that appears in the equation of state T^* , p^* and ρ^* :

$$\varepsilon^* = kT^* \quad (2.30)$$

$$v^* = \frac{kT^*}{p^*} \quad (2.31)$$

$$r = \frac{Mp^*}{kT^*\rho^*} = \frac{M}{p^*v^*} \quad (2.32)$$

where M is the molecular weight of the interested component.

In the original paper [7] ε^* was associated to the interaction energy between first segment of neighboring chains, but in time the meaning was converted in the proportional to the depth of the holes of the potential energy configuration [19].

The product $r\varepsilon^*$ represent the total molar energy of interaction, that is the energy necessary to convert a single mole of fluid from *close-packed* state to a state where the density tends to 0.

For that concern v^* , it is necessary to remember that although the Sanchez and Lacombe model used a lattice, the theory was suggested to describe and analyzed disordered structure. The *close-packed* state has to be considered similar to an amorphous species rather than a crystalline one and so the product rv^* can be identified as a molar volume of the *close-packed* state of the disorderly fluid [20].

The ratio between the molar energy interaction and the molar volume is defined as the characteristic pressure of the system $p^* = \varepsilon^*/v^*$ or the pressure of single components $p^* = \varepsilon^*_{ij}/v^*_{ij}$ and it is equal to the density of cohesive energy. p^* assumes the meaning of intermolecular interaction force index.

Because it is more convenient refer to parameter related to the macroscopic world and not to the molecular one, define a characteristic temperature for single species, as a ratio between interaction energy and Boltzmann's constant is possible:

$$T^* = \frac{\varepsilon^*}{k} \quad T_i^* = \frac{\varepsilon_i^*}{k} \quad (2.34)$$

and for each species present in the system, a characteristic density as a ratio between the molecular weight and the close-packed volume system occupied from the specie:

$$\rho_i^* = \frac{M_i}{r_i^0 v_i^*} \quad (2.35)$$

These last relationship shows that the characteristic quantities are similar to the ideal gas law:

$$p^* = \frac{\varepsilon^*}{v^*} = \frac{kT^*}{v^*} \Rightarrow p^* v^* = kT^* \quad (2.36)$$

As for the molecular parameter, even for the macroscopic parameter, exist combination of rules which allow to extend the theory of pure fluids to mixtures. In particular characteristic pressures are additives to couples according to the expression:

$$p^* = \sum_i \Phi_i p_i^* - \frac{1}{2} \sum_i \sum_j \Phi_i \Phi_j \Delta p_{ij}^* \quad (2.37)$$

Where p_i^* is the characteristic pressure for component i, Φ_i its molar fraction and Δp_{ij}^* a binary interaction parameter:

$$\Delta p_{ij}^* = p_i^* + p_j^* - 2p_{ij}^* \quad (2.38)$$

$$\rho^* = \frac{\sum_i N_i M_i}{\sum_j r_j^0 N_j v_j^*} = \frac{1}{\sum_i \frac{\omega_i}{\rho_i^*}} \quad (2.39)$$

ω_i is the weight fraction of component i-th in the mixture.

All the thermodynamic properties are helpful to find the necessary parameters to apply Sanchez and Lacombe model, but in practice pVT data are used because are available from the literature for the most common fluids. The parameters required from the equation of state are determined through the fitting with the experimental data [8] [20].

In case of low molecular weight fluids, these parameters are evaluated once the temperature T, heat of vaporization ΔH_v , vapor pressure and liquid specific volume v_i are fixed.

In case of a high molecular weight polymer the hypothesis is that r tends to infinity. In this case ρ^* , p^* and T^* are deducted from the fitting of pVT data available from the literature or obtained from direct experimental values.

When the existing pVT data are not sufficient for the interested polymer, density values, thermal expansion coefficient or compressibility information determined experimentally at ambient pressure and temperature are used, but with lower sensitiveness.

2.1.4 Solubility

Solubility of gas phase solved in a polymer at fixed temperature and pressure conditions is determined equating the chemical potential of penetrant solvent in the external phase and in the solution and imposing at the same time the validity of the equations of state for both phases.

The chemical potential expression is obtained from the Gibb's free energy derivation related to molar fraction of the same species at constant temperature, pressure and molar fractions of other components:

$$\mu_i = \left. \frac{\partial G}{\partial n_i} \right|_{T,p,n_{i \neq j}} \quad (2.40)$$

Although for the gasses other better theories were developed, Sanchez and Lacombe expression will be used afterwards for simplicity to describe gas and polymer phase.

Deriving the eq. 2.40 [19]:

$$\begin{aligned} \mu_1 = kT \left\{ \ln \phi_1 + \left(1 - \frac{r_1}{r_2}\right) (1 - \phi_1) + r_1 \tilde{\rho} \frac{\Delta p^*}{\tilde{\rho}_1^* kT} (1 - \phi_1)^2 \right. \\ \left. + r_1 \left[-\frac{\tilde{\rho}}{\tilde{T}_1} + \frac{\tilde{p}_1}{\tilde{T}_1 \tilde{\rho}} + \frac{(1 - \tilde{\rho}) \ln(1 - \tilde{\rho})}{\tilde{\rho}} + \frac{1}{r_1} \ln \tilde{\rho} \right] \right\} \end{aligned} \quad (2.41)$$

When the second phase is represented by a polymer, $r_2 \rightarrow \infty$:

$$\begin{aligned} \mu_1 = kT \left\{ \ln \phi_1 + (1 - \Phi_1) (1 - \phi_1) + r_1 \tilde{\rho} \frac{\Delta p^*}{\tilde{\rho}_1^* kT} (1 - \phi_1)^2 \right. \\ \left. + r_1 \left[-\frac{\tilde{\rho}}{\tilde{T}_1} + \frac{\tilde{p}_1}{\tilde{T}_1 \tilde{\rho}} + \frac{(1 - \tilde{\rho}) \ln(1 - \tilde{\rho})}{\tilde{\rho}} + \frac{1}{r_1} \ln \tilde{\rho} \right] \right\} \end{aligned} \quad (2.42)$$

The solubility is obtained solved simultaneously three equations [21]:

$$\left(\begin{aligned} \tilde{\rho} &= 1 - \exp \left[-\frac{\tilde{\rho}^2}{\tilde{T}} - \frac{\tilde{p}}{\tilde{T}} - \left(1 - \frac{\Phi_1}{r_1}\right) \tilde{\rho} \right] \end{aligned} \right) \quad (2.43)$$

$$\left(\begin{aligned} \tilde{\rho}_1 &= 1 - \exp \left[-\frac{\tilde{\rho}_1^2}{\tilde{T}_1} - \frac{\tilde{p}_1}{\tilde{T}_1} - \left(1 - \frac{\Phi_1}{r_1}\right) \tilde{\rho}_1 \right] \end{aligned} \right) \quad (2.44)$$

$$\left(\begin{aligned} \left[-\frac{\tilde{\rho}}{\tilde{T}_1} + \frac{\tilde{p}_1}{\tilde{T}_1 \tilde{\rho}} + \frac{(1 - \tilde{\rho}) \ln(1 - \tilde{\rho})}{\tilde{\rho}} + \frac{\ln \tilde{\rho}_1}{r_1^0} \right] r_1^0 &= \ln \Phi_1 + (1 - \Phi_1) \\ &+ \tilde{\rho} \frac{M_1 \Delta p^*}{\rho_1^* RT} (1 - \Phi_1)^2 + \\ \left[-\frac{\tilde{\rho}}{\tilde{T}_1} + \frac{\tilde{p}_1}{\tilde{T}_1 \tilde{\rho}} + \frac{(1 - \tilde{\rho}) \ln(1 - \tilde{\rho})}{\tilde{\rho}} + \frac{\ln \tilde{\rho}}{r_1} \right] r_1 & \end{aligned} \right) \quad (2.45)$$

At the end, ω_1 will be the uptake mass fraction of penetrant at the equilibrium

$$\omega_1 = \frac{\phi_1}{\phi_1 + (1 - \phi_1) \frac{\rho_2^*}{\rho_1^*}} \quad (2.46)$$

Chemical potentials of the components in the mixtures, as described from Sanchez and Lacombe equations, have the following properties:

- At low temperature and/or high pressure, reduced density tends to the unit $\tilde{\rho}, \tilde{\rho}_1 \rightarrow 1$. Under this condition Flory Huggins chemical potential are obtained;
- A unique interaction parameter $\Delta p^* = p_1^* + p_2^* - 2p_{12}^*$ is sufficient to completely characterized a binary mixture, because all the other parameters are already known for pure components [21].

This parameter is representative of the mixtures energy interactions and in particular it is positive if the interactions between gas phase and polymer are energetically less favorite than the interactions between the pure components. The interactions usually are described as function of an empiric parameter Ψ which represents p_{12}^* deviation from geometric average of p_1^* and p_2^* :

$$p_{12}^* = \Psi \sqrt{p_1^* p_2^*} \quad (2.47)$$

Solving the system previously described (eq. 2.43-2.45), the composition of the single components present in the mixture and its density are obtained. In particular change in volume is estimated:

$$\frac{\Delta V}{V_0} = \frac{\tilde{v}}{\phi_1 \tilde{v}_1 + (1 - \phi_1) \tilde{v}_2} = \frac{1}{\tilde{\rho} \rho^* (1 - \omega_1) \hat{v}_2^0} - 1 \quad (2.48)$$

where V_0 is the ideal volume of the mixture considering valid the single volume additivity and \hat{v}_2^0 the specific volume of pure polymer in the experimental conditions.

2.2 PC-SAFT

Perturbated-chain SAFT equation of state was developed by Gross and Sadowski [12] and it was created applying the perturbation theory of Barker and Henderson [22] [23] to a hard-chain reference fluid.

2.2.1 Pure Fluids

In the PC-SAFT the repulsive interaction, typical for a perturbation theory, are described with a hard-chain term derived by Chapman et al. [10]. The attractive interactions are separated into dispersive interactions and a contribution due to the association.

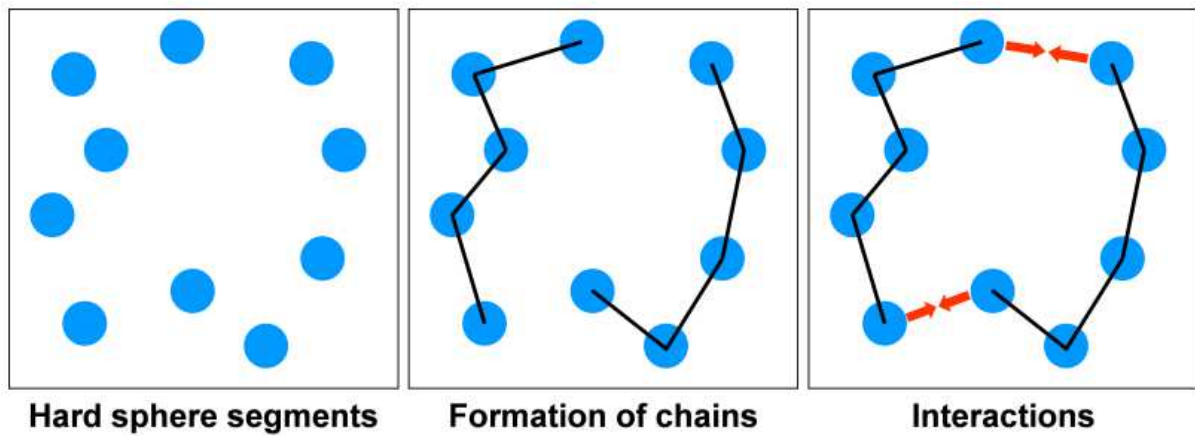


Figure 2.1: Hard-chain reference system considered in the PC-SAFT [24]

The compressibility factor Z is given as an ideal gas contribution (id), a repulsive contribute (hc), an attractive contribute (disp, chain) and a contribute due to the specific interaction such as hydrogen bonding or multiple interactions:

$$Z = Z^{id} + Z^{hc} + Z^{disp,chain} + Z^{assoc} \quad (2.49)$$

where $Z = pV/RT$ with p is the pressure, V the molar volume, T the temperature and R is the gas constant. In the eq. 2.49 $Z^{id} = 1$.

The repulsive contribute Z^{hc} is the residual hard chain contribution to the compressibility factor and is given by:

$$Z^{hc} = \bar{m}Z^{hs} - \sum_i x_i(m_i - 1)(g_{ii}^{hs})^{-1} \rho \frac{\partial g_{ii}^{hs}}{\partial \rho} \quad (2.50)$$

where Z^{hs} is the residual contribution of the hard-sphere fluid and $\bar{m} = x_i m_i$.

$$Z^{hs} = \frac{\xi_3}{(1 - \xi_3)} + \frac{3\xi_1\xi_2}{\xi_0(1 - \xi_3)^2} + \frac{3\xi_2^3 - \xi_3\xi_2^3}{\xi_0(1 - \xi_3)^3} \quad (2.51)$$

$$g_{ij}^{hs} = \frac{1}{(1 - \xi_3)} + \left(\frac{d_i d_j}{d_i + d_j} \right) \frac{3\xi_2}{(1 - \xi_3)^2} + \left(\frac{d_i d_j}{d_i + d_j} \right)^2 \frac{2\xi_2^2}{(1 - \xi_3)^3} \quad (2.52)$$

$$\begin{aligned} \rho \frac{\partial g_{ij}^{hs}}{\partial \rho} &= \frac{\xi_3}{(1 - \xi_3)^2} + \left(\frac{d_i d_j}{d_i + d_j} \right) \left(\frac{3\xi_2}{(1 - \xi_3)^2} + \frac{6\xi_2\xi_3}{(1 - \xi_3)^3} \right) \\ &+ \left(\frac{d_i d_j}{d_i + d_j} \right)^2 \left(\frac{4\xi_2^2}{(1 - \xi_3)^3} + \frac{6\xi_2^2\xi_3}{(1 - \xi_3)^4} \right) \end{aligned} \quad (2.53)$$

The temperature-dependent segment diameter d_i of component i is given by:

$$d_i = \sigma_i \left[1 - 0.12e^{\left(-3\frac{\epsilon_i}{kT}\right)} \right] \quad (2.54)$$

The attractive contribution $Z^{disp,chain}$ is the dispersion contribution to the compressibility factor and is given by:

$$Z^{disp,chain} = -2\pi\rho \frac{\partial(\eta I_1)}{\partial \eta} \overline{m^2 \epsilon \sigma^3} - \pi\rho\bar{m} \left[C_1 \frac{\partial(\eta I_2)}{\partial \eta} + C_2 \eta I_2 \right] \overline{m^2 \epsilon^2 \sigma^3} \quad (2.55)$$

where:

$$\begin{aligned} \frac{\partial(\eta I_1)}{\partial \eta} &= \sum_{j=0}^6 a_j(\bar{m}) (j + 1) \eta^j \\ \frac{\partial(\eta I_2)}{\partial \eta} &= \sum_{j=0}^6 b_j(\bar{m}) (j + 1) \eta^j \end{aligned} \quad (2.56)$$

C_1 and C_2 are abbreviation for compressibility expression.

The association contribution Z^{assoc} is given by:

$$Z^{assoc} = \rho \sum_i x_i \sum_j x_j \sum_{A_j} \left[\left(\frac{1}{X^{A_j}} - \frac{1}{2} \right) \frac{\partial X^{A_j}}{\partial \rho_i} \right] \quad (2.57)$$

And the association strength:

$$\Delta^{A_i B_j} = \sigma_{ij}^3 g_{ij}(d_{ij}) k^{A_i B_j} \left[e^{\left(\frac{\epsilon^{A_i B_j}}{kT} \right)} - 1 \right] \quad (2.58)$$

2.2.1.1 Pure-component parameter

2.2.1.1.1 Non-associating components

For the non-associating molecules, three pure component parameters are require:

- Segment diameter σ_i (Å)
- Segment number m_i
- Segment energy parameter ϵ_i/k (K)

These parameters are identified for this equation of state by fitting vapor pressure and pVT data found in literature or obtained from experimental tests.

2.2.1.1.2 Associating components

For the associating molecules, in addition to the pure-parameter described for the non-associating components, two different type of association sites are assumed (electron acceptor and electron donor), each of them existing twice per molecule.

- Association energy $\epsilon^{A_i B_i}$
- Association volume $k^{A_i B_i}$

2.2.2 Mixtures

In mixtures $\bar{m} = \sum_i x_i m_i$ and is the mean segment number.

Conventional combining rules for repulsive (hard chain) and attractive (dispersion) terms is applied in order to calculate the thermodynamic properties of the mixtures.

$$\sigma_{ij} = \frac{1}{2}(\sigma_i + \sigma_j) \quad (2.59)$$

$$\varepsilon_{ij} = (1 - k_{ij})\sqrt{\varepsilon_i\varepsilon_j} \quad (2.60)$$

Binary interaction parameter k_{ij} is introduced to correct the dispersion energy parameter.

For cross associating system, for example, ethanol and butanol, the strength of the cross associating interactions between the two associating substances is described applying simple combination rules suggested by Wolbach and Sandler [25] without using any other adjustable parameters:

$$\varepsilon^{A_i B_j} = \frac{1}{2}(\varepsilon^{A_i B_i} + \varepsilon^{A_j B_j}) \quad (2.61)$$

$$k^{A_i B_j} = \sqrt{k^{A_i B_i} k^{A_j B_j}} \left(\frac{\sqrt{\sigma_i \sigma_j}}{(1/2)(\sigma_i + \sigma_j)} \right)^3 \quad (2.62)$$

Binary interaction parameter k_{ij} is determined by fitting with solubility data in pure solvent.

Compounds which have OH-groups should be modeled as associating compounds with at least two association-site types, each having one or two sites.

The association volume $k^{A_i B_j}$ prove to have less influence on the results of the solubility calculations. Therefore, this parameter can be excluded from the parameter estimation, reducing the number of adjustable parameters.

2.2.3 Solubility

The fugacity coefficient in the mixture is related to the residual chemical potential μ_i^{res} , the Boltzmann's constant k , temperature T , and to compressibility factor Z :

$$\ln \varphi_i = \frac{\mu_i^{res}(T, \nu)}{kT} - \ln Z \quad (2.63)$$

The compressibility factor Z is defined as a function of pressure p , molar volume ν , Boltzmann's constant k , Avogadro number N_{AV} and temperature T :

$$(2.64)$$

$$Z \equiv \frac{pv}{kN_{AV}T}$$

The residual chemical potential is the partial derivation of the residual Helmholtz free energy A^{res} divided by the number of molecules N with respect to the concentration x_i at constant temperature and volume:

$$\begin{aligned} \frac{\mu_i^{res}(T, v)}{kT} &= \frac{A^{res}}{NkT} + Z - 1 + \left(\frac{\partial(A^{res}/NkT)}{\partial x_i} \right)_{T, v, x_{k \neq i}} \\ &\quad - \sum_j \left[x_j \left(\frac{\partial(A^{res}/NkT)}{\partial x_j} \right)_{T, v, x_{k \neq j}} \right] \end{aligned} \quad (2.65)$$

With Eqs 2.63 and 2.65, the fugacity coefficient becomes:

$$\begin{aligned} \ln \varphi_i &= \frac{A^{res}}{NkT} + \left(\frac{\partial(A^{res}/NkT)}{\partial x_i} \right)_{T, v, x_{k \neq i}} - \sum_j \left[x_j \left(\frac{\partial(A^{res}/NkT)}{\partial x_j} \right)_{T, v, x_{k \neq j}} \right] + Z \\ &\quad - 1 - \ln Z \end{aligned} \quad (2.66)$$

2.3 NELF Model

Sanchez and Lacombe and PC-SAFT theories allow a good estimation of the vapor or gas solubility in rubbery polymers. The case of glassy polymers is different because the equilibrium structure is not present and the equations used in the previous paragraphs are no longer valid.

Starting from the Sanchez and Lacombe work, Doghieri and Sarti developed the NELF (*Non-Equilibrium Lattice Fluid*) [26] [27] that allows to calculate sorption isotherms of gas and vapors in glassy polymers through the introduction of order parameter able to describe the non-equilibrium state in polymer.

Because the order parameter is not a quantity uniquely defined, its choice becomes important in the data analysis phase. The parameters have to be [28]:

- 1) A macroscopic quantity and easily measurable;
- 2) Represent the non-equilibrium state of the polymer, characterized by a free excess volume related to its equilibrium values;
- 3) Be an internal state variable, namely Z where its change speed dZ/dt is a thermodynamic property:

$$\frac{dZ}{dt} = f(T, p, \omega, Z) \quad (2.67)$$

NELF model identifies partial polymeric density ρ_{pol} as an order parameter and it has to be:

- 1) A macroscopic quantity, easily measurable;
- 2) Higher free volume corresponds to lower polymer density
- 3) Appropriate rheological consideration that a polymer shows due to a mechanical stress allow to elaborate a constitutive equation typical for viscoelastic solids:

$$\frac{d\rho_{pol}}{dt} = f(T, p, \omega, \rho_{pol}) \quad (2.68)$$

The Gibb's free energy of the mixture is only function of temperature T , pressure p , composition ω and partial polymeric density ρ_{pol} because the use of the only internal variable allows an easier usage of the thermodynamic properties.

$$G = G(T, p, \omega_i, \rho_{pol}) \quad (2.69)$$

And in an equivalent way, replacing the mass fractions ω_i with the molar ones n_i :

$$G = G(T, p, n_i, \rho_{pol}) \quad (2.70)$$

Differentiating:

$$dG = -SdT + VdP + \sum_i \mu_i dn_i + Ad\rho_{pol} \quad (2.71)$$

where S , V and μ_i are the non equilibrium entropy, volume and chemical potential of species i -th and $A = \partial G / \partial n_i |_{T,p,n_{i \neq j}, \rho_{pol}}$ is the affinity regard the order parameter chosen.

Some considerations are possible:

- Chemical potential value $\mu_i = \partial G / \partial n_i |_{T,p,n_{i \neq j}, \rho_{pol}}$ is different from chemical potential in the equilibrium condition working at the same operative conditions as temperature, pressure and composition;
- Based on second law of thermodynamic, reliability and time derivative of the order parameter have to be discordant in sign because $dG/dt = dG/d\rho_{pol} d\rho_{pol}/dt = A d\rho_{pol}/dt \leq 0$.

In glassy systems the evolution of the order parameter (macroscopically equal to a polymer swelling) is negligible in pseudoequilibrium conditions:

$$\frac{d\rho_{pol}}{dt} = f(T, p, \omega, \rho_{pol}) \approx 0 \quad (2.72)$$

- From the eq. 2.72 the partial density value is not unique, but depends on the previous history (mechanical, thermal, or chemical) of the polymer.

A penetrant sorbed in a glassy polymer determines a volume changes in the polymer itself. This change, essential for the solute adsorption, is linear with the stress field that is generated as a result of the rearrangement of the chains.

In agreement with rheological laws, the relationship stress-volume deformation is evaluated with the use of appropriate spring, condenser models (Maxwell, Voigt, etc) where the mechanical properties of the system (elasticity and viscous absorption coefficients) are related to the relaxation time over the lag τ .

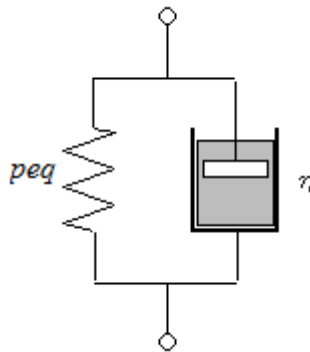


Figure 2.2: Voigt viscoelastic model

As a consequence, the NELF model was developed starting from the rheological Voigt model (Fig. 2.2).

$$p = p^{eq} + \eta \frac{1}{V_{pol}} \frac{dV_{pol}}{dt} \quad (2.73)$$

At a generic instant of time the pressure exerted on the system p depends on the elastic contribute p^{eq} , the polymeric phase volume V_{pol} and the viscous assorption coefficient η . In the Eq. 2.71 the elastic contribute depends only from the thermodynamic properties of the system and it have not constraints of linearity unlike what happen in the pure rheology.

Because:

$$\frac{1}{V} \frac{dV}{dt} = - \frac{d \ln p}{dt} \quad (2.74)$$

The eq. 2.72 becomes:

$$\frac{d \ln \rho_{pol}}{dt} = \frac{p^{eq} - p}{\eta} \quad (2.75)$$

that represents the order parameter evolution.

The pure polymeric phase density ρ_{pol}^0 knowledge is the initial condition of this problem.

The pseudo equilibrium condition is reached when the state of the system is invariant in the observation time. In this situation the chemical potential for the penetrant inside the polymer and in the bulk phase must be equal.

Starting from Sanchez and Lacombe expressions of the Gibb's free energy, the chemical potential expressions are obtained as function of the composition:

$$G = NrRT^* \left\{ -\tilde{\rho} + \frac{\tilde{\rho}}{\tilde{p}} + \tilde{T} \left[\frac{(1 - \tilde{\rho}) \ln(1 - \tilde{\rho})}{\tilde{\rho}} + \frac{1}{r} \ln \tilde{\rho} \right] \right\} \quad (2.76)$$

for binary mixture, imposing the mixing rule and fixing $Nr = n_1 r_1 + n_2 r_2$:

$$G = NrRT^* \left\{ -\tilde{\rho} + \frac{\tilde{\rho}}{\tilde{p}} + \tilde{T} \left[\frac{(1 - \tilde{\rho}) \ln(1 - \tilde{\rho})}{\tilde{\rho}} + \frac{1}{r} \ln \tilde{\rho} + \sum_i \frac{\phi_i}{r_i} \ln(\phi_i \tilde{\rho}) \right] \right\} \quad (2.77)$$

The Eq. 2.76 is simplified when in the binary system one component is a polymer because $r_2 \rightarrow \infty$:

$$G = NrRT^* \left\{ -\tilde{\rho} + \frac{\tilde{\rho}}{\tilde{p}} + \tilde{T} \left[\frac{(1 - \tilde{\rho}) \ln(1 - \tilde{\rho})}{\tilde{\rho}} + \frac{1}{r} \ln \tilde{\rho} + \frac{\phi_i}{r_i} \ln(\phi_i \tilde{\rho}) \right] \right\} \quad (2.78)$$

The characteristic equation of state at the equilibrium is obtained as usual minimizing the free energy, bringing back at the result provided by Sanchez and Lacombe. Deriving Gibb's free energy to the composition, chemical potential at non-equilibrium condition as function of temperature, pressure, composition and partial density are obtained:

$$\mu_i = \left. \frac{\partial G}{\partial n_i} \right|_{T, p, n_{i \neq j}, \rho_{pol}} = \mu_i(T, p, \omega_i, \rho_{pol}) \quad (2.79)$$

Because polymeric partial density results connected to the reduced density by the equation $\tilde{\rho} = \rho_{pol}/(\omega_{pol}\rho^*)$, all the variables are expressible through quantity related to the mixture.

Less than additive constant [27]:

$$\begin{aligned} \mu_i = kT \left\{ \ln \left(\frac{\omega_1 \rho_2}{\omega_2 \rho_1^*} \right) \right. \\ - \frac{M_1 p_1^*}{\rho_1^* R T_1^*} \left\{ \left[1 + \left(\frac{T_1^* p^*}{T^* p_1^*} - 1 \right) \frac{\omega_2 \rho^*}{\rho_2} \right] \ln \left(1 - \frac{\rho_2}{\omega_2 \rho^*} \right) + \frac{T_1^* p^*}{T^* p_1^*} \right. \\ \left. \left. + \frac{\rho_2}{\omega_2 \rho^*} \left[\frac{T_1^*}{T} \left(1 + \frac{p^*}{p_1^*} - \left(\omega_2 \frac{\rho^*}{\rho_2} \right)^2 \frac{\Delta p^*}{p_1^*} \right) \right] \right\} + 1 \right\} \end{aligned} \quad (2.80)$$

In this last expression the first three addends are related to the entropic contribution to the chemical potential, while the fourth is due to the energetic contribution. It was observed that changes in partial polymeric density significantly affect entropic contributes: increasing polymeric density, chemical potential increases and consequently the solubility decreases.

The knowledge of the characteristic parameter (p^*, T^*, ρ^*) , polymeric partial density $\rho_{pol} = \rho_2$ and the binary interaction parameter Δp^* is important for the use of chemical potential expression. These parameters are determined from experimental measurements or by the fitting of the solubility data. In the absence of the experimental data, the equation that describe the first order kinetics evolution coupled to the corresponding initial condition and to the relationship [26]:

$$\Delta p^* = (\sqrt{p_1^*} - \sqrt{p_2^*})^2 \quad (2.81)$$

provides an estimation at the first order interaction. The sensitiveness of this model is high if the polymer density determination is considered, but is too low for the binary interaction parameter which is rarely far from the value obtained with eq. 2.81. Alternately to the eq. 2.81, the use of the expression $\Delta p^* = p_1^* + p_2^* - 2\psi\sqrt{p_1^* p_2^*}$, once the empirically parameter ψ is introduced as in the Sanchez Lacombe model.

As said before, the solubility calculation is based on the imposition of the pseudo equilibrium condition between the gas (penetrant) and the solid (polymer) phase. Using chemical potential by Sanchez and Lacombe for the bulk phase and by the eq. 2.80 for the mixture, pseudo equilibrium condition becomes:

$$\begin{aligned}
& \left[-\frac{\tilde{\rho}_1}{\tilde{T}_1} + \frac{\tilde{p}_1}{\tilde{T}_1 \tilde{\rho}_1} + \frac{(1 - \tilde{\rho}_1) \ln(1 - \tilde{\rho}_1)}{\tilde{\rho}_1} + \frac{\ln \tilde{\rho}_1}{r_1^0} \right] r_1^0 \\
& = \ln(\tilde{\rho} \phi_1) - \left(r_1^0 + \frac{r_1 - r_1^0}{\tilde{\rho}} \right) \ln(1 - \tilde{\rho}) - r_1 \\
& - \tilde{\rho} r_1^0 \frac{V_1^*}{RT} (p_1^* + p^* - \phi_2^2 \Delta p^*)
\end{aligned} \tag{2.82}$$

Solved in terms of ϕ_1 , it allows to obtain the mass uptake of penetrant.

2.4 Affine network theory

The mechanical constraint due to the crosslink degree inside a polymer can be explained by the affine network theory.

The affine model assumes that cross links are firmly connected to the macroscopic body and network deform in the same way with the macroscopic deformation.

A polymer network may be characterized by the number of chains inside it, including those with only one end attached:

$$v = \frac{1}{2}(\mu_j \phi + v_{ends}) \quad (2.83)$$

where μ_j is the number of the junctions inside the network, ϕ is their functionality, v_{ends} the number of ends of chains [15].

For a perfect network for which $v_{ends} = 0$:

$$v_e = v = \frac{1}{2}(\mu_j \phi) \quad (2.84)$$

where v_e is the effective number of chains.

The cycle rank ξ is a quantity that characterized the network with higher generality and regards the nature of its imperfections. This quantity is used to characterize the elastic response of the network. In a perfect network ξ is the difference between the number of chains and the number of junctions:

$$\xi = v - \mu_j = v \left(1 - \frac{2}{\phi}\right) \quad (2.85)$$

A important characteristic typical for the polymeric network is the interaction between chains and junctions [15].

The average number Γ of junctions within the region of radius $\langle r^2 \rangle_0^{1/2}$ offers a quantitative measure of the degree of interpretation and it is given by:

$$\Gamma = \frac{4\pi}{3} \langle r^2 \rangle_0^{3/2} \frac{\mu_j}{V^0} \quad (2.86)$$

where V^0 is the volume of the network in its state of reference.

According to the assumption that the transformation of chain vectors is affine in the change in position gradient tensor λ that defines the macroscopic strain, the free energy is:

$$\Delta A_{\text{aff}} = \frac{\nu}{2} kT (\lambda_x^2 + \lambda_y^2 + \lambda_z^2 - 3) - \mu_j kT \ln \left(\frac{V}{V_0} \right) \quad (2.87)$$

where $\lambda_x, \lambda_y, \lambda_z$ are the principal extension ratios measured relative to the dimensions of the specimen.

The stress is obtained as a function of strain by differentiation of eq. 2.87. For uniaxial elongation parallel to the x-axis, $\lambda_x = \lambda = L/L^0$ and $\lambda_y = \lambda_z = (V/V_0\lambda)^{1/2}$ and the force of retraction for the affine network is:

$$f_{\text{aff}} = \left(\frac{\partial \Delta_{el}}{\partial L} \right)_{T,V} = \frac{\left(\frac{\partial \Delta_{el}}{\partial \lambda} \right)_{T,V}}{L^0} = \left(\frac{\nu kT}{L^0} \right) \left(\lambda - \frac{V}{V^0} \lambda^2 \right) = \left(\frac{\nu kT}{L_{i,V}} \right) \left(\frac{V}{V^0} \right)^{2/3} (\alpha - \alpha^{-2}) \quad (2.88)$$

Where $\alpha = L/L_{i,V} = \lambda(V/V^0)^{-1/3}$ is the extension ratio relative to the length $L_{i,V} = L^0(V/V^0)^{1/3}$ of the isotropic specimen at the volume V predominant in the elongated state.

2.5 Calculation tools

Excel worksheet, fortran code and worksheet implemented with fortran routine were set up to solve phase equilibria and mass transport problem in polymer solute systems of interest, for the case of a single solute or for a mixture of several different solutes. Thermodynamic properties involved in phase equilibria and mass transport properties are calculated after non-equilibrium version of Sanchez-Lacombe lattice fluid theory (NELF) for the case of glassy systems and after PC-SAFT EoS implemented with affine network relation for polymer elasticity. Details for the calculation tools set up and used in this work are described in more details in the following sections, with reference to the specific applications to which they are associated.

Chapter 3

IN-PLANE STRESS MEASUREMENT

The knowledge of transport properties is a theme of considerable importance in a lot of productive sectors using polymeric materials. The maintenance of dimensional stability is an important key in many fields. The sorption of an external phase may induce swelling which causes material deformation, varying the characteristics with positive or negative effects depending on the application concerned.

The mass transport in polymeric thin coating is influenced by:

- Solute/polymer properties;
- Operative conditions (temperature and/or pressure)
- Activity of solute
- Geometry and chemical and mechanical history of polymeric coating.

The analysis of volumetric properties and state of stress are important in the mass transport field and the problem arising are different.

Many elements characterize the analysis of volumetric properties and stress state originated from the mass transport in polymeric materials.

The aim of the present work is to design an apparatus which measures the in-plane stress that arises in polymeric coating below the glass transition temperature (T_g) as result of vapor sorption/desorption processes.

3.1 Bending Beam

The bending-beam is a simple technique to determine the mechanical characteristics and the properties associated in a polymeric coating [30] [31] [32] [33] [34]. It is based on the measure of the deflection of a free end of a beam coated with a thin layer of polymeric coating, over the time. The mechanical properties of the beam are known and from the deflection values determines the change in stress state. The bending-beam is due to different phenomena:

- Mass transport;
- Thermal gradients;
- Mechanical stress.

The bending-beam is applied using a thin film of polymeric material coated on a supported beam with known mechanical characteristics. The in-plane stress and the other information related are calculated from the deflection applying the suitable mathematical models. In particular the technique is used to determine:

- Stress state in the polymer [35] [36] [37] [38]
- Glass transition temperature of polymer [35] [39]
- Beginning of breaking process [35]
- Elastic stiffness and thermal expansion coefficient for the polymer [40]
- Elastic modulus of the polymer [36]
- Fickian and non-Fickian diffusion of low molecular weight solvents in glassy polymers [41] [42] [43].

This technique is used in different fields of polymeric science but its use is not simple or trivial because it depends on different parameters:

- Support material;
- Preparation of the sample;
- Bending measure;
- Polymeric thickness;
- Elastic modulus.

3.1.1 Choice of support material

The beam to measure the bending is usually a small and thin cantilever with a rectangular section. The beam geometry greatly influences the instrument sensibility: increases with its length and decreases with its thickness. It is necessary reach an appropriate compromise between these possibilities because the excessive stretching and contemporary thinning of the beam would result in excessive bending due to the own weight.

It is necessary that the beam works inside the elastic region during the test, because in case of yield the data analysis should be explained with elastic-plastic or viscoelastic models.

A list of materials used as support in the stress measurements was compiled by Campbell [31], but determining in advance the right material is not so easy.

The characteristics such as surface finish, flatness of the substrates, elastic modulus, limit the possibility to use the same beam for many tests. For these reasons, the experimental tests were carried out on disposable cantilever made with readily available materials.

3.1.2 Preparation of the sample

The polymer is deposited on the metallic beam through the solvent casting technique. This casting is followed by 24h of evaporation under hood vacuum at ambient temperature. Subsequently a thermal treatment of annealing for 1h under vacuum and temperature higher than T_g is made. A treatment of controlled cooling under vacuum conditions follows the latter.

Annealing process is useful because it reduces the stress due to the solvent evaporation. During the substrate deposition, the polymer remains constrained due to the contact forces at the interface that freeze inside a stress state which tends to bend the support.

Confine this stress phenomena is possible taking care that the evaporation of solvents is slow and controlled, but delete it is impossible.

3.1.3 Bending measure

The placement of the beam inside the measure system plays an important role because the deflection measurement is in situ. The sample has to be tight to the original location [44]. Special care should be devoted to fixing the beam in a right way: the solution adopted provides the locking of the substrate between two threaded nuts in turn blocked by two locknuts.

The measure system sensitiveness is related to the characteristics and geometry of the support and in the same way from the detection system used. The methods able to measure the deflection of the beam are different:

- Direct observation [35] [41]
- Laser pointer [37] [39]
- Mechanical methods (assessment of the force necessary to ensure the free end balance) [45]
- Interferometer methods [31]

- Inductance transducer [31]
- Capacitive transducer [33].

The direct observation is the simplest technique, but with the less sensitiveness in case of human observer. Using tools to perform the measurement automatically, for example optical micrometer, this drawback is solved.

The laser pointer is the most used technique in case of liquid phases because the correction to be made for the different refraction index in air and in liquid is very simple [46].

The inductance and capacitive transducers allow to reach higher sensitiveness (deflection of 10^{-6} - 10^{-9} mm), but the measurements are affected by high background noise and to the limited use at the ambient temperature [32].

The interferometer methods gives the best results, but it is used in the atomic force microscope due to its constructive complexity.

In a large scale only the direct observation or the laser pointer are usable.

3.1.4 Polymer thickness and mechanical properties

The polymer thickness knowledge is necessary to calculate the state of stress. The polymer thickness is evaluated by means of weight variations, is the sample change is not significant. In case of important swelling during the sorption process the laser interferometer in situ is used.

The knowledge of the mechanical properties of the support is important to analyzed the deflection data.

3.2 Stress state

Stresses in coating deforms the substrate on which the polymer is deposited, consequently there is a curvature of it [31] [41] (Fig. 3.1).

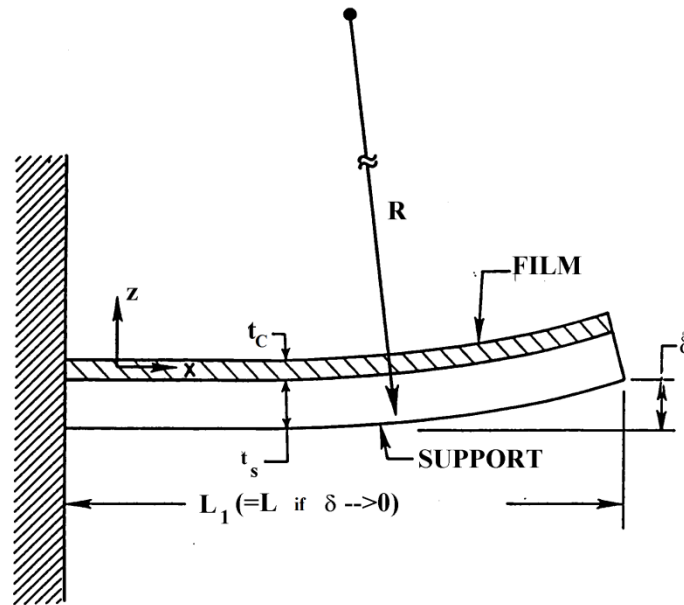


Figure 3.1: Scheme of the model support and polymer

This state of stress (σ) can be calculated from the knowledge of:

- Radius of curvature (r);
- Thickness of polymeric layer (t_c);
- Thickness of substrate layer (t_s);
- Elastic modulus of substrate (E_s);
- Poisson coefficient of substrate (ν_s).

Assuming there is a good adhesion between polymeric film and substrate, and accounting for the fact that the radius of curvature is much bigger than the substrate and film thicknesses and that the beam width is less than half of its length, the average stress state can be expressed as [33] [34]:

$$\sigma = \frac{E_s t_s^2}{(1 - \nu_s) 6 r t_c} \quad (3.1)$$

The radius of curvature can be determined from the bending of the beam (\square), applying the theorem of Pythagoras and considering that at the initial state the cantilever is horizontal ($r = \infty$).

$$r \approx \frac{L^2}{2\delta} \quad (3.2)$$

where L is the length of the beam.

Including (3.2) in (3.1):

$$\sigma = \frac{2\delta E_s t_s^2}{(1 - \nu_s) 6L^2 t_c} \quad (3.3)$$

The term $(1 - \nu_s)$ born from the biaxial tension field and is neglected when the deflection is lower than half of the support thickness. From the equation (3.3), the sensitiveness increases increasing the length of the beam and decreasing its thickness, if the other parameters remain equal.

The stresses in the polymeric coating are due to the ability of the polymer to reach higher or lower length compared to that which would reach the free support.

The stress definition born from the action that the support exerts on the polymeric film to prevent the return to unstressed condition. A tensile stress will produce a concave curvature, while a compressive stress a convex bending.

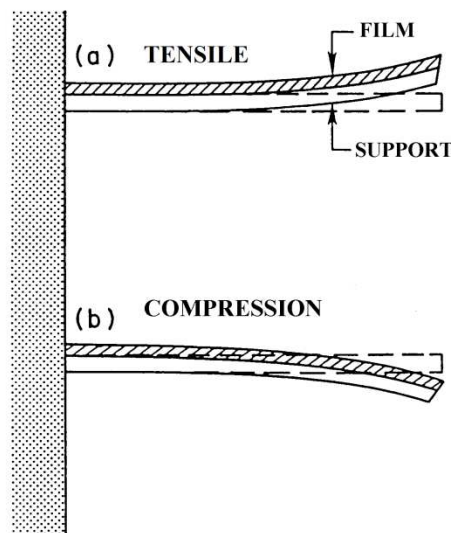


Figure 3.2: Relation between stress and curvature

The solvent evaporation during the preparation of the sample produce a tensile stress with a concave curvature.

The bending beam technique measures the total stress due to:

- thermal contribution;
- equilibrium and mass transport processes.

Both of them might be compressive or tensile.

From the knowledge of the stress state of the beam, the relative variation of volume of the polymeric film between initial (V_0) and final (V_1) as induced by the sorption/desorption phenomena can be determined applying a neo Hookean model. This is non-linear with the

stress, but quadratic and it is based on the elastic modulus of the polymer (E_c).

$$T_{xx} - T_{yy} = G(\alpha_x^2 - \alpha_y^2) = \sigma = \frac{E_c}{3} \left[\left(\frac{V_0}{V_1} \right)^{2/3} - \left(\frac{V_1}{V_0} \right)^{4/3} \right] \quad (3.4)$$

3.3 Materials & Methods

3.3.1 General apparatus description

The experimental apparatus used for the preliminary tests was built during past years at the Memlab laboratory. As shown in Fig. 3.3 the apparatus is composed by:

- Penetrant reservoir
- Pressure transducer
- Sample compartment
- Optical micrometer
- Nitrogen trap
- Vacuum pump

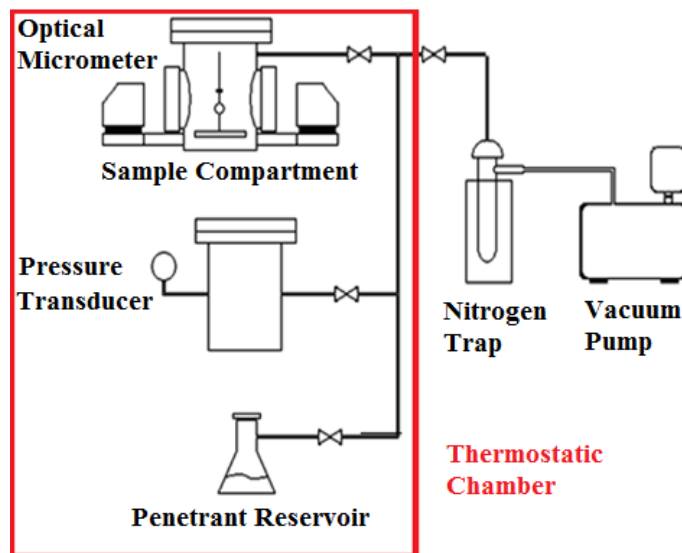


Figure 3.3: Experimental Apparatus

The sample compartment is made in stainless steel and two glass observation port allows the optical micrometer to making the measurement. The glass observation port works up to vacuum conditions and 8 bar, while the temperature depends on the thermostatic chamber range.

Inside the sample compartment the beam coated with the polymer and a reference system are placed and fixed (Fig. 3.4).

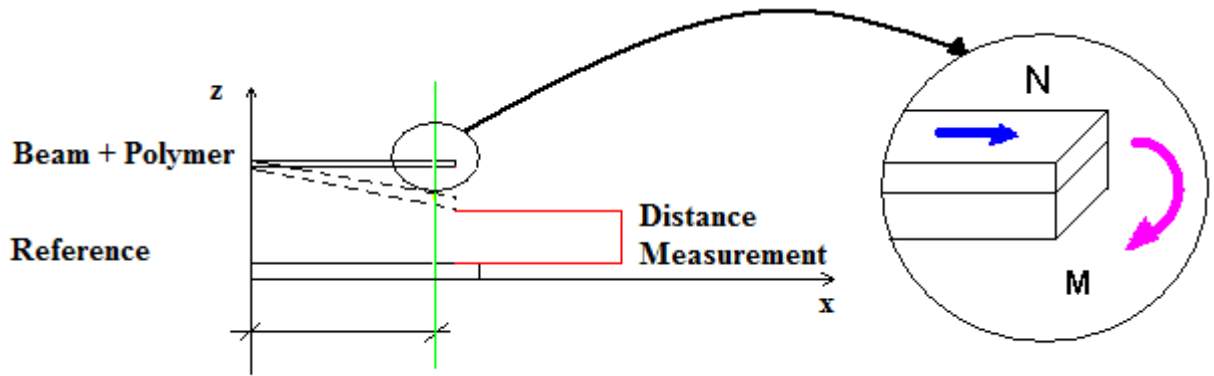


Figure 3.4: Scheme of sample beam and reference system inside the sample compartment

The deflection is measured with a direct observation by an optical micrometer at linear CCD with image sensor CMOS *Keyence model LS-7030-M*, where the characteristics are reported in Tab. 3.1.

Type	Micrometer with image sensor
Measurement range	from 0.3 to 30 mm
Minimum size measured	0.3 mm
Light source	LED green GaN
Accuracy	$\pm 2 \text{ } \mu\text{m}$
Repeatability	$\pm 0.15 \text{ } \mu\text{m}$
Sampling rate	Up to 2400 scan/sec
Operative conditions	Temperature: 0-50 °C, Umidity: 35-85%

Table 3.1: Technical specification of the optical micrometer *Keyence LS-7030M*

The high-intensity GaN green LED radiates light, which will be changed into uniform parallel light through the special diffusion unit and collimator lens and emitted to the target in the measuring range. Then the shadow image of the target will appear on the HL-CCD (high-speed linear CCD) through the telecentric optical system. The output incident signal of the HL-CCD will be processed by the DE (digital edge-detection) processor in the controller and CPU. As a result, the dimensions of the target will be displayed and output.

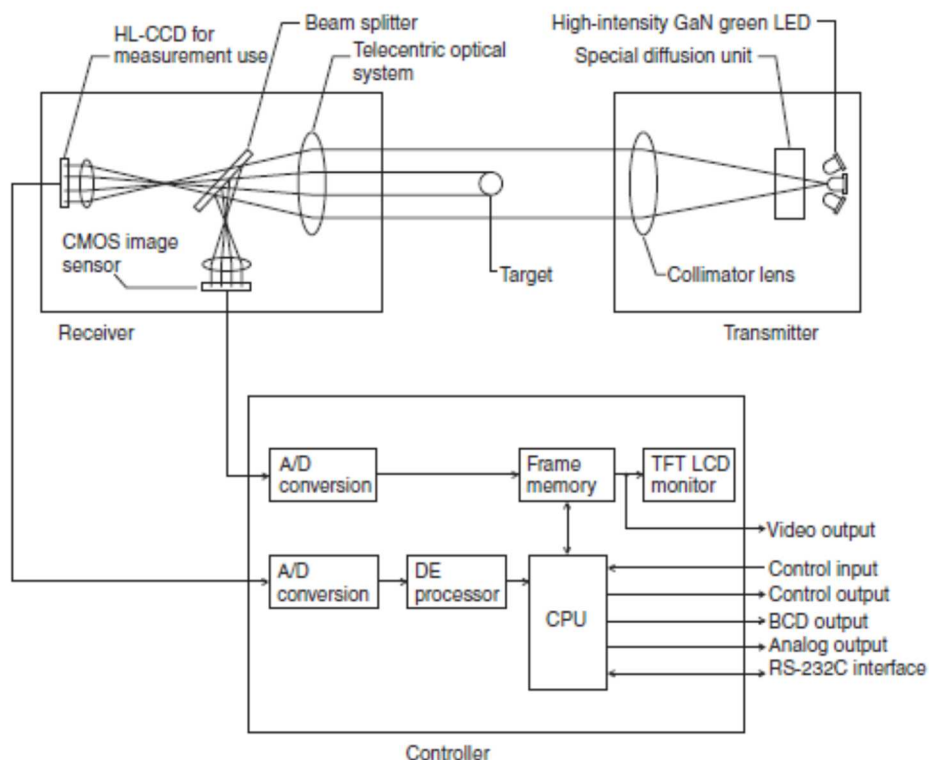


Figure 3.5: Operation diagram of optical the micrometer *Keyence LS-7030M*

The system allows simultaneously two different measurement between pairs of points with higher brightness gradient to a threshold level. In this study the distance between the free end of the beam and the reference system (bending) and the thickness of the reference system were measured. The measured data and the sample image are displayed in a dedicated controller (*Keyence LS7501*). The distances are transferred via RS232 to an electronic elaborator for storing.

To reduce errors due to the placement of the sample inside the sample compartment with respect to the measuring axis, the micrometer is located on a pair of positioners able to move in two directions (*Physik Instrumente*). The first one allows the horizontal alignment between transmitter and receiver with the sample beam, while the vertical one permits to move the ray of light orthogonal to the same sample.

Because the test temperature are lower than the glass transition temperature of the polymer, this is set and controlled by thermostatic chamber made in Plexiglas. The whole instrumentation, accepted the viewer, nitrogen trap and the vacuum pump are placed inside the thermostatic chamber to reduce the fluctuations between night and day.

The solvent in liquid phase is inside a flask and it is evaporated inside a reservoir with a capacity of 12 L up to the desire pressure. The filling is preceded by the evacuation of the entire system and the blanketing which helps to eliminate the air inside the flask. The vacuum system consists in a Edward's pump and in a liquid nitrogen trap and it is used during the evacuation and blanketing of the system.

3.3.2 Material

The experimental tests were carried out using toluene and n-pentane as solute and polystyrene (PS) provided by Versalis as polymer. The experiments were made in a range of temperature (30-45°C) and with a solute content up to 20%.

	Mw [g/mol]	ρ [g/cm ³]	Tg [°C]
PS, Versalis	270000	1,05	103
n-pentane, Aldrich	72,15	0,626	36 (T _b)
Toluene, Aldrich	92,14	0,865	110 (T _b)

Table 3.2: Physical properties of polymer and solvents used

The sample were prepared by solvent casting technique from a solution of toluene (1 wt%) and as supports were used stainless steel and spring steel beams (Table 3.3).

	Thickness[mm]	E[MPa] @ 25°C	PoissonCoefficient	Size (LxW) [mm]
Stainless Steel	0,5	210000	0,3	50x10
Spring Steel	0,5	210000	0,3	50x10
Spring Steel	0,1	210598	0,305	50x0,75

Table 3.3: Mechanical properties of materials used as support

After the deposition, the polymer coating were placed under a vacuum wood at the ambient temperature overnight. After that the samples were thermally treated in a vacuum oven at 120°C for 1h and cooled in a controlled way inside the oven until the ambient temperature is reached. In this way the solvent removal and the deleting of the existing stresses were obtained.

Because the thickness measurement is very important for the in-plane stress calculation and as reported in paragraph 3.3.6 the coating thickness is lower than 5 μ m, it was evaluated using a sensitive balance. From the knowledge of the size and the initial (without coating) and the final (after thermal treatment) weight of the beams, its thickness was evaluated.

The beam length, as the coating thickness, mainly influences the equilibrium values of the beam bending. Making explicit the equation 3.2, the deflection value depends by the beam length considered in the measurement:

$$\delta \approx \frac{L^2}{2r} \quad (3.5)$$

The attention should be paid on the point in which the bending is evaluated experimentally. During the tests the measurement were carried out 2 mm before the free end of the beam to avoid that the deflection causing the output from the measuring line.

3.3.3 Apparatus set-up

The apparatus described in the paragraph 3.1 was used with polyetherurethane (PEUT), polyvinylacetate (PVAc) and polycarbonate (PC) as polymers. The tests were performed at 40°C using acetonitrile (CH₃CN) as solute up to 35% inside the system. With these systems polymer-solvent the configuration illustrated in Fig. 3.3 worked appropriately.

However using PS with toluene or n-pentane the problems identified were related to:

- Sorption of solutes by grease vacuum;
- Leakages inside the sample compartment;
- Weakness in the bending beam.

3.3.3.1 Sorption of solutes by grease vacuum

The sorption of solutes by grease vacuum was solved using the same configuration, but changing the type of sealant. The choice saw the use of a fluorinated grease, less close to the aromatic solvents.

This grease has a high thermal stability (-20 to 250°C), good resistance to aggressive media and is neutral towards plastic materials. Furthermore shows low evaporation under vacuum conditions.

3.3.3.2 Leakages inside the sample compartment

Leakages inside the sample compartment were reduced making some changes to the original configuration (Fig. 3.3).

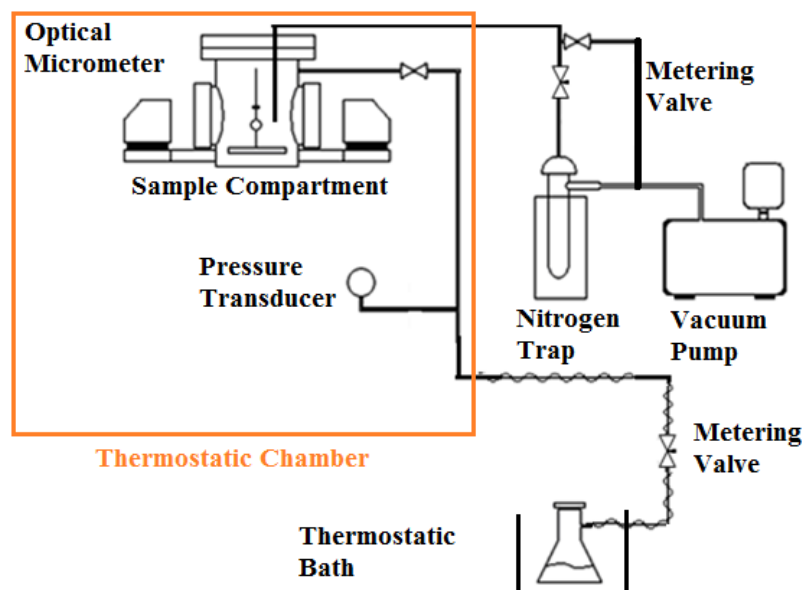


Figure 3.6: Apparatus set-up

To reduce the total volume of the system, the pre-expansion reservoir was removed placing the penetrant reservoir outside the thermostatic chamber in a thermostatic bath. It will be possible to work with a little bit temperature inside the penetrant flask then in the thermostatic to reduce the effect due to the lowering of the temperature in vacuum condition. With this new configuration is also possible to reduce the waiting time to heat the vapor inside the pre-expansion chamber up to the working temperature.

Two metering valves were added upstream and downstream of the sample compartment to work in a dynamic way. However, the time to work in flow depends on the capacity of the nitrogen trap. the maximum quantity of liquid nitrogen inside the dewar allows to work up to 8 hours.

The penetrant reservoir volume was increased because of the need to work in flow from 100 mL to 500-600 mL.

To evaluate the fluctuations in the pressure values during the tests, the pressure transducer was connected via RS232 cable to the PC.

3.3.3.3 Weakness in the bending beam

The experiments to evaluate the coating thickness and the right material as support were done using PS and toluene as solute with characteristics reported in Tab.2. The tests were carried out at 40°C and at 10% of toluene inside the system. The vapor pressure at the operating condition is 8,1 mbar calculated with the Wagner's parameters [47]. The polymer was deposited on the support as reported in paragraph 3.3.2.

Because the diffusion coefficient of toluene at 40°C and 10% of its activity is around $3 \cdot 10^{-12} \text{ cm}^2/\text{s}$ and considering that the coefficient is related to the thickness by the time lag method [48]. Considering the diffusion coefficient constant:

$$\tau = \frac{l^2}{6D} \quad (3.6)$$

Where τ is the time lag, D the diffusion coefficient of solute in the polymer and l is the coating thickness.

Imposing to the equation (3.6) the thickness (l) equal to 1 μm , the time lag results close to some minutes. Working with 1-2 μm of polymer coated on the beam allows to perform the experiments in a short time because the characteristic time for the diffusion is low, less than 1 hours.

As explained in the chapter 3.1, the choice of the more suitable material as support can be made *a priori* only from the knowledge of the mechanical properties.

Starting from a support made in stainless steel (50x10x0,5 mm) available in the Memlab laboratory the first tests were performed.

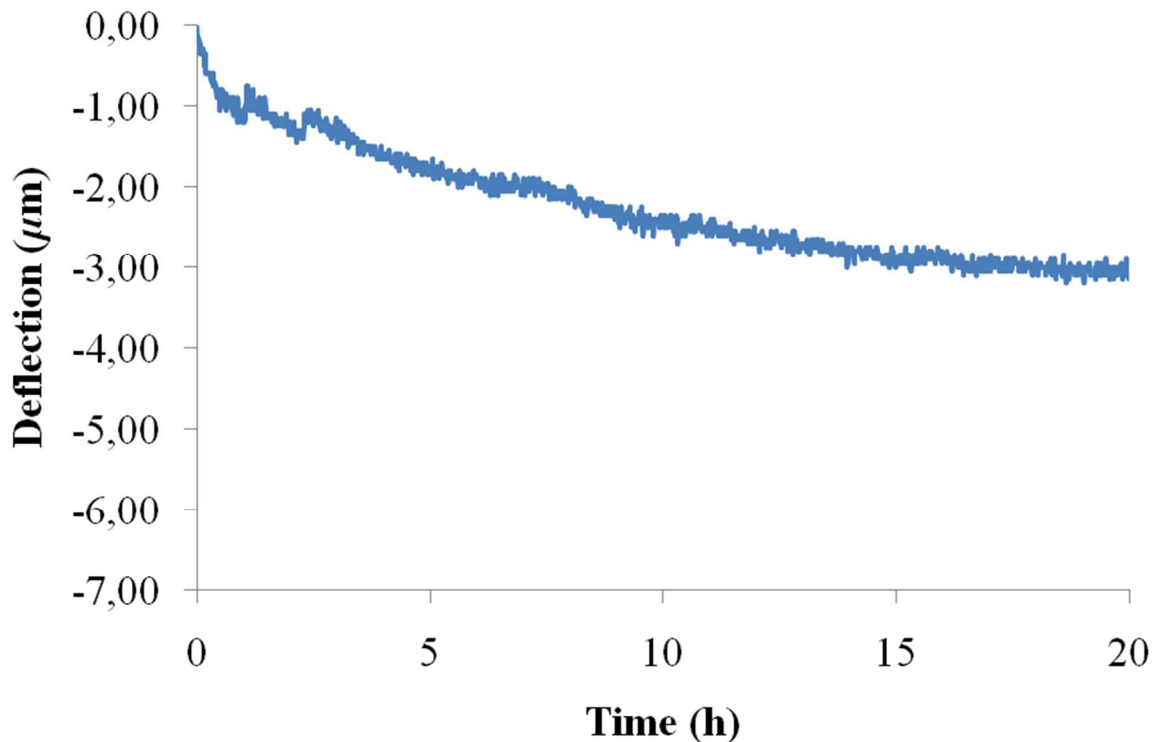


Figure 3.7: Deflection of stainless steel support coated with 5 μm polymer film

As shown in Fig.3.7, the stainless steel support available in the laboratory is not suitable because already using 5 μm of polymer thickness the deflection signal is close to the accuracy reported in Tab. 3.1. These support were rejected because the signal for 1 μm of PS would result less than 1 μm .

Subsequently two other supports made in spring steel and with different thickness 0,5 and 0,1 mm with the dimensions reported in Tab. 3.3 were tried.

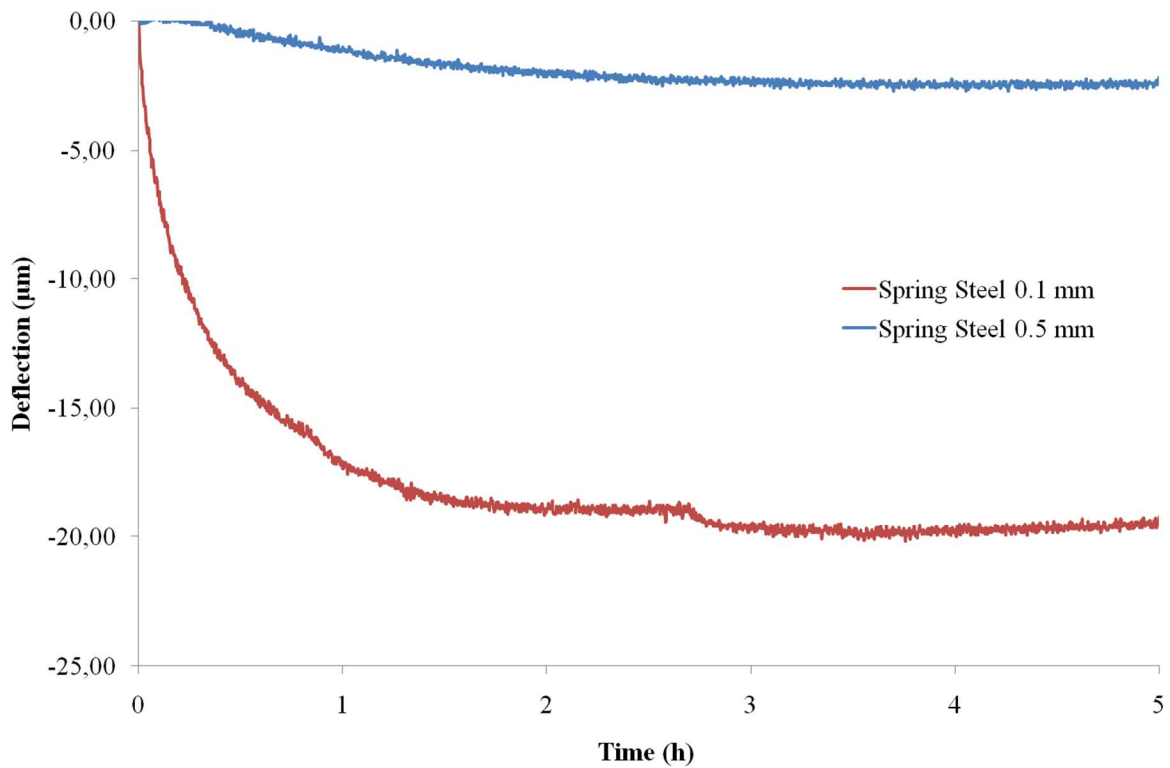


Figure 3.8: Deflection of spring steel support coated with 1 µm polymer film at different support thickness

The passage from 0,5 to 0,1 mm as support thickness improve considerably the bending signal. As a result of these consideration the further experiments were conducted with spring steel support (50x7,5x0,1 mm).

The elastic modulus for this type of material was calculated using three points bending technique made with a rheometer in a range of temperature. The technique is illustrated in Fig. 3.9 [49]:

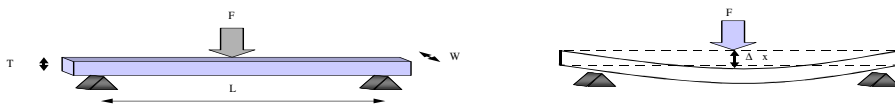


Figure 3.9: Geometry in a three points bending technique

The sample, prepared in the form of rectangular beam characterize by known thickness T and length W , it is placed between two “knives”, seat at distance L from each other. If the

instrument works in a control of deformation, the beam will be subject to a linear deflection λx implemented by a motor, that through a knife vertically flexes the beam in a sinusoidal manner with the frequency. The output signal will be the force F and because stress and tensile deformations are needed, forces and linear deflections have to be transformed thanks to correlations.

The situation in case of three points bending is complicated because the lower face of the beam is in tensile conditions while the upper one is compressed. Even in this case the ratio between stress and deformation is proportional with the ratio between force and linear deflection by a geometric shape factor K :

$$\frac{\tau}{\varepsilon} = K \frac{F}{\Delta x} \quad (3.7)$$

For three point bending the eq. (3.7) becomes [49]:

$$K = \frac{4WT^3}{L^3} \quad (3.8)$$

In order to exploit to the maximum the instrument, the geometric factor K has a fundamental rule. Every rheometer can performed deformations (linear or angular) and measure force or torques within the specifications for which is designed. In flexural geometry (Fig. 3.9), the force measurement can take place in a specific range because below the transducer is not able to provide the required load and above the sensitiveness is close to the background noises. In an analogous way the displacement feasible in a fixed range too. Gives a shift range, fixed for a rheometer based on the specimen size, too small movements compared to this scale are not actionable.

Therefore the working range limit depends on the elastic modulus values for a fixed geometry. The geometry factor is helpful not to exceed the instrument range.

Figure 3.10 shows a typical graphic for the operative range able to describe the situation reported in Fig. 3.9. On the abscissa appears the complex Young's modulus E^* :

$$|E^*| = \sqrt{E'^2 + E''^2} \quad (3.9)$$

while in ordinate the specimen thickness, the only variable modifiable in the eq. (3.8).

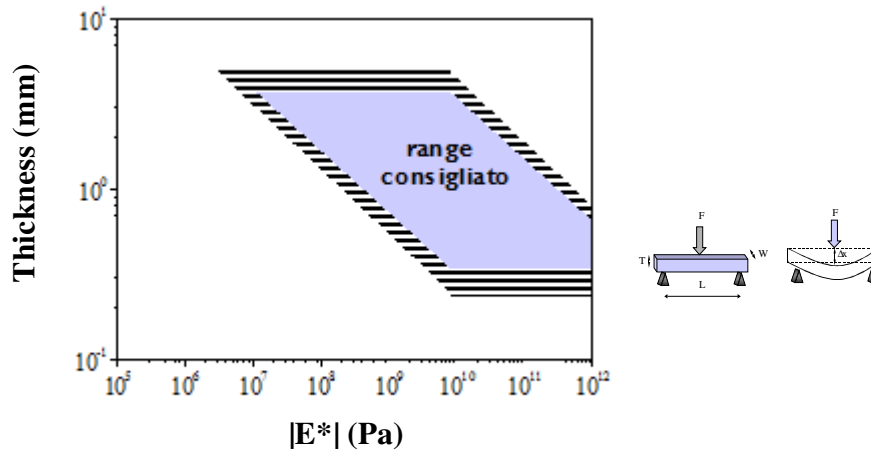


Figure 3.10: Working range in a three point bending geometry

Increasing the beam thickness it will be possible to measure lower Young's modulus values. When the elastic modulus is too small, the force is small too and is the deflection Δx is equal, the force values will be higher in relation to the specimen thickness. The right region of the graph is limited by the maximum values of force that the instrument is able to perform. If the elastic modulus is too high, even if the applied force is maximum, deformations will be small and confused with the background noise. A smaller thickness in this case will help, with equal force, to generate higher bending.

The experiments to evaluate the Young's modulus of the metallic beam were carried out with a temperature sweep tests. Deformation amplitude and angular frequency are maintained constant while temperature is changing according to a programmed ramp. The heating rate must not be too high because the sample has to warm up properly.

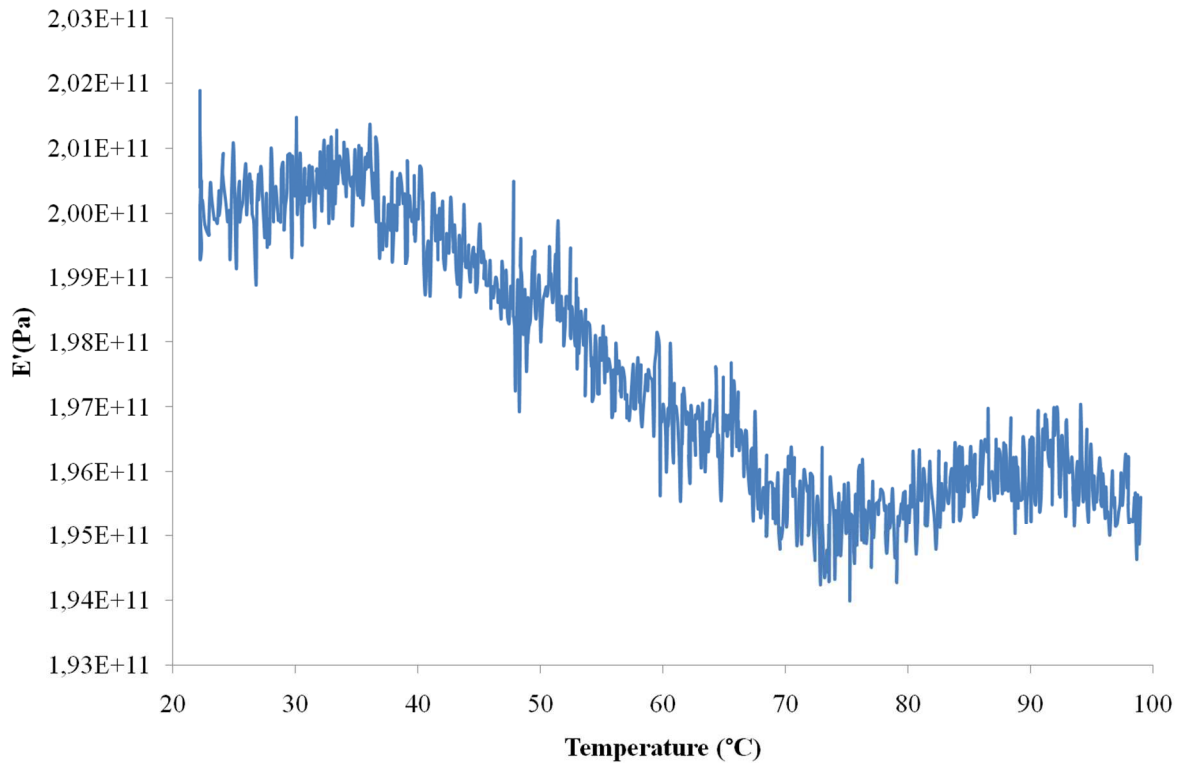


Figure 3.11: Young's modulus VS temperature in case of spring steel beams

The temperature range investigated was between the ambient temperature and 100°C. The elastic modulus is more or less constant in a interval between ambient temperature and 40°C and after 75°C to the end of the temperature inquired.

3.3.4 Equation of state calculation for analysis of bending beam data

The processing of the data obtained from the direct observation of the bending of the coated beam describe in the next chapter was conducted by the help of excel sheet built with the aim of obtain stress and volume change information.

The excel sheet was developed ad hoc in this work using the equation reported in the following chapter. The input data are:

- Beam deflection;
- Elastic modulus;
- Poisson coefficient;
- Beam size;
- Coating thickness

while the output value is the stress during the observation time.

Another excel sheet was developed to determine the volume change after different amount of solvent in the system. Even in this case the equations used are reported in the next chapter.

The stress state obtained from the previous analysis will be the input with initial volume and elastic modulus of the polymer.

The modeling of this problem was done to pass from volume to mass data. In particular to obtain mass uptake values comparable with the mass uptake data obtained from a direct measurement by the QCM. The tool able to do that is a excel sheet developed in the past from the Memlab team. The sheet can be used with a large number of equation of state but in this work only the PC-SAFT and Sanchez and Lacombe were used to describe the equilibria while the NELF was used to describe the non equilibrium part. Specifically these equations are contained inside excel library.

The first step in the use of this excel file is to determine with the help of the selected equation of state the parameter required. In particular in input information is related to the PVT data of pure solvent because the parameter are derived from the fitting with them. The same procedure is followed for the polymer.

Once the equation of state parameters are known, the binary interaction parameter has to be evaluated. In particular the input data will be the solubility ones obtained experimentally or from the literature in the equilibrium conditions. The excel file will be capable to fitted the equilibrium data changing only the binary interaction parameter.

At this point known the binary interaction parameter and the swelling coefficient obtained from the volume change data acquired experimentally, mass uptake values will be determinate in the non-equilibrium region by the NELF.

3.3.5 Quartz Crystal Microbalance

Parallel to measurement taken at the bending beam cantilever apparatus, phase equilibrium behavior in the same polymer-solvent systems was investigated by means of an apparatus based on a quartz crystal microbalance (QCM); this experimental apparatus was properly designed and assembled in the DICAM laboratory for low-pressure vapor sorption experiments. The QCM microbalance is a compact and versatile device, and one of the most sensitive mass detector available. The technique is based on variation of resonant frequency of crystals to external condition; in a QCM configuration, a quartz crystal resonant frequency is measured as a function of a mass placed on it. An 8 MHz quartz disk placed between gold electrodes was coated on one face by spin coating and the analysis is indeed performed on supported polymer film, just as for the case of bending beam apparatus. The selected crystal package is one of the most common used on microbalance, and allows to obtain suitable samples for sorption measurements.

By a properly made system, crystal was placed in a closed volume immersed in a water bath, whose temperature was set by a heated and refrigerated circulating bath (Thermo Fisher scientific) and measured by an internal thermocouple (sensitivity 0.1°C). Before each test, the system was evacuated by air and samples dried by a two-step rotary vane vacuum pump

(Edwards vacuum), following standard procedures. The penetrant was stored in a reservoir as a liquid, and entered in the measuring system by vapor expansion through a manual valve. Both vacuum and vapor pressure were measured by a pressure gauge (Edwards Barocell, range 0-100 mbar)

An oscillating circuit (ElbaTech S.r.l., Marciana, LI, Italy) was used to power a crystal inserted in a well-controlled environment. The oscillating signal was compared with a reference by the circuit, and resulting wave sent to a computer input. The resonant frequency value was measured by an internally-clocked high-precision PCI 6601 from National Instrument, and values acquired over time by a supplied software. Due to the circuitry characteristics, the sensitivity of the system is 0.1 Hz, and the reproducibility about 5Hz. A complete scheme of the sorption system is reported in Figure 1.

To have a good conversion of the frequency signal into mass values several operations were needed before starting a sorption test. New quartz crystals were first cleaned by 5 minutes sonication immersed in HPLC grade toluene (5 minutes, 25 MHz ultrasonication water bath), then measured into the experimental system for resonant frequency at experimental conditions desired. The same crystal was then spin coated; a 2% wt. toluene solution was used at ambient conditions, and the rotational speed was finely set to obtain the desired sample thickness, as explained below. Then the sample was treated for aging normalization (120°C for 30 min and slow cooling, high vacuum). Finally, the coated sample was loaded in the QCM system and the frequency measured at high vacuum conditions.

An absolute resonant frequency decrease were obtained after depositing cycles, attributable to the PS dry mass deposited on top of the crystal face. To evaluate the sample mass, the Sauerbrey equation was applied to the frequency difference:

$$\Delta m = -\frac{A\sqrt{\rho_q\mu_q}}{2f_0^2}\Delta f \quad (3.10)$$

The equation describe a linear decrease of frequency due to a mass gain on crystal surface; A is the crystal surface area, ρ_q is the crystal density 2.648 g/cm³, μ_q is the quartz shear modulus for the selected package (2.947×10¹¹ g/(cm s²)) and f_0 the absolute resonant frequency. The reported equation was developed for well distributed thin (rigid) system oscillating in air; however viscosity difference are usually accounted just for liquid environment, and the relative upper mass limit described from the author as $\Delta f/f_0 \leq 2\%$ frequency decrease was not exceeded in any case.

The film thickness was evaluated as the theoretical volume (density from technical datasheet, 1.05 g/cm³ at 25°C), supposed homogeneous on the crystal surface. This value was confirmed as average thickness by diffusion coefficient evaluation from literature, as a function of toluene pressure [49]. The thickness value has a crucial effect on good sorption determination, as described for volumetric tests. This was chosen far above the limit thickness value for bulk behavior, as a function of polymer type and properties, but sufficiently low to have a relatively short diffusion time to avoid concentration gradient over thickness, and to well

distinguish the Fickian diffusive zone and the relaxation zone respectively. Tested samples had an averaged thickness between 400 and 550 nm.

Fig. 3.12 shows a schematic design of QCM.

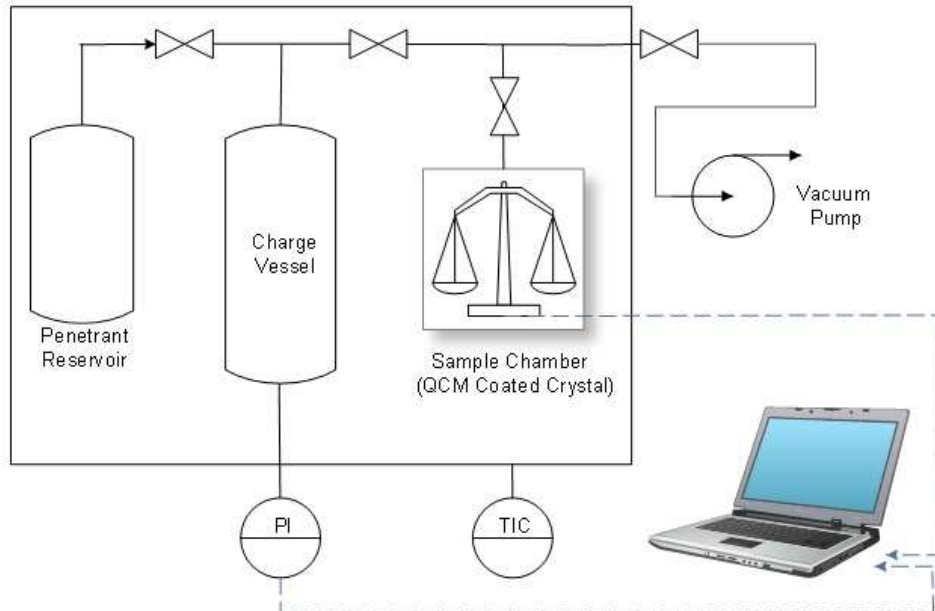


Figure 3.12: QCM apparatus

3.5 Experimental Test

3.5.1 Polymer thickness VS Bending signal

The bending signal was tested working with different thickness of PS on the spring steel support. Two different thickness, 1 and 3 μm , were compared.

The Fig. 3.13 shows the results obtained and the deflection seems to be linear with the polymer amount. For both curves the first part (0-50 $\text{s}^{1/2}$) is super imposable, confirming that the diffusion coefficient is equal but the characteristic time of diffusion is different as explained in the equation (3.6).

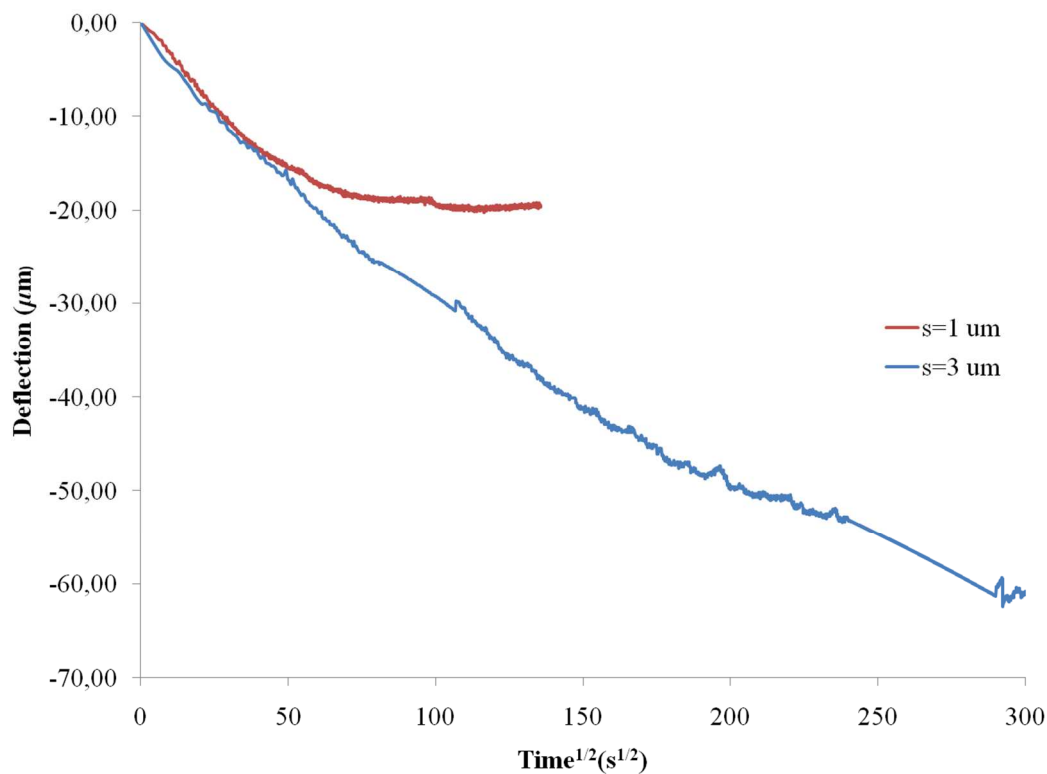


Figure 3.13: Deflection of spring steel support coated with different thickness of polymer

3.5.2 Static VS Dynamic configuration

Remember that at this part of the study the dynamic configuration can operate as such in a manner dependent on the capacity of the dewar containing liquid nitrogen, static and dynamic configuration were compared. The experiments were carried out at 10% of toluene inside the system, at 40°C and using supports coated with 1 μm of polystyrene.

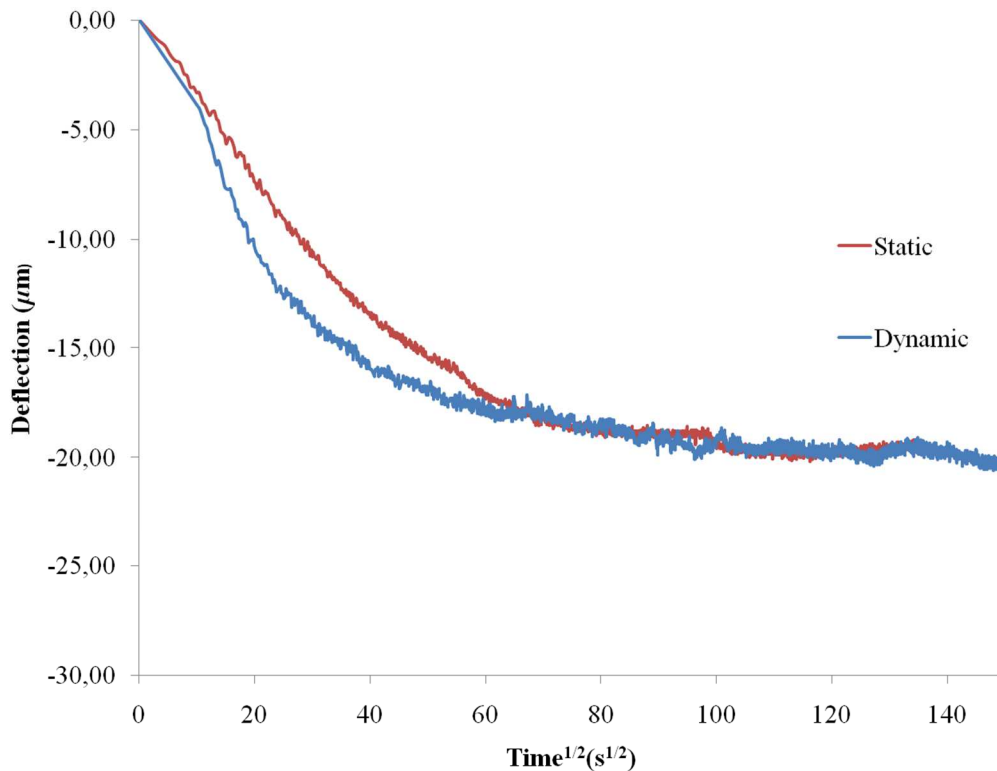


Figure 3.14: Deflection of spring steel support coated with 17μm polymer film working in a static or dynamic way

Figure 3.14 shows what happens working uploading the sample compartment at the right activity of penetrant (static) or uploading the system continuously (dynamic). In the static way the limit is the leakage and then the entry of air inside the compartment. In the second case the limit is the liquid nitrogen capacity.

In a limited range of time, 6 hours, the effect due to the incoming air is not so evident.

The difference visible in the first moments (0-40 s^{1/2}) are due to the time necessary to reach the operative activity in the system, but from the Fig. 6 both experiments have the same characteristic time of diffusion. Furthermore it is end in the same time and with the same values in both cases.

3.5.3 Experiments in flow

A set of experiments were performed increasing the fugacity of the system in two steps: from 0 to 10% and from 10% to 15%. the activity was increased every 20 h circa.

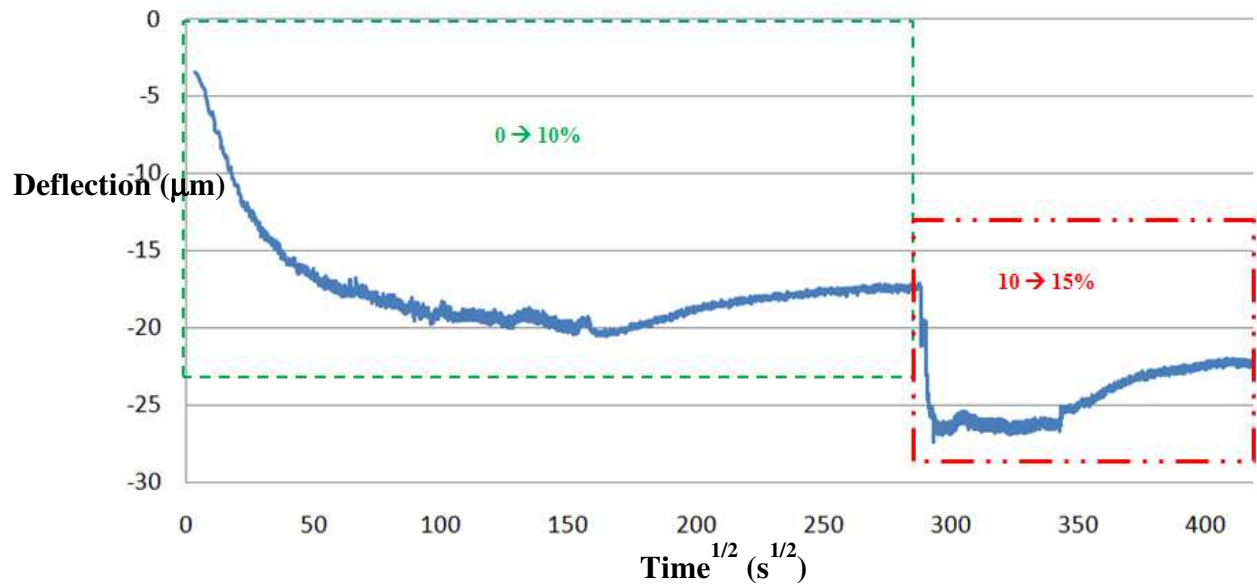


Figure 3.15: Deflection of spring steel support coated with 1 μ m polymer film increasing the activity inside the system

The tests were carried out working in dynamic way during the day and in a static way during the night because the dewar capacity is limited. During the static conditions the pressure increases because the air enter in the system and the deflection reached higher values (less negative). This effect could be related to the relaxation phenomena or to the change in the operative condition (fugacity).

To explained it, the vacuum pump output was connected by a flexible pipe to the vacuum wood. In this way the dynamic test duration in not dependent on the amount of liquid nitrogen used.

From this moment forward the experiments were performed in flow for the entire test time.

Subsequent test were obtained working with n-pentane and toluene as penetrants and increasing the fugacity of the system with steps of 5% every 24 hours up to 20%.

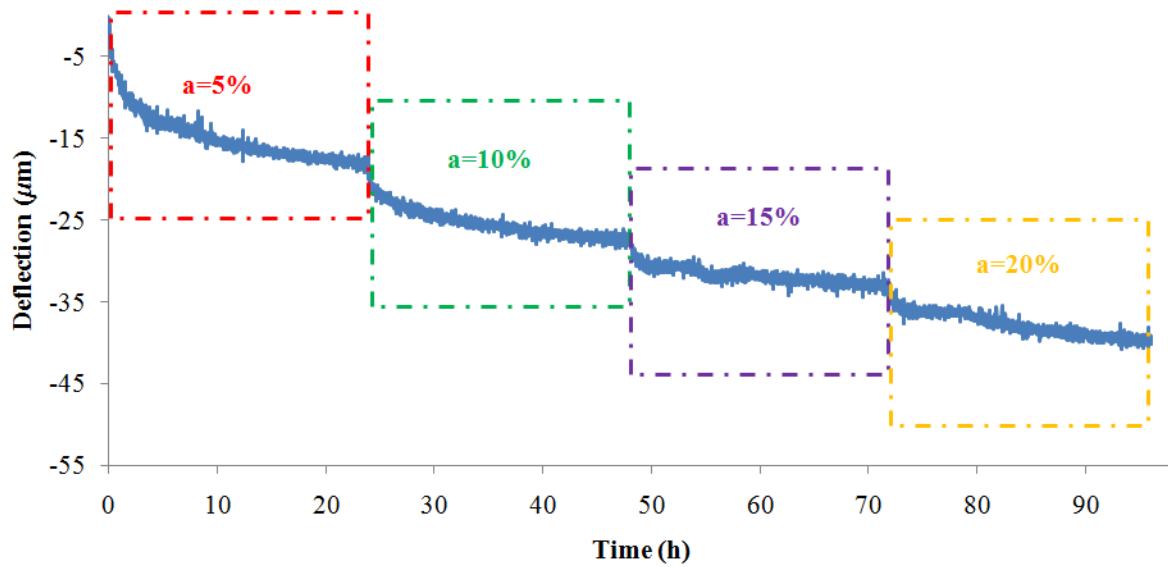


Figure 3.16: Deflection of spring steel support coated with 17-nm polymer film increasing of 5% every 24 h the fugacity

Figure 3.16 shows what happen for n-pentane, but in case of toluene the situation is similar, increasing the activity at fixed time working totally in flow. The behavior observed in Fig. 3.15 where the deflection increased, here it is not present. So the cause was attributable to the activity change due to the incoming air.

3.6 Data Analysis

The results of stress and volume change in time for the polymeric coating were obtained imposing sequences of increasing concentration steps of n-pentane in the system. In particular the fugacity of the system was incremented with steps of 5% every 24 h up to 20% as maximum fugacity. Examples of results that can be obtained from this kind of tests is offered in subsequent figures. Within the relatively small temperature range the thermostatic chamber allows to explore, the differences in terms of volume change are clear, although not so easy to express in quantitative terms. Data for volume change estimated this way can be used to calculate polymer density as function of solute fugacity and from the latter information, through the use of NELF model [28] [50] [51], the mass of solute absorbed or released in the system can be ultimately evaluated at all steps examined in the procedure. This specific analysis is now in order and it will be performed in the follow up of this work, together with the comparison with mass uptake results which can be obtained by means of more specific techniques.

3.6.1 n-pentane

The experiments were carried out increasing the amount of n-pentane inside the system of 5% every 24 h up to 20%. The temperatures investigated were 30-35-40-45°C and the results in terms of in-plane stress measured are illustrated in Fig. 3.17.

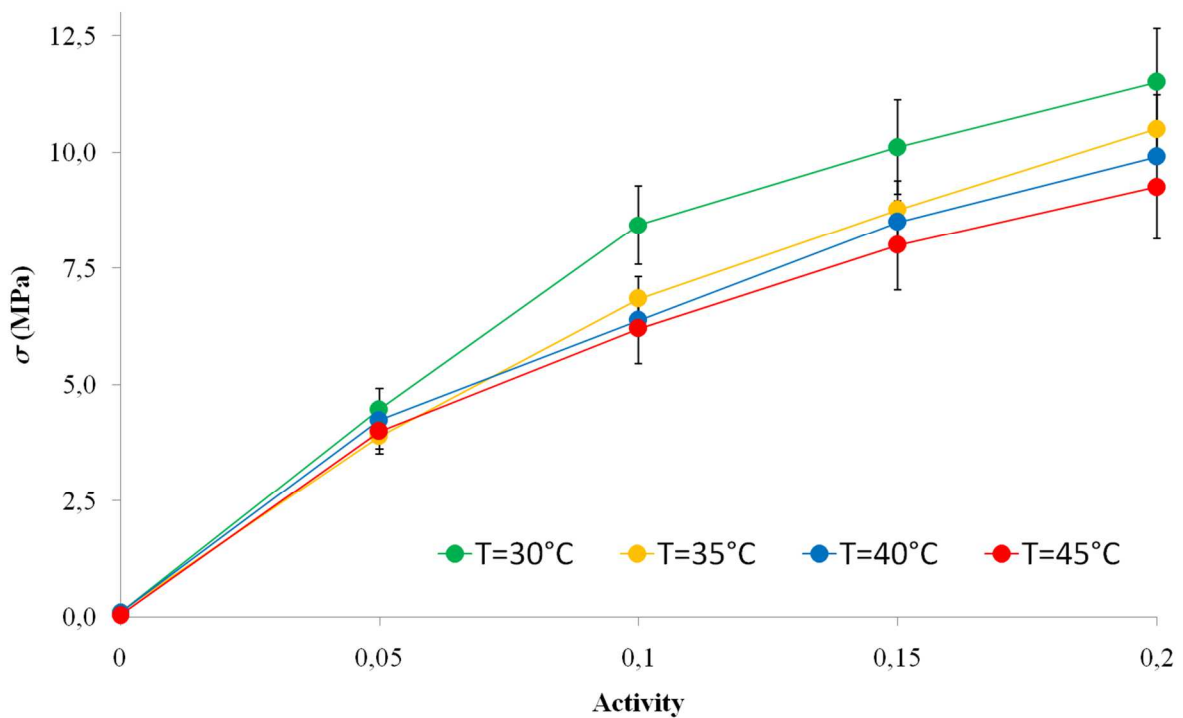


Figure 3.17: in-plane stress state VS penetrant activity

Even if the temperatures investigated were not so distant each other differences in terms of in-plane stress results were obtained. Its trend increasing the amount of n-pentane in the sample compartment seems to be similar varying the temperatures.

Applying the eq. 3.4, once the in-plane stress is known, the change in volume is achieved. The figure 3.18 shows the change in volume at different fugacity of m-pentane in the system.

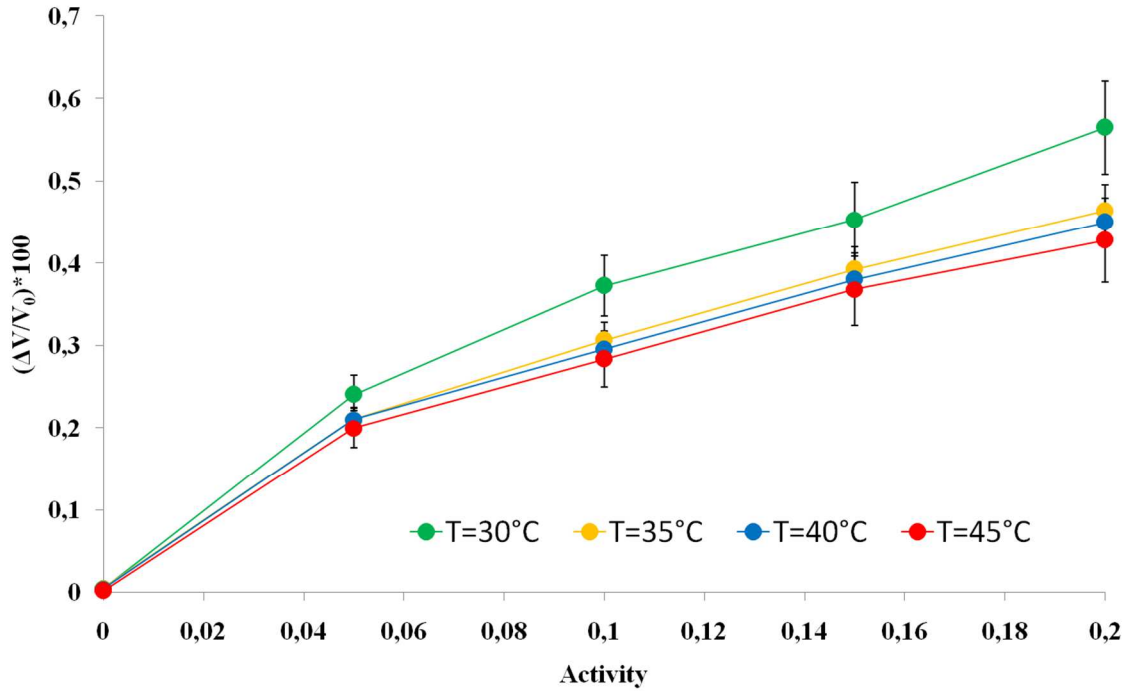


Figure 3.18: Volume change VS penetrant activity

From the change in volume results and applying the NELF model described in the chapter 2, the mass uptake of penetrant in the polymer is evaluated.

To evaluate the binary interaction parameter k_{ij} between the PS and the penetrant, equilibrium data obtained with a magnetic suspension balance [52] and with a quartz helical spring [53] were used. The equation of state used to its evaluation were Sanchez and Lacombe and PC-SAFT.

Swelling coefficient was evaluated at all temperatures investigated from the volume change data. It was evaluated for all temperatures at different activity and then for each temperature an average swelling coefficient was obtained.

$$k_{swelling} = \frac{\frac{V_i - V_{i-1}}{V_0}}{p_i - p_{i-1}} \quad (3.10)$$

Temperature [°C]	K_{swelling}
30	0.358
35	0,302
40	0,256
45	0.206

Table 3.4: Swelling coefficient evaluate experimentally applying eq. 3.10

Figures 3.19 and 3.20 shows the equilibrium (dashed line) and non equilibrium (continuous line) regions using PC-SAFT EoS (3.19) or Sanchez and Lacombe (3.20) to predict these trends.

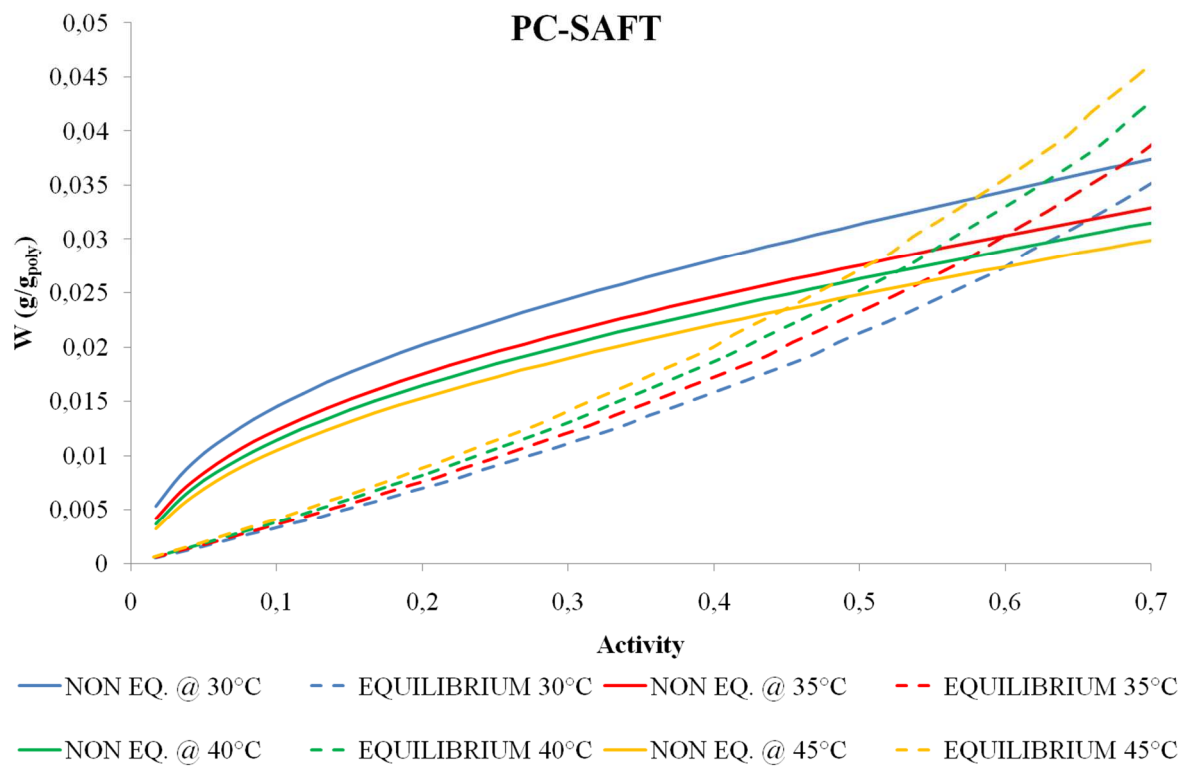


Figure 3.19: Mass uptake prediction using PC-SAFT EoS and NELF model

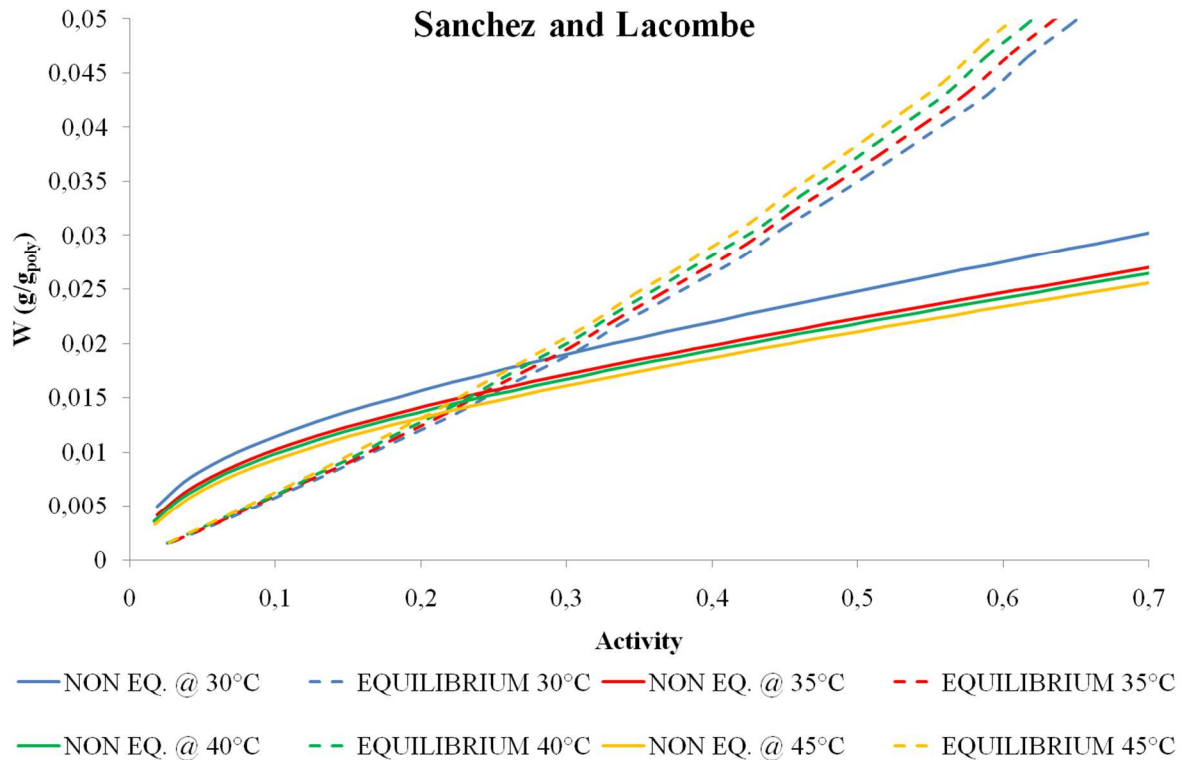


Figure 3.20: Mass uptake prediction using SL EoS and NELF model

In both cases in the non-equilibrium area increasing the temperature the mass uptake of n-pentane decreases in a most obvious way for the PC-SAFT predictions, while in the equilibrium area the situation is opposite: increasing the temperature the mass uptake increases.

Using different equation of state the slope at non-equilibrium seems to be the same, but at the equilibrium the mass uptake of penetrant reach higher values fixed the activity of the system.

3.6.2 Toluene

The experiments were carried out increasing the amount of n-pentane inside the system of 2,2 and 5% every 24 h up to 20%. The temperature investigated was 30°C and the results in terms of in-plane stress measured are illustrated in Fig. 3.21.

Only one temperature was selected because for this penetrant some data at 30°C and different rate were available and obtained with a direct mass uptake measurement with a QCM apparatus described in paragraph 3.3.4. These datas were achieved by Davide Pierleoni during his PhD activity.

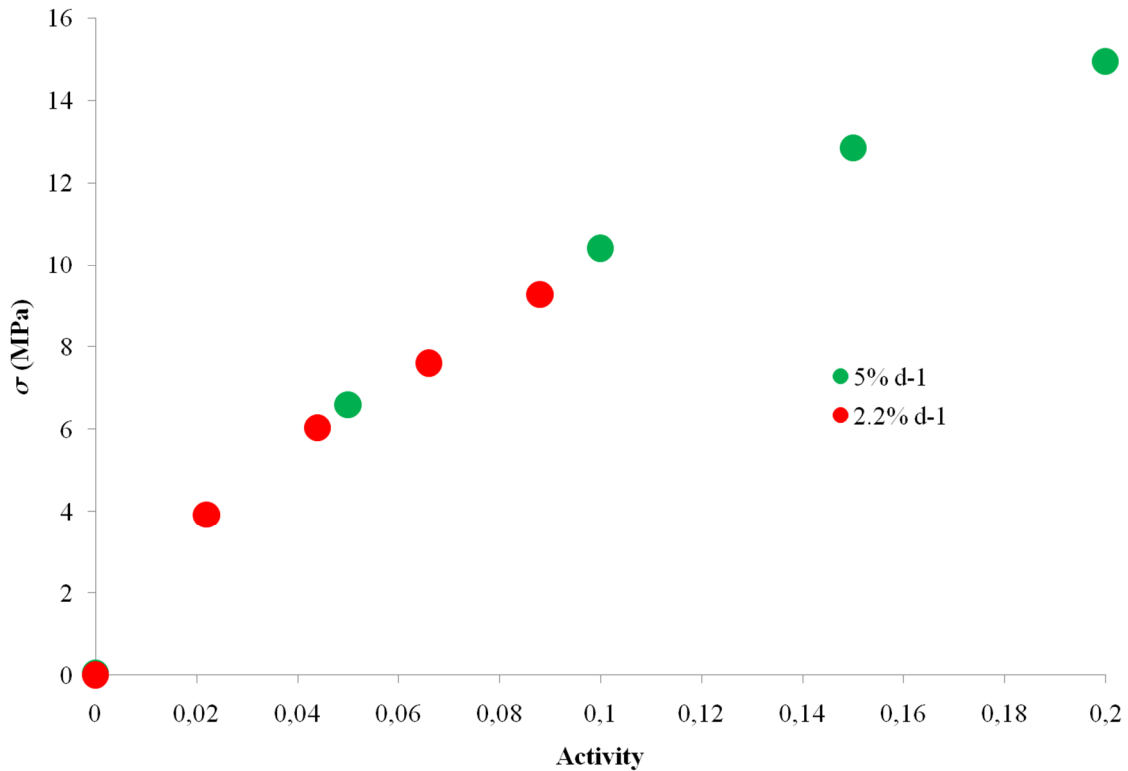


Figure 3.21: in-plane stress state VS penetrant activity

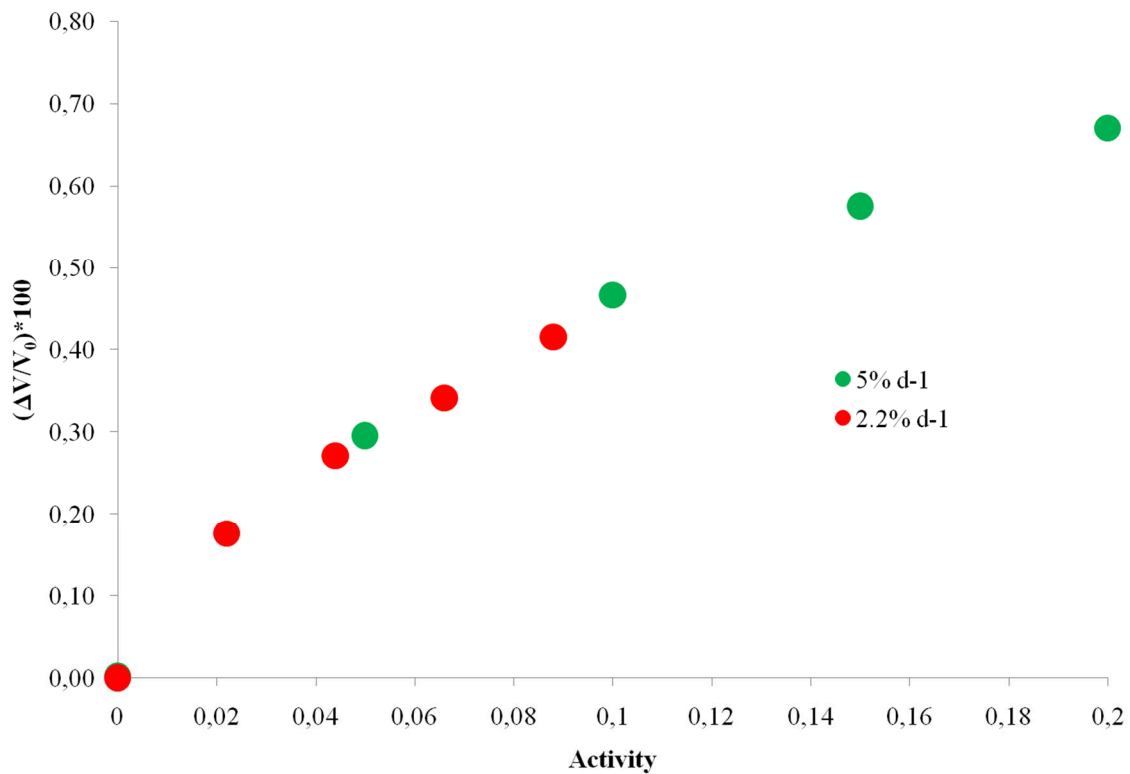


Figure 3.22: Volume change VS penetrant activity

Figures 3.21 and 3.22 displays the in-plane stress and volume change versus the activity of toluene in the system at different speed rate of solvent increment. Changing the speed, the in plane stress e consequently volume change not appear to mutate their slope.

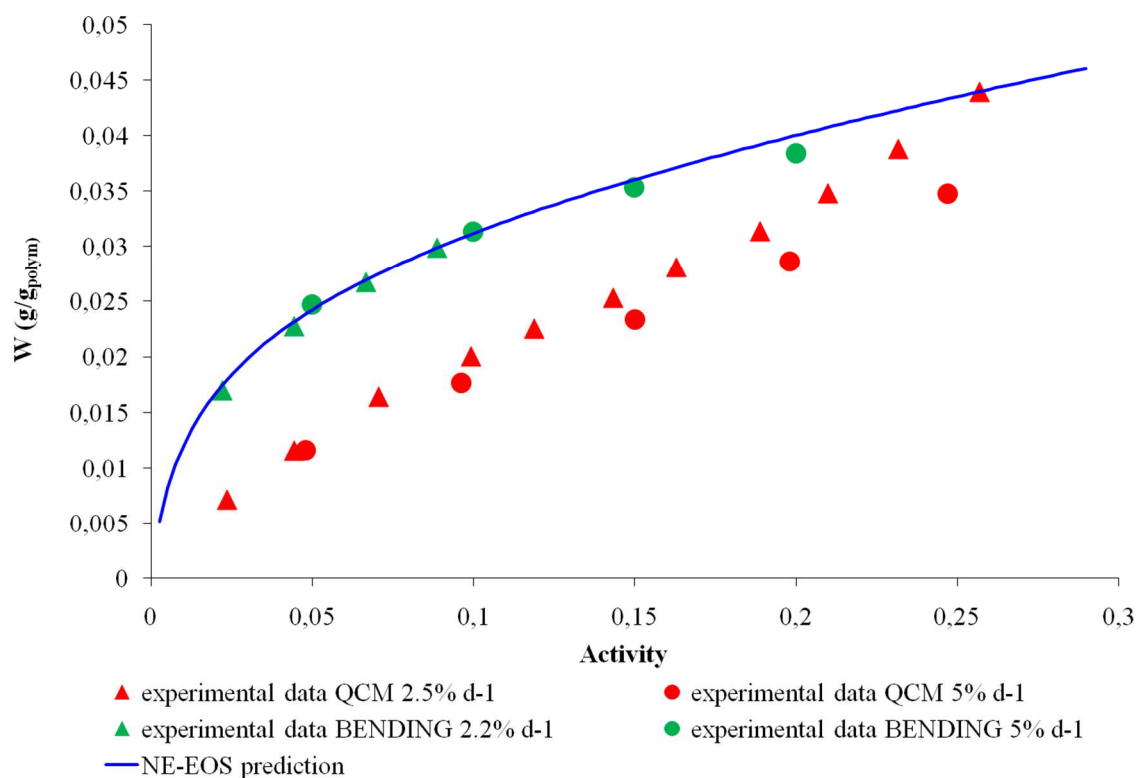


Figure 3.23: QCM VS BENDING

Figure 3.23 shows the comparison between directly mass uptake data obtained from QCM and predicted data obtained from in-plane stress measurement applying PC-SAFT and NELF model.

From the results acquired with the QCM the slope changes with the speed rate. Figure 3.24 described better what happen at different speed rate.

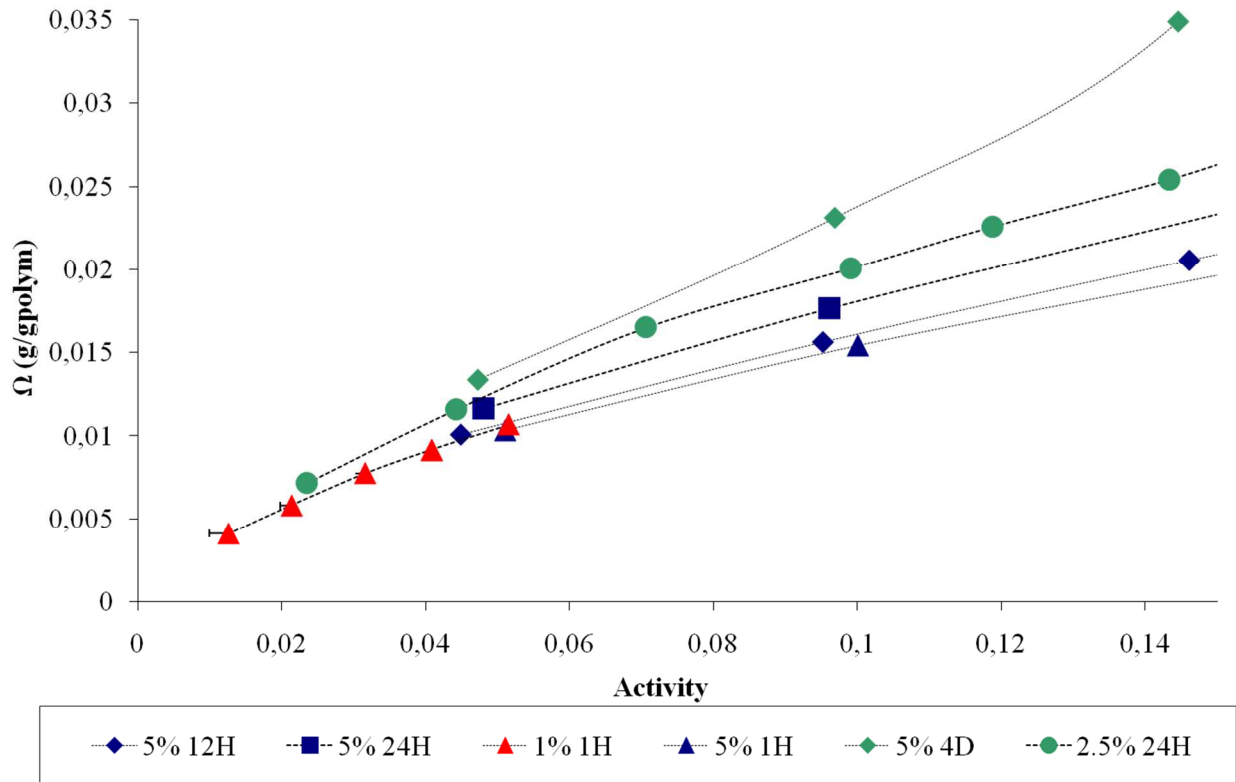


Figure 3.24: Mass uptake VS toluene activity at different speed rate obtained from QCM

Differenced attributable to the change in speed rate are not evident in the results obtained from in-plane stress measurement, where the stress state seems to be uninfluenced from this.

3.7 Conclusions

The results of stress and volume change in time for the polymeric coating were obtained imposing sequences of increasing concentration steps of n-pentane and toluene in the system. In particular the fugacity of the system was incremented with steps of 5% every 24 h up to 20% as maximum fugacity in case of n-pentane, while with steps of 2,2 and 5% every 24 h in case of toluene. The experiments were carried out at 4 different temperature: 30, 35, 40 and 45°C for n-pentane and at a single temperature (30°C) for toluene. Within the relatively small temperature range the thermostatic chamber allow to explore, the differences in terms of volume change are clear, although not so easy to express in quantitative terms.

Data for volume change estimated this way can be used to calculate polymer density as function of solute fugacity and from the latter information, through the use of NELF model, the mass of solute absorbed or released in the system can be ultimately evaluated at all steps examined in the procedure. This specific analysis was compared with mass uptake results which can be obtained by means of more specific techniques (QCM) for toluene, while for n-pentane it is still under observation.

Concerning the comparison between toluene results, in-plane stress measurements with this procedure have shown that the stress and so the volume changes not modified changing steps of fugacity increment, while results obtained with QCM have displayed that increasing the speed rate volume change decreases. Discrepancy between mass uptake calculated after bending beam data or measured through QCM apparatus suggests a revision of the procedure used to estimate the volume change from stress measurements in bending beam experiments. Indeed, a rather simple relation for elastic stress-strain relation have been used in this case for the polymer-solute system and implemented with parameter taken from pure polymer rheological measurements.

On the other hand, it has been proved in this work that measurement from QCM and bending beam apparatuses can provide distinct information about thermodynamic and stress state in glassy system which experience relaxation phenomena induced by vapor sorption. The procedures set up in this work will be used in future works for an extensive analysis of relaxation of both stress relaxation and thermodynamic properties in polymer-solute glassy systems, in the attempt to establish constitutive relations for mechanical, volumetric and sorption properties in non-equilibrium states below the glass transition temperature.

Chapter 4

ORGANIC SOLVENT NANOFILTRATION

Organic Solvent Nanofiltration (OSN) is a membrane separation process which received considerable attention in recent years, aimed at the recovery/purification of organic streams by rejection of relatively high molecular weight component. The availability of new membranes characterized by very high permeability to solvent components and high selectivity to solutes very much contributed to the interest grown around OSN. Together with high solvent flux, OSN membrane must guarantee resistance to solvent components and the two features can be combined, e.g., by properly tuning the degree of crosslinking in a polymeric material characterized by good affinity to solvent species in the feed. The above characteristics make OSN membrane a very interesting subject in this work and to the analysis of the effect of network elasticity on mass transport properties in OSN membrane is devoted this section of the report.

To describe the flux or the rejection through OSN membranes, the transport mechanism of solvents or solutes has to be understood. The models proposed until now, based on:

- Solution-diffusion;
- Pore flow;
- Solution-diffusion with imperfections

differ in the mechanical description of the permeation, that is the driving force for this type of transport and in the number of parameters that have to be fitted or obtained from independent measurement [54].

The work was specifically aimed at characterizing and representing the complex trend of rejection exhibited by OSN membranes, which is still under discussion.

The aim of this chapter is to characterize in terms of performance two different commercial PDMS-based membranes and on the experimental results develop a model based on a thermodynamic and mechanical approach able to describe the flux and the rejection.

4.1 Definition

Organic solvent nanofiltration (OSN) is a membrane pressure driven process, where a feed stream at 30-50 bars and containing molecules (cut-off 200-1000 Da) and organic solvents are split in two different streams. The permeate is at 1 bar and contains molecules able to pass through the membrane, while the retentate is at the same pressure of the feed and contains the molecules that are not able to pass through it.

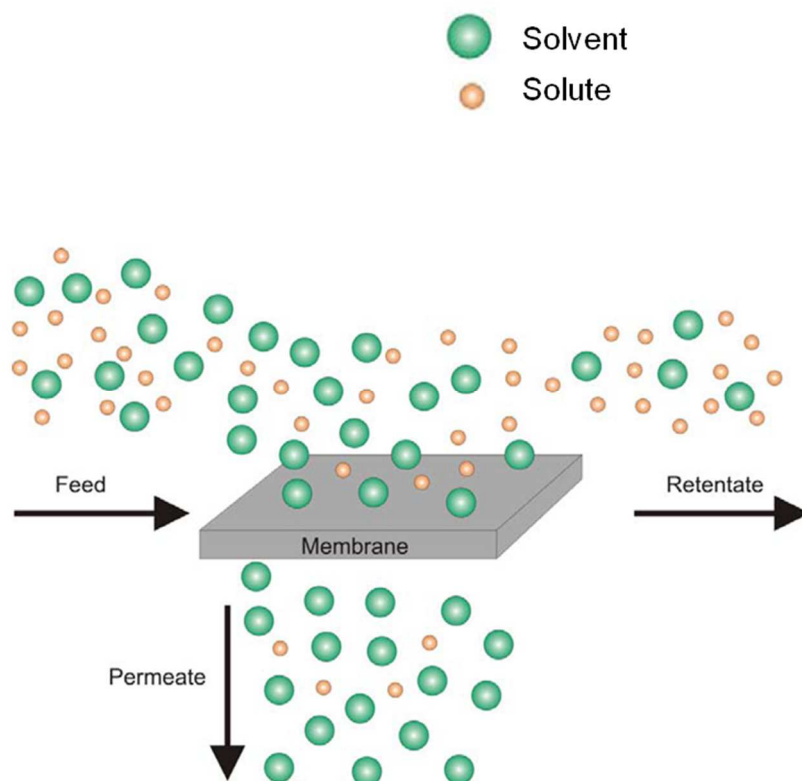


Figure 4.1: Organic solvent nanofiltration scheme

The process performances are influenced by:

- Solvent/solute properties;
- Solvent/ solute composition;
- Operative conditions (temperature and/ or pressure).

Because the change in phase are not occur during the filtration, the OSN is a low energy demand process.

Usually only one “pure” stream can be obtained and due to this reason the OSN is combined with other unit operation such as distillation.

One of the greatest challenges of the OSN is the development of solvent stable membranes. The membranes material should not only exhibit chemical stability, but also mechanical resistance, high selectivity and high fluxes. Membranes can be made of polymers (organic

material) or ceramic (inorganic material) but the first group of them has found much wider application [55].

Rubbery and glassy polymers are used. Rubbery materials such as polydimethylsiloxan (PDMS) have been extensively researched because they have high tendency to swell, which leads to high fluxes [55].

Glassy polymers, such as polyamides and polyimides have high chemical and thermal stability. They usually have lower fluxes than rubbery polymers.

4.2. Theory background

4.2.1 Membrane performance

Membrane performances are evaluated by the flux. Solvent flux is obtained by measuring the weight of the volume permeated per unit area per unit time using the following equation:

$$J = \frac{m}{A * t} \quad (4.1)$$

For the binary mixture the rejections of the test compounds is determined by following equation:

$$R_i(\%) = \left(1 - \frac{C_{p,i}}{C_{r,i}}\right) * 100 \quad (4.2)$$

Membrane rejection is defined as the percentage of one minus the ratio between the composition of component i in the permeate and in the retentate side.

From a process point of view, the separation coefficient or selectivity $\alpha_{i,j}$ is defined in analogy to distillation processes as

$$\alpha_{i,j} = \frac{x_{i,perm}}{x_{i,feed}} * \frac{x_{j,feed}}{x_{j,perm}} \quad (4.3)$$

And can be used to characterize the ability of a membrane to separate two components i and j from each other [56].

4.2.2 Young's modulus

To characterize the physical properties of polymer films, creep measurements are usually performed to estimate the time dependent increase of film deformation at constant stress. Those measurements provide information about the viscoelastic behavior of polymers and therewith also allow the determination of viscosity and Young's modulus [57].

The time-dependent elongation $\varepsilon(t)$ determined in creep experiments with or without VOC loading is given by:

$$\varepsilon(t) = \frac{L(t) - L_0}{L_0} \quad (4.4)$$

$L(t)$ represents the film length at time t and L_0 the film length of the straight-strained state at time zero. The creep compliance $F(t)$ is defined as:

$$F(t) = \frac{\varepsilon(t)}{\sigma_0} \quad (4.5)$$

The stress σ_0 which is required is assumed to be constant during the whole creep experiment. σ_0 is required which is assumed here to be constant during the whole creep experiment. This is valid for small elongations since σ_0 is obtained by:

$$\sigma_0 = \frac{F_0}{A_0} \quad (4.6)$$

where F_0 is the applied (constant) force and A_0 is the cross sectional area of the polymer film which might decrease at high elongations. However, for the experiments performed in this work the film elongation was below 2%.

The Young's modulus is calculated as a slope of the elastic region.

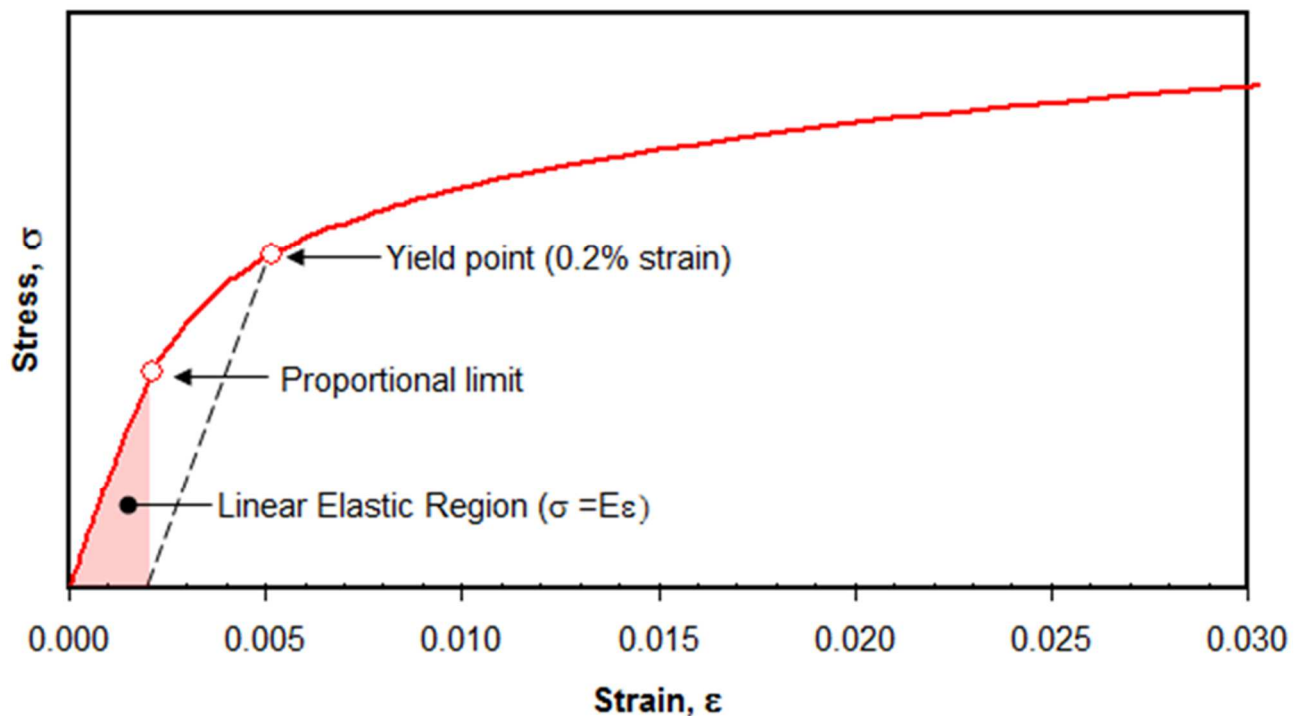


Figure 4.2: Typical stress-strain graphic

4.2.3 Sorption

Solubility and diffusivity values of organic liquid species in polymers are required in order to perform the calculations that support membrane separation process design.

Lee et al [58] measured the swelling induced by a series of organic solvents in PDMS in order to study the applicability of this matrix in microfluidic devices, and found that solvent induced swelling decreases with increasing the difference between solubility parameter of the solvent and PDMS, thus indicating a predominant effect of energetic interactions on the solubility.

The measurement of liquid solubility in polymers can be performed gravimetrically, directly measuring the mass uptake.

$$c = \frac{m - m_0}{m_0} \quad (4.7)$$

4.3 Materials and Methods

4.3.1 Materials

Four different, solvents namely toluene, n-hexane, ethanol and butanol were used in the characterization. Table 4.1 summarized the main properties of the mentioned solvents.

As solutes, 2 different n-alkanes with different chain lengths were used. A summary of the used n-alkanes is shown in Table 4.2.

Two different membranes were tested. In both membranes the active layer is a silicone separation layer with a thickness of some microns.

The first one PDMS_1 is a TFC OSN membrane based on a silicone separation layer. Its silicone separation layer is applied as a coating and then cross-linked by irradiation to avoid swelling in organic solvents; this cross-linking process has been patented [59]. This membrane can work at a maximum temperature of 60°C and a feed pressure up to 35 bar.

The second one is PDMS_2. This membrane can work at a maximum temperature of 80°C and a feed pressure up to 35 bar.

Solvent	Formula	Molecularweight t kg/kmol-1	Viscosit y (mPa s)	SurfaceTensio n (mN m-1)	Boiling Point °C	Solubilityparamet er (Mpa 0,5)
Toluene	C7H8	92,14	0,59	28,5	110,6	18,3
n-Hexane	C6H14	86	0,31	18,4	69	14,9
Ethanol	C2H6O1	46	1,08	22,3	78	26,2
Butanol	C4H10O1	74	3	24,6	118	28,7

Table 4.1: Physicochemical properties of the used solvents [60] [61]

Solute	Formula	Molecularweight kg/kmol-1	Solubilityparameter (Mpa 0,5)
Dodecane	C12H26	170,34	16,1
Docosane	C22H46	310,61	16,7

Table 4.2: n-alkanes used as solutes [60] [61]

4.3.2 Experimental Procedure

4.3.2.1 OSN experimental setup and procedure

Membrane screening was carried out using METCell Cross-Flow system connecting 2 filtration cells with individual areas of 0,0017 m² in series.

The METcell Cross-Flow system, purchased from Evonik MET, consisting in a high-pressure filtration cells suitable for reverse osmosis (RO) and nanofiltration (NF), an organic solvent compatible gear pump and tank base. All parts resist up to 69 barg. A total of about 600-700 mL of solution is circulated between the tank and the filtration cells and filtration takes place in cross flow. The appropriate pressure was insured by nitrogen bottle and a fine-tuning pressure gauge.

Once the membrane was installed in the test cell, the steady state is reached after 15-20 min after that the operating pressure is applied. For the retention measurements, two permeate samples per test cell and one feed sample was taken after 30 minutes. All sample were analyzed three times using gas chromatography (GC 17a, Shimadzu) applying a flame ionization detector (FID) using helium as the carrier and a capillary column, HP-5 with a diameter of 0.32 mm and a film thickness of 0.25 μm

For the flux measurements permeate was continuously extracted and weighted at constant interval of time.

The membrane was carefully rinsed by the solvent used between each filtration experiment.

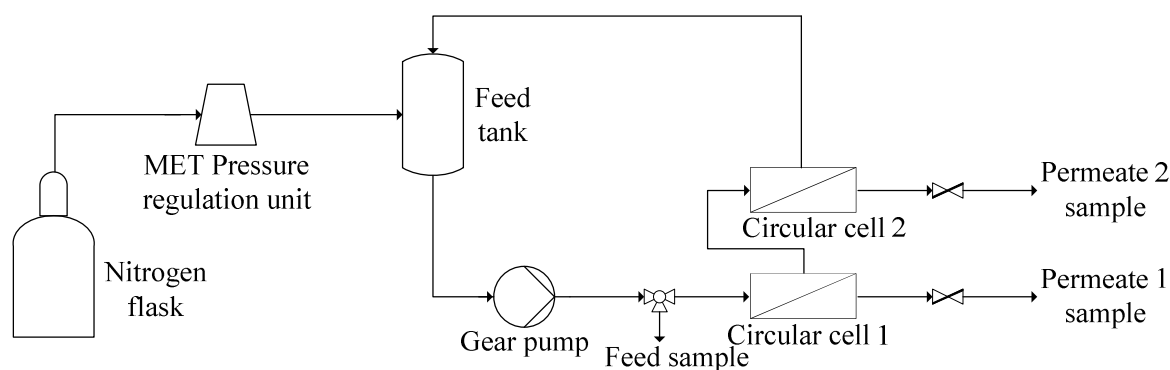


Figure4.1: Flow diagram of the OSN testcell apparatus (Evonik MET cell)

Membranes characterization was performed at the ambient temperature and at different mixtures compositions. The first experiments were carried out with pure toluene at 35 bar. Afterwards the experiments with three different binary solvent mixtures (25 wt%, 50 wt%, 75 wt%) of toluene/n-hexane were carried out at 35 bar. Subsequently, the pure flux of n-hexane is measured at 35 bar. Different n-alkanes were added to n-hexane and the retention was measured in pure n-hexane and in different composition of the binary mixtures toluene/n-

hexane. Finally, the retention of n-alkanes solved in pure toluene was measured. The same method was used for the experiments using alcohols (ethanol or butanol) or the binary mixtures alcohols/(toluene or n-hexane). The Table 4.3 shows a summary of all realized experiments.

Solvent 1	Solvent 2	Solute	TMP (bar)
Toluene	-	-	35
n-Hexane	-	-	35
Ethanol	-	-	35
Butanol	-	-	35
Toluene	n-Hexane (0,25,50,75 wt%)	n-Alkanes (0,0.5 wt%)	35
Toluene	Ethanol (0,25,50,75 wt%)	n-Alkanes (0,0.5 wt%)	35
Toluene	Butanol (0,25,50,75 wt%)	n-Alkanes (0,0.5 wt%)	35
n-Hexane	Ethanol (0,25,50,75 wt%)	n-Alkanes (0,0.5 wt%)	35
n-Hexane	Butanol (0,25,50,75 wt%)	n-Alkanes (0,0.5 wt%)	35

Table 4.3: Summary of the performed experiments

The quantity of n-alkanes added to the pure solvent or binary mixtures was around 0,5 wt%.

4.3.2.2 Young's modulus measurement

The Young's modulus of these membranes was measured using a DMA 2980 at 25°C in dry conditions and at different concentration of toluene and n-hexane. A detailed description of the apparatus is given by Mueller et al [62].

The central device of the creep apparatus is a measuring chamber that is arranged in an air thermostat (Fig. 4.2). Within this chamber, two film-tension clamps are positioned which fasten the polymer film. The upper clamp is connected to a VOC resistant force transducer that measures the force of up to 20 N with a reproducibility of 0.003 N. The force is applied to the clamped polymer film by a linear drive (PhysikInstrumente) that is connected via a shaft to the lower clamp. The linear drive is able to perform linear steps with a minimum step size of 100 nm in a range of up to 50 mm with a maximum force of 120 N. This large force is needed to move the bellow, which divides the low-pressure area (inner measuring cell) from the mechanical actuator which is situated outside the measuring cell. Since the lower clamp is directly connected to linear drive, the latter directly measures the position of the clamp. Because of isothermal conditions, the heat expansion of the shaft can be neglected. The control of the linear drive and therewith of the constant force applied to the polymer sample is performed by a LabView program. The measuring chamber and the earlier designed sorption

apparatus are built in a vapor-flow-through design to solve the problem of inevitable leakage into the equipment. Thus, the pressure in the cell can be kept constant over long times better than 0.1 mbar between 0.1 and 1330 mbar. The temperature of the cell is controlled by means of an air thermostat bath, which is equipped with heating and cooling devices to keep the temperature constant better than 0.03 K in the range between 20 and 85°C. The temperature gradient within the air thermostat was determined to be about 0.1 K; the one within the measurement cell is even lower. The temperature in the double-wall VOC vaporizer is controlled by means of a conventional liquid thermostat. Temperatures in the vaporizer and in the measuring chamber (next to the sample) are measured using a calibrated resistance thermometer (PT100). The measuring chamber as well as vaporizer can each be evacuated by means of a vacuum pump.

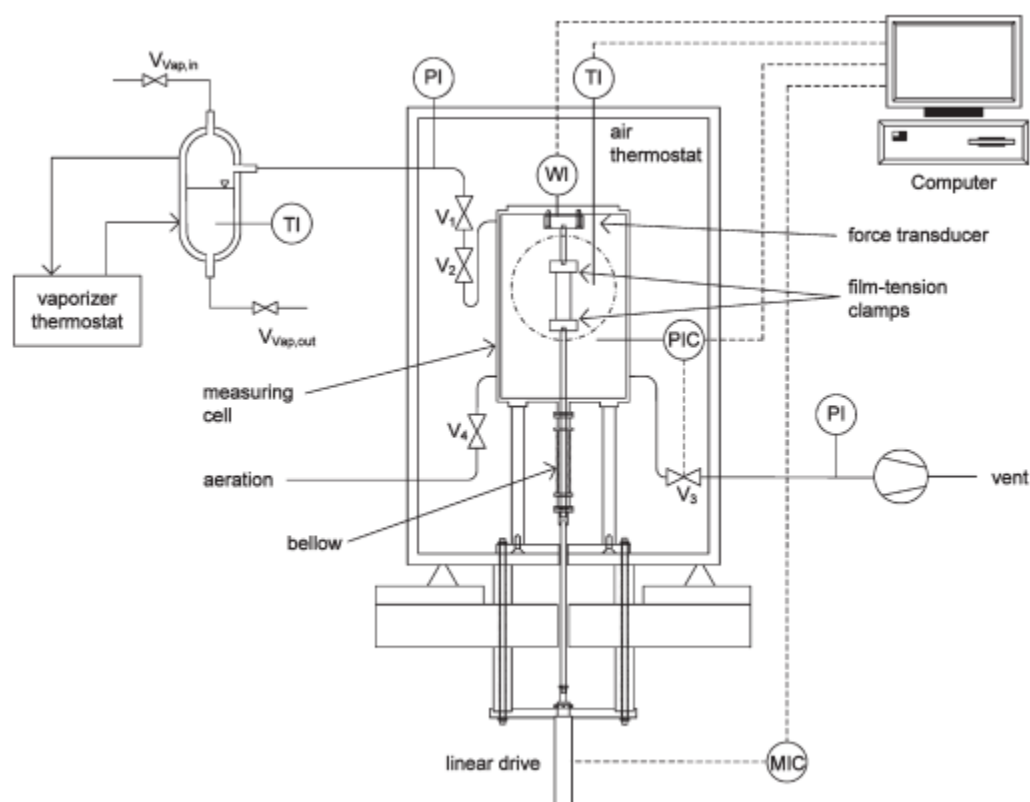


Figure 4.2: Flow sheet of the creep apparatus for isothermal and isobaric vapor measurements especially at low pressures [62]

Only the active layer was used for these types of experiments. The sizes of the membrane used were 15X45 mm while the thickness for the different experiments varies in the range of 4-6 μm . For the determination of elastic modulus of dry and loaded polymer, the increasing strain was measured under constant stress.

For that purpose, a film of active layer was attached to the clamps within the measuring chamber. After heating and evacuation of the apparatus a dry measurement was performed lengthening the sample of 0.005 mm per minute until the material wasn't any more in the elastic region.

After that, the pressure in the measurement chamber was increased by opening valves V1 and V2 and closing valves V3 and V4 (Fig. 4.2). After reaching the desired pressure, the inlet valve V2 was set to achieve a desired flow of 0.1 (mbar L)/s, and the pressure control was set into operation. These isothermal and isobaric conditions were maintained for the whole measurement. After reaching the equilibrium, the lower clamp was carefully driven downward by the linear drive until the film was tightly strained as for the dry experiment. To ensure reproducibility, creep curves at 25°C and different toluene and n-hexane loadings were measured at least twice.

4.3.2.3 Sorption measurement

The solubility of pure solvents in two membrane active layers was measured gravimetrically, directly measuring the mass uptake in liquid sorption experiments [62].

The sorption experiments can be performed according to a classical blot and weight method: samples will be immersed in vials or flasks filled with liquid, placed in a thermostatic bath and weighted at regular time intervals. The membrane will be isolated from the support layer because it has been seen that even the support layer can absorb some liquid cover and distort the real value.

In order to weight the samples and register the mass uptake, the samples were removed from liquid, quickly dried with a paper towel, weighted on the analytical balance and then re-immersed in the liquid. In this way the mass uptake in function of time was obtained.

For the most volatile solvents, such type of technique may induce errors in the evaluation of solubility, due to evaporation of the solvent absorbed during the sample weight measurement.

From these experiments information about diffusivity coefficients are also obtained. In particular Fig. 4.3 shows a typical trend obtained after several weigh.

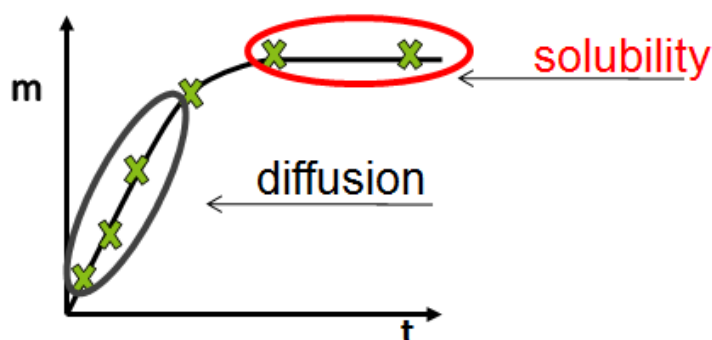


Figure 4.3: Typical trend obtained from sorption measurements

The slope of the linear part in the above plot allows for the determination of the diffusion coefficient, while the steady-state value represents the sorption contribution.

The identification of diffusion contribution is not always easy because in some case the diffusion is too fast that after the first weigh the mass values does not change.

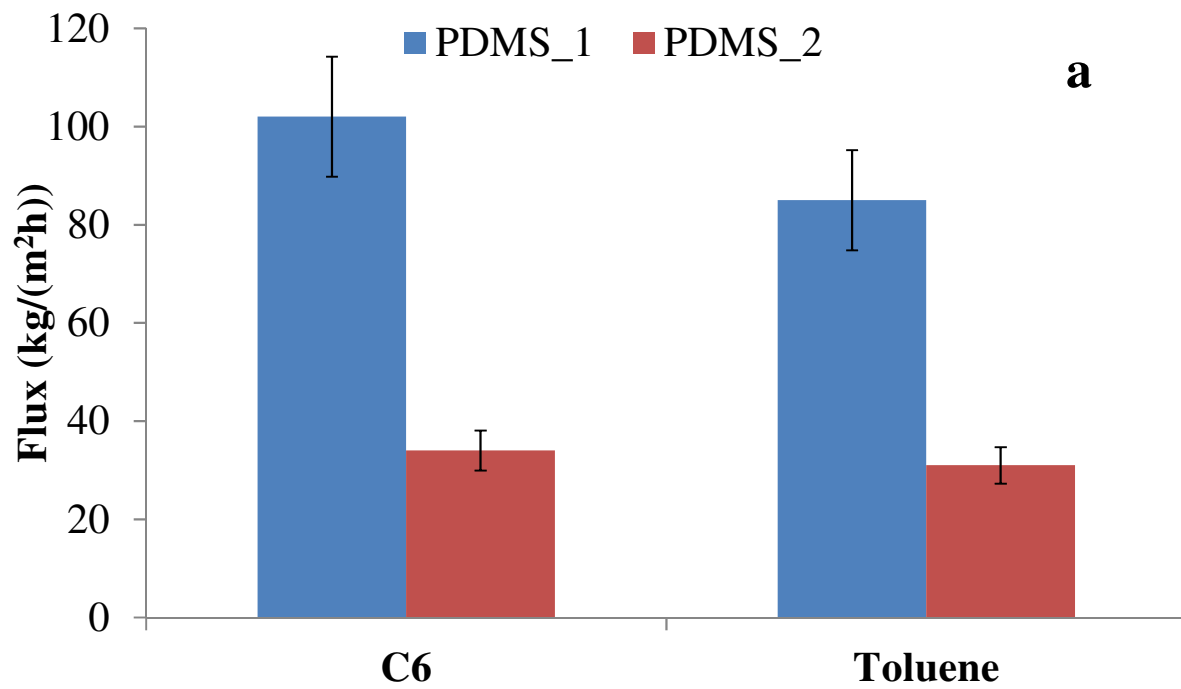
4.4 Experimental Results

4.4.1 Performance characterization

Figures 4.4 a,b show the results obtained in terms of flux using the OSN filtration system described in the previous paragraph.

Focus the attention on the toluene and n-hexane, the flux of the second solvent is three times higher for PDMS_1 than for the other membrane.

In case of alcohols (Fig. 4.4 b) the situation is opposite because the flux is higher for PDMS_2 and the differences with the other membrane are not so evident as in case of alkanes.



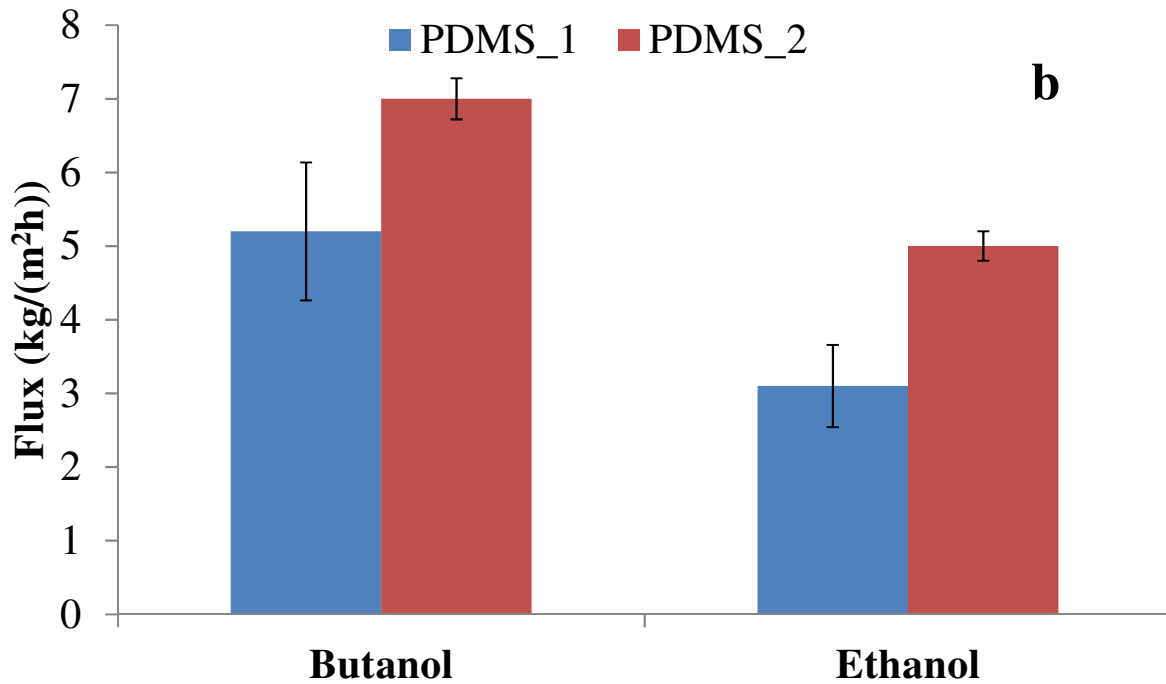


Figure 4.4 a,b:Solvents flux evaluated experimentally

4.4.1.1 Toluene-Hexane mixture

Figures 4.5 reports normalized flux versus weight composition of component i in the feed side. Working with similar solvents inside the mixture (toluene-hexane) the trend is linear for both species and in particular increasing the composition of component i , normalized flux increases. Representing the flux, as normalized, important differences are not appreciable for different membranes. Referring to the previous plots (Fig. 4.4 a,b) the differences in terms of flux remain and PDMS_1 shows three times higher flux than PDMS_2.

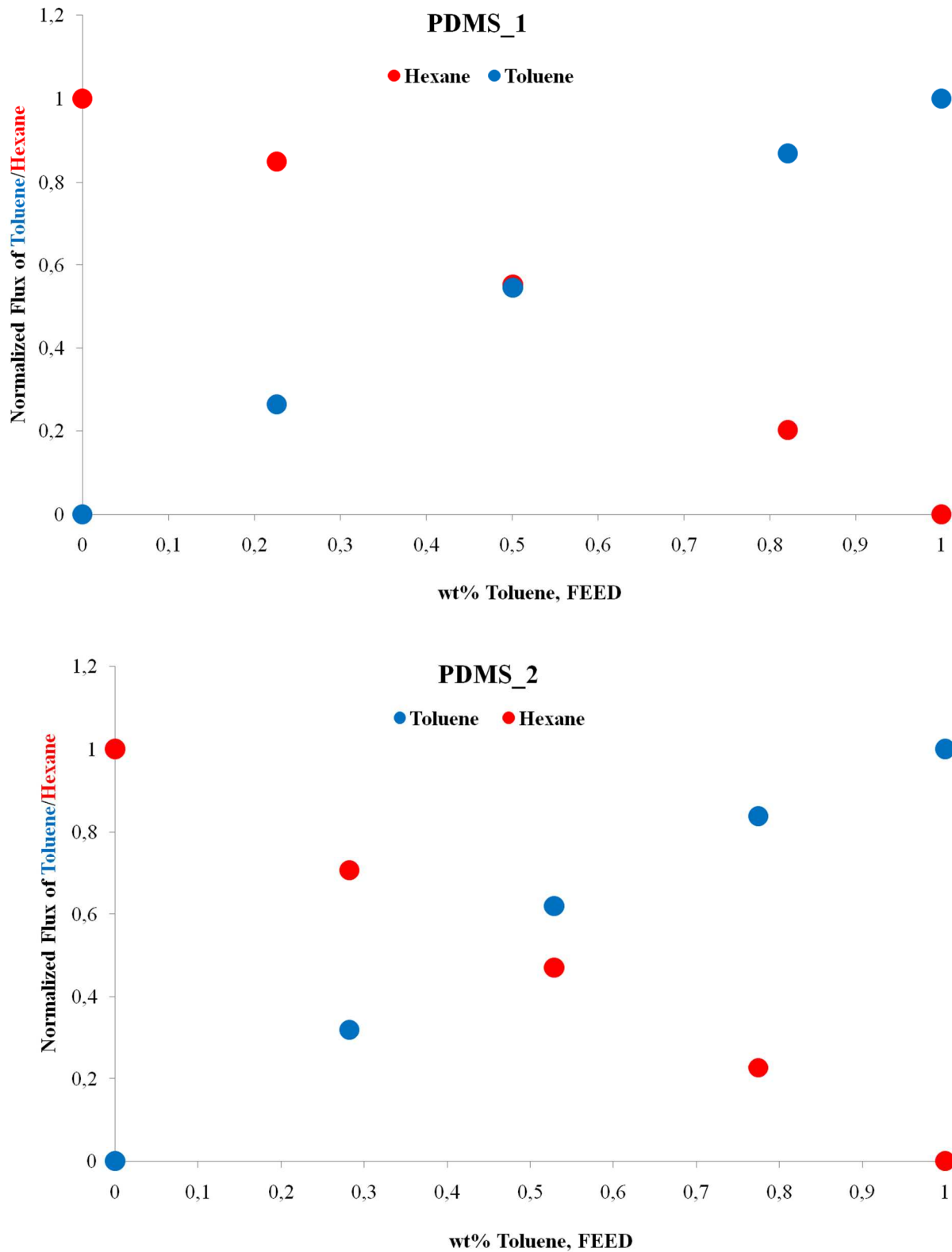


Figure 4.5 a,b: Normalized flux of toluene and n-hexane vs toluene feed composition

Adding 0,5 wt% to this mixture, the rejection in terms of dodecane and docosane able to pass through the membrane was measured.

Figures 4.6 a,b show that the solute rejection does not change with the composition of the component i and in both cases is two times higher for the alkane with the higher molecular weight.

PDMS_1 proved the higher flux but lower rejection than PDMS_2.

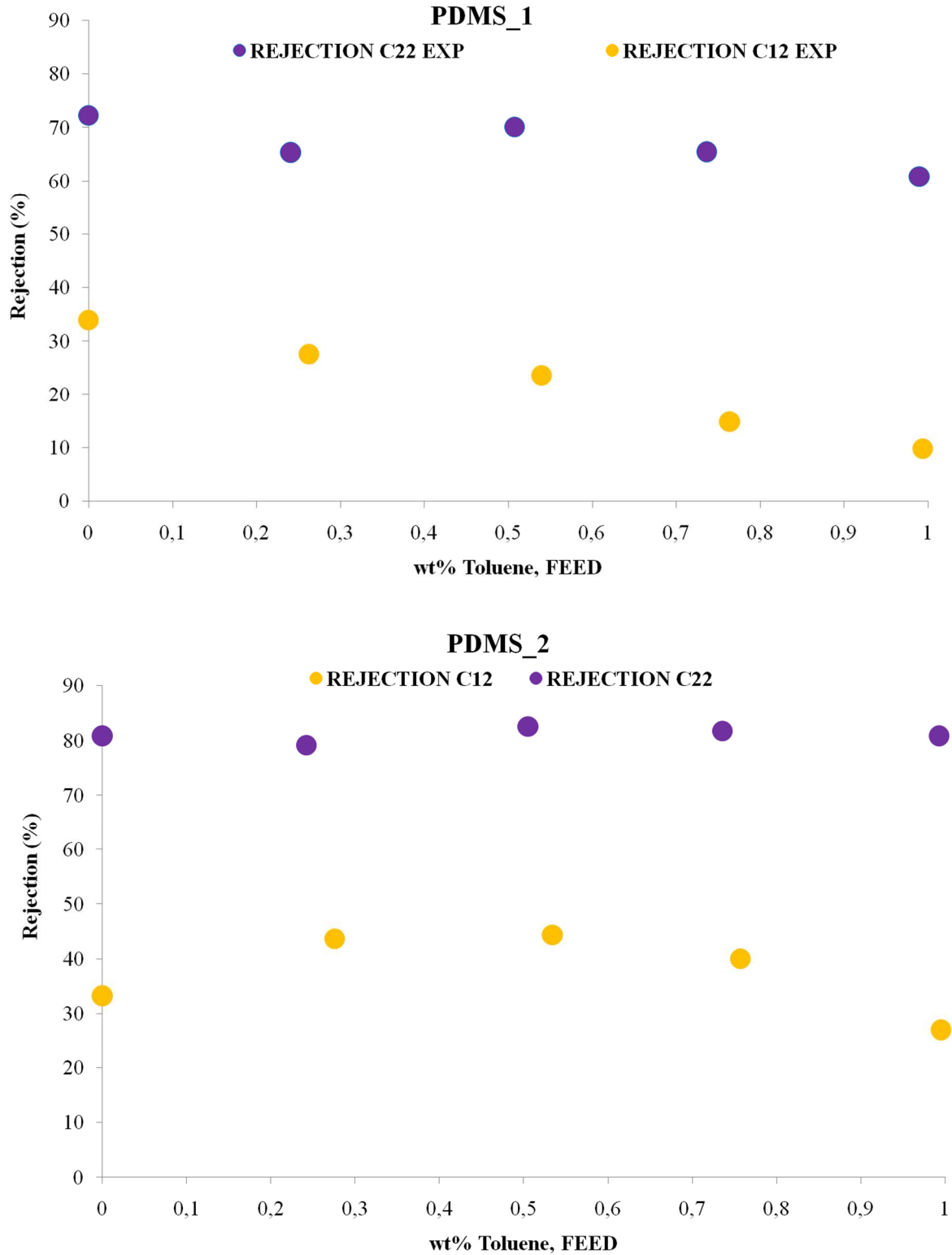


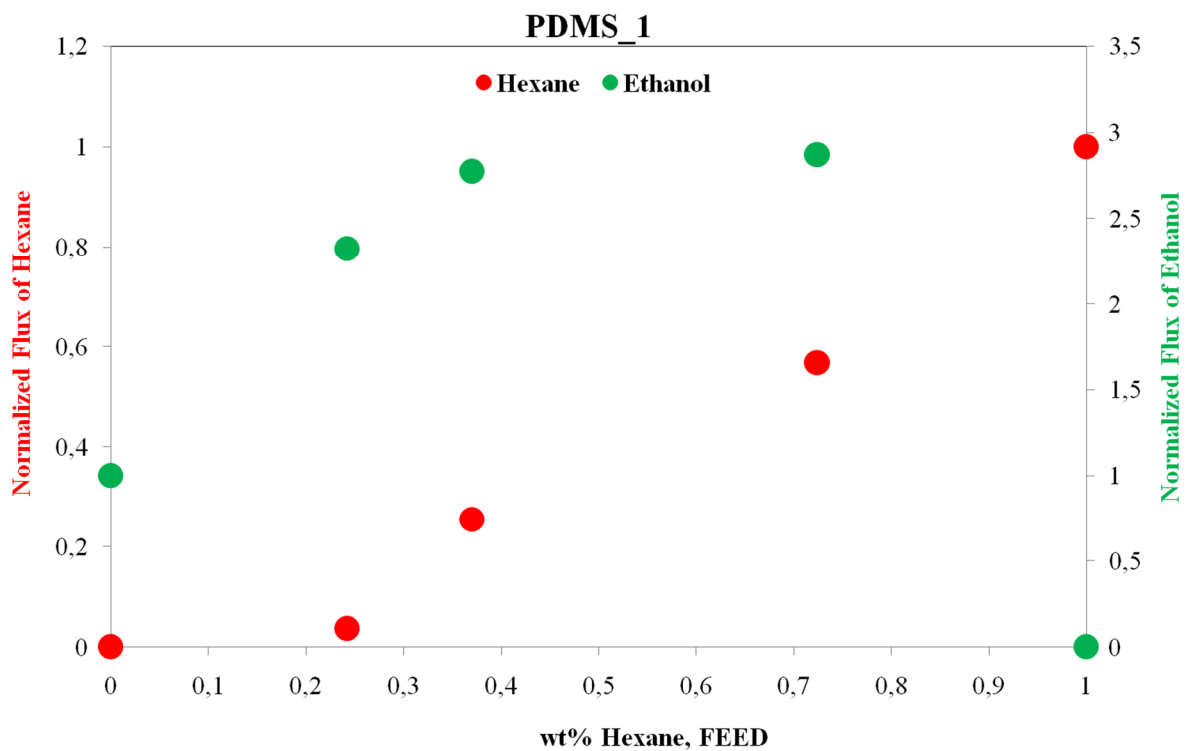
Figure 4.6 a,b: Rejection of solutes vs toluene feed composition in toluene-hexane mixture

4.4.1.2 Hexane-Ethanol mixture

Figure 4.7 shows normalized flux versus weight composition of component i in the feed side.

If the mixture is formed by different solvents for nature the normalized flux trend is not linear as in Fig. 4.5 but normalized flux of ethanol presents a maximum around 75% of alcohol inside the mixture. This phenomena is predominant for PDMS_1 than for PDMS_2 probably because the flux is higher.

Normalized flux for hexane is linear increasing alkane content in the mixture.



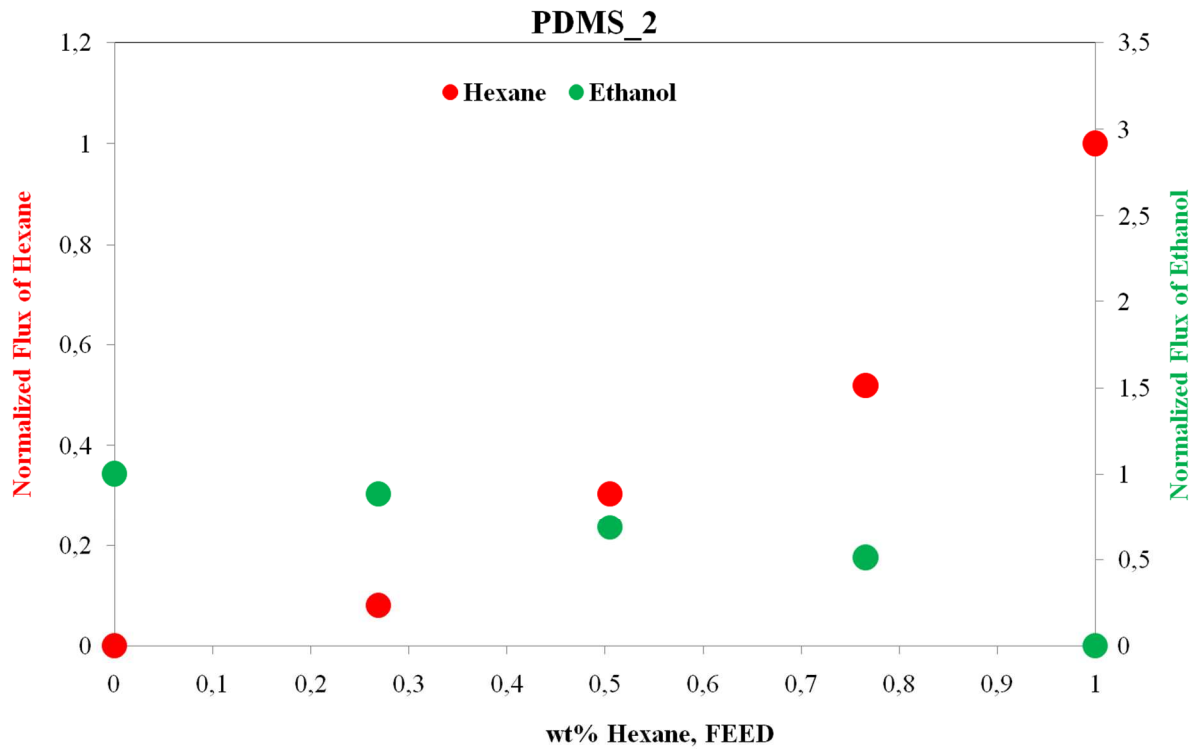


Figure 4.7 a,b: Normalized flux of n-hexane and ethanol vs n-hexane feed composition

As in the previous case the rejection of solutes is obtained adding 0,5 wt% of dodecane and docosane to this mixture.

Figures 4.8 a,b show that the solute rejection change with the composition passing from negative to positive values.

Dodecane presents a minimum of rejection close to 75% of alcohol in the mixture, while for docosane the point at 99.5 wt% of alcohol and 0.5 wt% of alkane is not present because at the ambient temperature docosane is insoluble in ethanol.

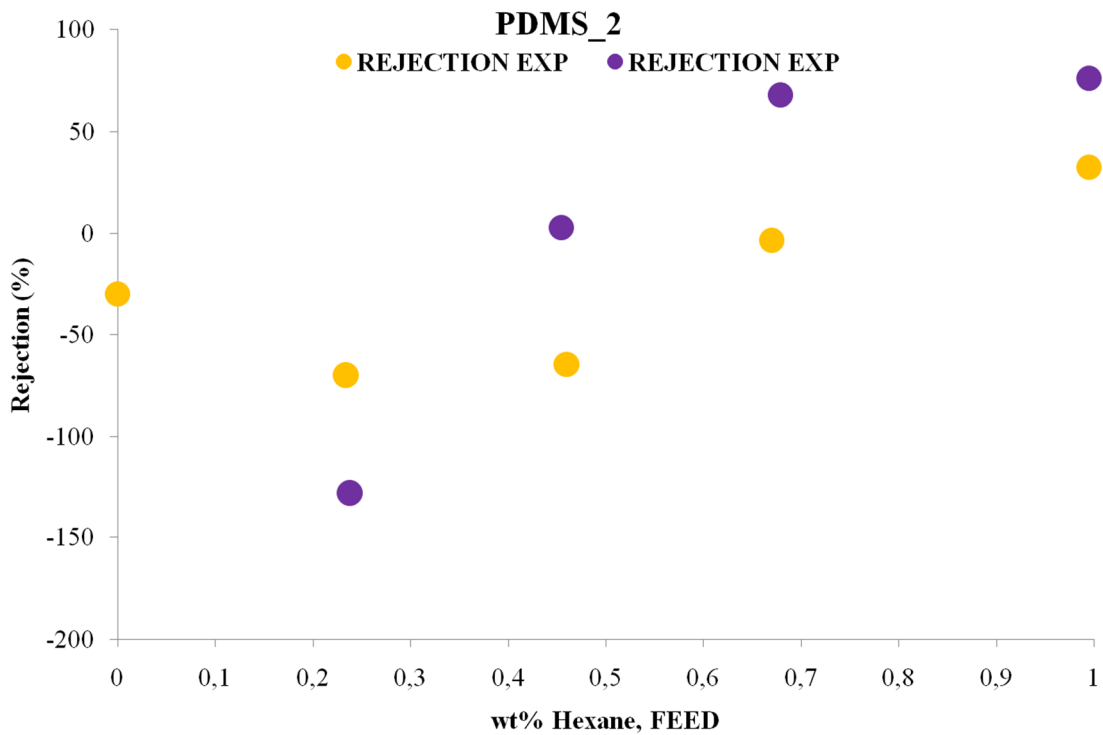


Figure 4.8 a,b: Rejection of solutes vs n-hexane feed composition in hexane-ethanol mixture

In Appendix A, all the other binary and ternary mixtures results in terms of experimental flux and alkanes rejection will be find.

4.4.2 Young's modulus measurements

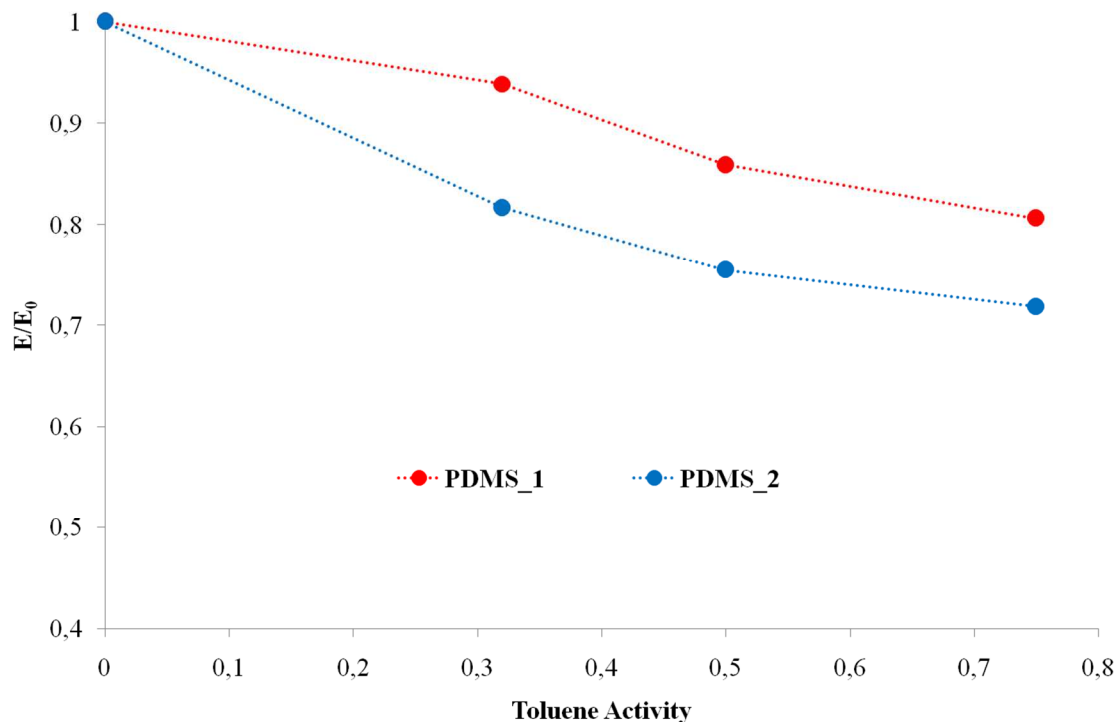
Figures 4.9 a,b show the reduction of the ratio between the elastic modulus at a specific condition (E) and in dry conditions (E_0) changing the fugacity of toluene and n-hexane in the system.

Only toluene and n-hexane were selected to evaluate the elastic modulus change because usually are more compatible to the swelling of PDMS matrix.

Because the evaluation of the effective active layer thickness is not so easy, the ratio between the elastic modulus and not the absolute value is reported in the following figures.

Figure 4.9 a represents what happen increasing the content of toluene in the system. The reduction of elastic modulus ratio is about 20% passing from 0 to 75% of toluene in the system for PDMS_1, while the same increment of fugacity in the system lead a reduction of 40% in case of PDMS_2.

Figure 4.9 b shows that the reduction of elastic modulus working with n-hexane as solvent, is less evident because from 0 to 75% is about 15% for both membrane, but the lowering passing from 0 to 25% is 15% for PDMS_2 and 2% for the other membrane.



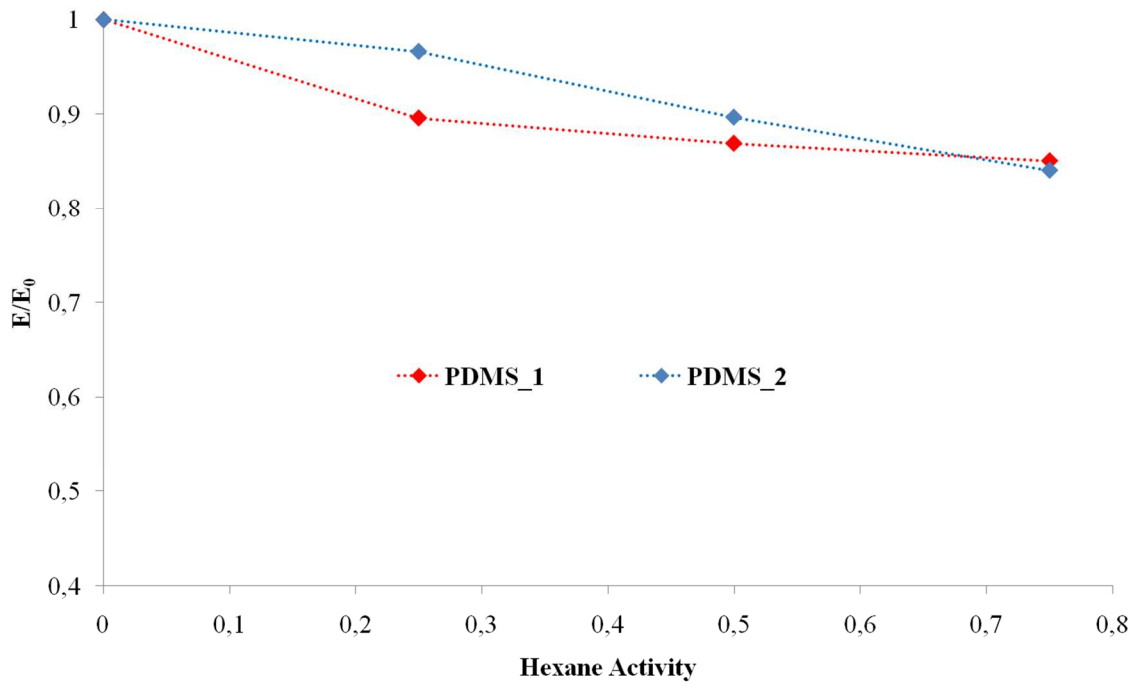


Figure 4.9 a,b:Ratio between the elastic modulus and the elastic modulus in dry conditions VS toluene/n-hexane content

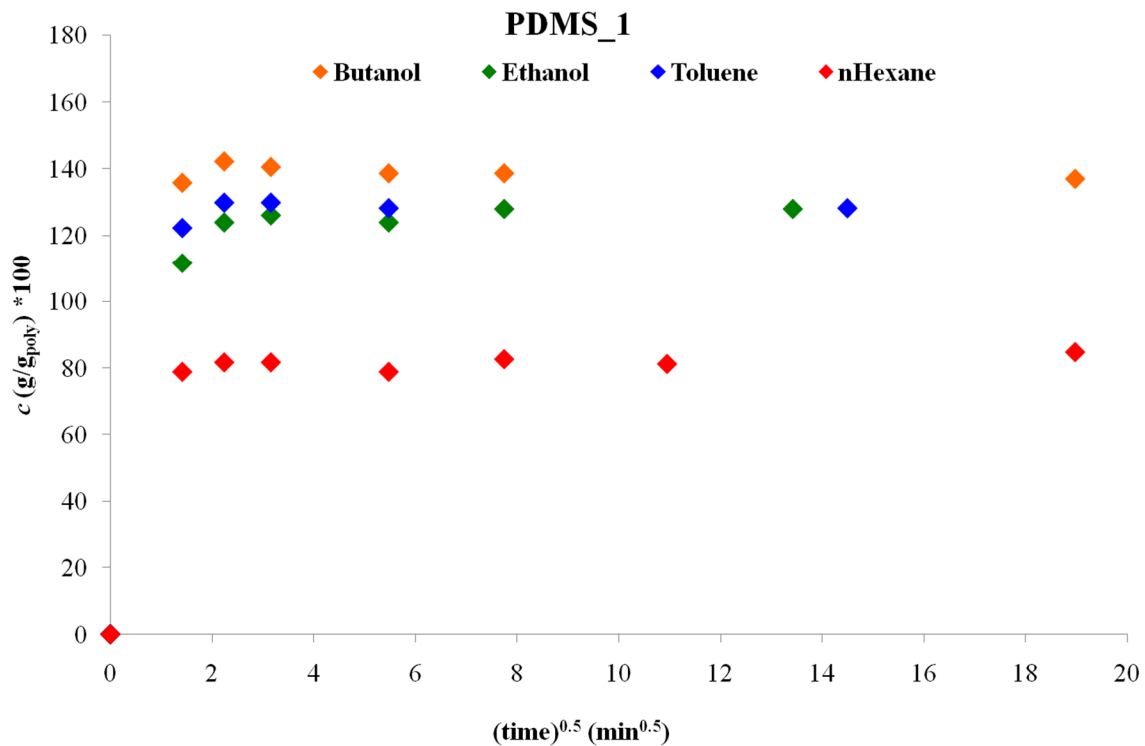
The higher elastic modulus reduction observed for PDMS_2 is to be attributed to the higher crosslink degree present in this membrane, visible in the lower values of experimental flux obtained in the previous test.

4.4.3 Sorption measurements

Sorption was evaluated for all the pure solvents and for different solvents the equilibrium in the membranes were reached after 2-5 minutes. Due to this reason, it was not possible to calculate the diffusion coefficient from the slope of the linear region.

In both materials the sorption value followed the trend: Butanol > Ethanol > Toluene > n-Hexane even if with n-hexane the operative error is bigger because the boiling point temperature is lower than with the other solvents.

The solubility values for PDMS_2 are 50% lower than with PDMS_1 for all pure solvents except for the n-hexane where the value is higher than 60% due to the bigger error in the measurements.



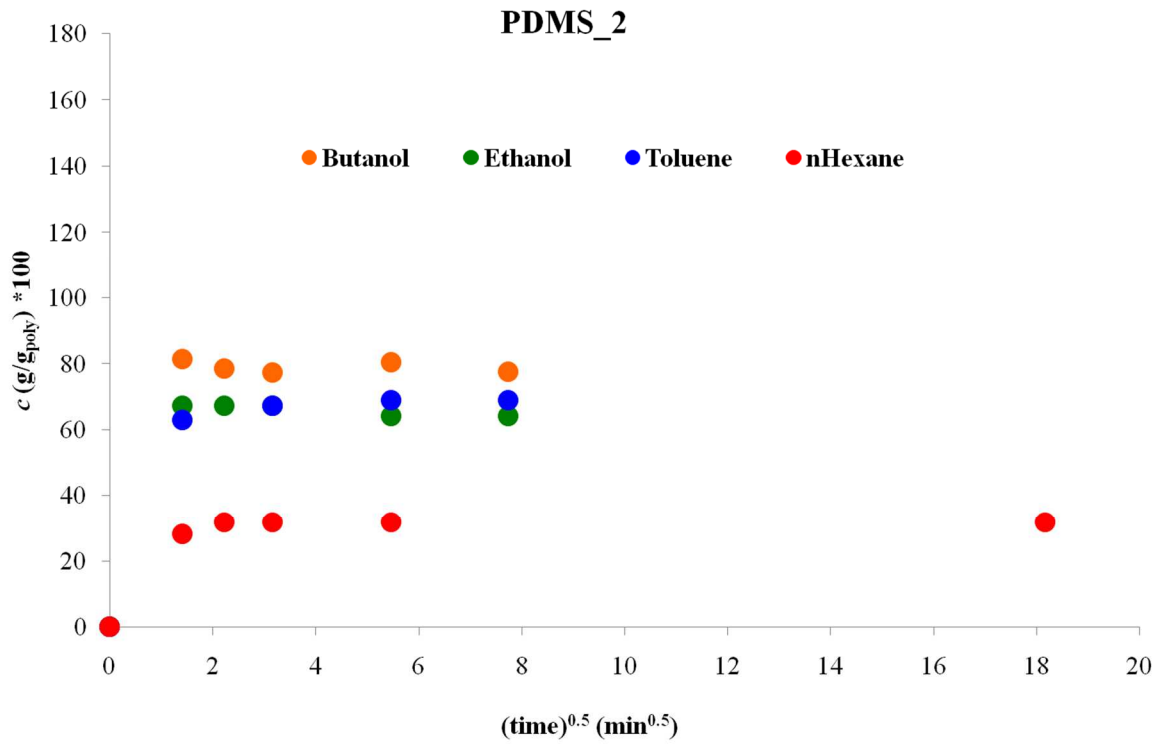


Figure 4.10 a,b: Percentage sorption VS square root of time for PDMS_1 and PDMS_2

The fact that the sorption is lower for PDMS_2 explains why the crosslink degree is higher for this membrane, as consequence of the lower experimental flux and higher reduction in the elastic modulus ratio.

4.5 Modeling

4.5.1 Transport Modeling

From the beginning of the membrane development, a large number of researcher focused the attention on the description of the transport mechanism through membranes.

The knowledge of the basic mechanism is important because:

- Allows to approach new situation with confidence;
- Reduce the number of experiments;
- Is able to predict new phenomena [64].

Transport models are the instruments to understand membrane transport [65] and they can be applied for prediction and design.

The availability of the model parameters allows performing prediction of the process performance at a different process scale.

In the past years many studies were published with the idea to model the transport at the membrane scale.

As said before to predict flux and rejection through porous or dense membranes, the transport mechanism of solutes and solvents has to be understood.

Unlike the aqueous system, steric and electrostatic separation mechanisms are not enough to describe an organic system. Properties of solvents and solutes and binary interaction parameters between these have to be known and the separation capability cannot be described only with the information of the MWCO [66].

Models used until now were:

- Solution-diffusion [67] [68]
- Pore flow [69]
- Solution-diffusion with imperfections [70].

The choice of the most suitable model depends on the physical structure of the membrane: porous or dense. All these models differ in the mechanical description of the permeation, driving force for this type of process, and as consequence on the number of parameters that have to be fitted or obtained experimentally.

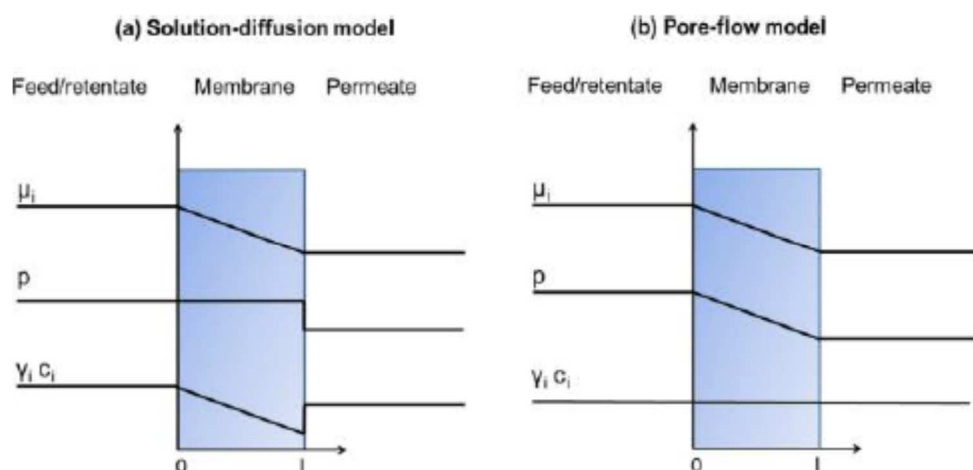


Figure 4.11: Profiles of chemical potential, pressure and solvent activity characteristic for a pressure-driven filtration of component i through a membrane according to a) solution diffusion and b) pore-flow transport models [68]

According with Fig. 4.11, solution-diffusion model is usually used to describe transport through a dense membrane because change in pressure occurs in the permeate side (the membrane pressure is equal to the feed pressure), while pore-flow model is based on the assumption that through the membrane is via pores which are larger as compared to the solute and solvent molecular diameters.

Because the membranes considered in the study are made in PDMS, the decision was to consider both of them as dense and use a solution-diffusion model to describe transport mechanism.

4.5.1.1 Solution-Diffusion Model based on Fick's law

Several models have been developed to describe the permeation of organic solvents through dense polymeric membranes. The most common model was proposed by Lonsdale and Marten [71] in 1965 and subsequently from Wijmans and Baker who gave an excellent review and compared the solution-diffusion model with the pore-flow model [68]. In this model the transport occurs only by diffusion. First the component that needs to be transported dissolves in the membrane. Once dissolved in the polymer network, the penetrant molecules diffuse through the membrane and in a third step desorb from the membrane at the side of the lower chemical potential. Different components are separated due to differences in sorption and diffusion.

With the solution-diffusion theory the mutual cross-coupling effects are not take into account.

The classical solution-diffusion theory is described by Fick's first law that relates the diffusive flux to the concentration under the assumption of the steady-state conditions.

$$J_i = -\dot{D}_i(z) \frac{dc_i(z)}{dz} \quad (4.8)$$

With \dot{D}_i as fickian diffusion coefficient and c_i as molar concentration. Under the assumption that the diffusion coefficient and molar concentration are constant:

$$J_i = -\rho \frac{D_{im}}{w_m} \frac{dw_i}{dz} = \frac{\rho D_{im}}{l \bar{w}_m} (w_{i,0} - w_{i,l}) \quad (4.9)$$

$w_{i,0}$ and $w_{i,l}$ are the weight fractions of the component i in the membrane on the feed and permeate interface and l is the thickness of the effective membrane active layer.

$w_{i,0}$ and $w_{i,l}$ can be determined assuming that the fluids and the membrane material are in equilibrium at the interface.

\bar{w}_m is the average weight fraction in the membrane.

$$\bar{w}_m = 1 - \bar{w}_{i,m} \quad (4.10)$$

$$\bar{w}_{i,m} = \frac{w_{i,0} + w_{i,l}}{2} \quad (4.11)$$

The effective or swollen thickness is calculated knowing the thickness in dry conditions and the density values.

$$l = \frac{l_0 \rho_m}{2 \rho_{0,m}} \left(\frac{1}{w_{m,0}} + \frac{1}{w_{m,l}} \right) \quad (4.12)$$

Anyway this approach is simplified and in some case has failed to describe the membrane flux correctly.

The simplifications are related to:

- Neglects the concentration dependence of Fickian diffusion coefficient;
- Neglects sorption dependence of the concentration;
- Considers the transport of solvent and solutes as completely independent of each other.

4.5.1.1.1 Fick's law analysis for binary mixtures

Describing binary mixture permeation, system included a ternary mixture of the polymer and two permeants. Eqs. (4.13) and (4.14) represent transport equations for two penetrants i and j , while Eq. (4.15) is the transport equation for polymer.

$$n_i = (n_i + n_j + n_m)w_i - \rho D_{im} \frac{dw_i}{dz} \quad (4.13)$$

$$n_j = (n_i + n_j + n_m)w_j - \rho D_{jm} \frac{dw_j}{dz} \quad (4.14)$$

$$n_m = (n_i + n_j + n_m)w_m - \rho D_{mm} \frac{dw_m}{dz} \quad (4.15)$$

Usually at the steady state $n_m = 0$.

The total mass flux of component i , n_i , is comprised of the mass flux resulting from the bulk motion of the permeants and mass flux resulting from diffusion relative to the bulk flux [72].

Eqs. (4.13) and (4.14) can be solved for n_i and n_j in:

$$n_i = \frac{\rho D_{im}}{w_m l} (1 - w_j)(w_{i,0} - w_{i,l}) + \frac{\rho D_{jm}}{w_m l} w_i (w_{j,0} - w_{j,l}) \quad (4.16)$$

$$n_j = \frac{\rho D_{im}}{w_m l} (w_j)(w_{i,0} - w_{i,l}) + \frac{\rho D_{jm}}{w_m l} (1 - w_i)(w_{j,0} - w_{j,l}) \quad (4.17)$$

Ternary mixtures are composed by two solvents, one solute and the polymer and the equations related are reported in Appendix B.

4.5.1.2 Solution-Diffusion Model based on Maxwell-Stefan equation

The Maxwell-Stefan equations (MS) were developed to describe multicomponent diffusion in gases at low density [73] [74], but have to be extended with good success to dense gases, liquid and polymers [73].

The Maxwell-Stefan equation predicts a general diffusive coupling via composition dependent multicomponent diffusion coefficient in system of three or more components. Unlike the classical solution-diffusion theory in this case the cross-coupling effect is not negligible.

The generalized Maxwell-Stefan equations for isothermal multicomponent mixtures can be written:

$$d_i = - \sum_{i \neq j} \frac{x_i x_j}{D_{ij}} (v_i - v_j) \quad (4.18)$$

Where D_{ij} are multicomponent diffusion coefficients [73], x_i is the mole fraction of i in the mixture and v_i the velocity of i relative to stationary coordinates. The term d_i is a generalized force for component i .

The velocity is converted in flux:

$$J_i = w_i \rho v_i \quad (4.19)$$

Where ρ is the mass density of the membrane, solvent and solute mixtures.

The flux of the membrane material at the steady-state is always zero and it is not useful to use the mole fractions when one of the components is a polymer, particularly if its molecular weight is unknown.

4.5.1.2.1 Maxwell-Stefan equation for binary mixtures

After other relationship mentioned from Paul et al [74] in a review is possible to obtain the MS equations for the ternary system $i-j-m$:

$$n_i = \frac{\rho D_{im} \left(1 + \frac{\bar{w}_l}{\bar{w}_m} \varepsilon_2\right) (w_{i0} - w_{il}) + \rho D_{jm} \left(\frac{\bar{w}_l}{\bar{w}_m} \varepsilon_1\right) (w_{j0} - w_{jl})}{\bar{w}_m l \left(1 + \frac{\bar{w}_l}{\bar{w}_m} \varepsilon_2 + \frac{\bar{w}_j}{\bar{w}_m} \varepsilon_1\right)} \quad (4.20)$$

$$n_j = \frac{\rho D_{jm} \left(1 + \frac{\bar{w}_j}{\bar{w}_m} \varepsilon_1\right) (w_{j0} - w_{jl}) + \rho D_{im} \left(\frac{\bar{w}_j}{\bar{w}_m} \varepsilon_2\right) (w_{i0} - w_{il})}{\bar{w}_m l \left(1 + \frac{\bar{w}_j}{\bar{w}_m} \varepsilon_1 + \frac{\bar{w}_l}{\bar{w}_m} \varepsilon_2\right)} \quad (4.21)$$

Where $\varepsilon_1, \varepsilon_2$ terms are:

$$\varepsilon_1 = \frac{D_{im}}{D_{ij}} \quad (4.22)$$

$$\varepsilon_2 = \frac{D_{jm}}{D_{ij}}$$

In absence of frictional coupling, the MS equations for the unidirectional case become equal to the Fick's law for 1 component.

Similar to the classical solution diffusion model, Maxwell-Stefan equation does not require a priori specification of which species is the solute and which is the solvent.

For the ternary mixture, the equations are reported in Appendix C.

4.5.2 Mixtures thermodynamics

Diffusion and sorption determines the flux and the rejection through the membrane because the molecule firstly needs to sorb into the membrane and then diffuse through it.

The first approach to determine the sorption behavior is the measurement of sorption isotherms. The second one uses binary interaction parameters, which can be estimated from experimental VLE data, in order to predict the behavior of the multicomponent system.

In this work, the second approach was used and in particular PC-SAFT equation of state (Chapter 2) was used in addition at sorption test with pure solvents. PC-SAFT equation of state is useful to evaluate the composition of component i inside the membrane feed and retentate side, where the pressures are different.

In Table 1 and 2 pure components and polymers PC-SAFT parameters used in this work are reported.

Components	m/M (mol/g)	σ (Å)	ϵ (K)	$\epsilon^{A_i B_i}$ (K)	$k^{A_i B_i}$	Ref.
Toluene	0.03055	3.716	285.69	-	-	[12]
n-hexane	0.03548	3.798	236.77	-	-	[12]
Ethanol	0.05172	3.177	198.24	2653.4	0.03238	[76]
Butanol	0.03716	3.614	259.59	2544.5	0.01	[12]
Dodecane	0.03115	3.895	249.21	-	-	[12]
Docosane	0.02885	3.958	258.99	-	-	[77]

Table 4.3: Pure-component PC-SAFT parameters for solvents and solute used

The membranes investigated were considered chemically similar, as a result of the experimental data. The parameters used for both of them were the same found for the PDMS.

Components	m/M (mol/g)	σ (Å)	ϵ (K)	$\epsilon^{A_i B_i}$ (K)	$k^{A_i B_i}$	Ref.
PDMS	0.03460	3.3820	165	-	-	[78]
PDMS_1	0.03460	3.3820	165	-	-	[this work]
PDMS_2	0.03460	3.3820	165	-	-	[this work]

Table 4.4: Pure-component PC-SAFT parameters membranes

4.5.3 Mechanics: Crosslink Degree

The characteristics introduced in the membrane to resist to the organic solvents were considered in the model by the crosslink degree. The differences saw from the performance experiments were due to the different compaction of the structure.

Various models can be adopted to describe the contribution of the crosslink: affine network theory, phantom network theory, etc. In this work the affine network theory was used as described in Chapter 2.

The crosslink degree was introduced as an elastic pressure that has to be added to the pressure calculated with the PC-SAFT.

$$p^{elast} = -\frac{A^{elast}}{V} - \frac{\lambda_{\perp}}{\lambda_{\parallel}^2} \frac{\partial(A^{elast}/V)}{\partial\lambda_{\perp}} \quad (4.23)$$

λ_{\perp} represents the stretching out of plane, while λ_{\parallel} represents the stretching in plane. In this way the model developed allows to consider that the membrane is able to swell in two different ways: out of plane (Fig. 4.12 a) or in all directions (Fig. 4.12 b).

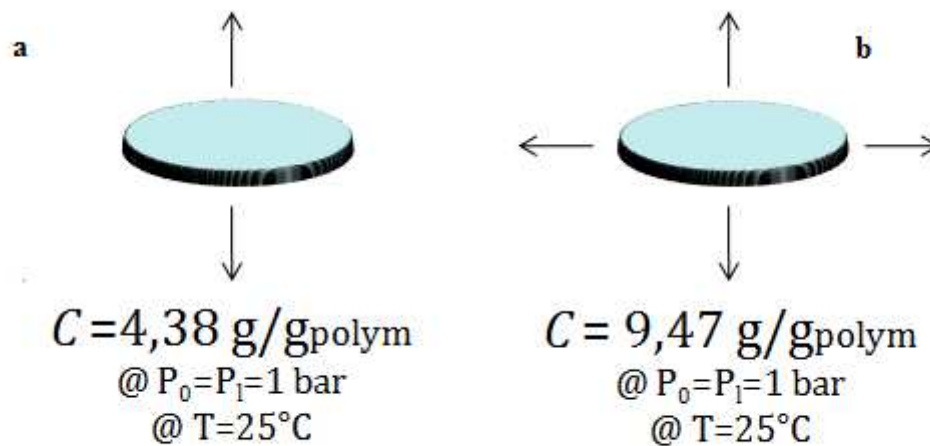


Figure 4.12 a,b : Solubility of component i inside the membrane depending on which the swelling take place

From Fig. 4.12 a,b emerges that at the same operative conditions of pressure and temperature and for the same chemical species the solubility reaches 2 times higher values if the membrane is able to swell in all direction rather than only along the thickness.

Because the membranes are not able to swell in all the directions inside the filtration system, only the swelling out of plane was considered in the calculation.

4.5.4 Mixtures Thermodynamics and Mechanics

To calculate thermodynamic properties an interaction parameter k_{ij} is used as an adjustable binary parameter that induces a correction to default geometric-mean rule for the pair potential energy.

Different procedure can be adopted to evaluate the binary interaction parameter between solvents and membrane:

- From sorption experiments;
- From literature values;
- Imposing equal to zero.

Binary interaction parameters between solvents were calculated from the VLE found in literature as a result of the procedure illustrated in Fig. 4.13.

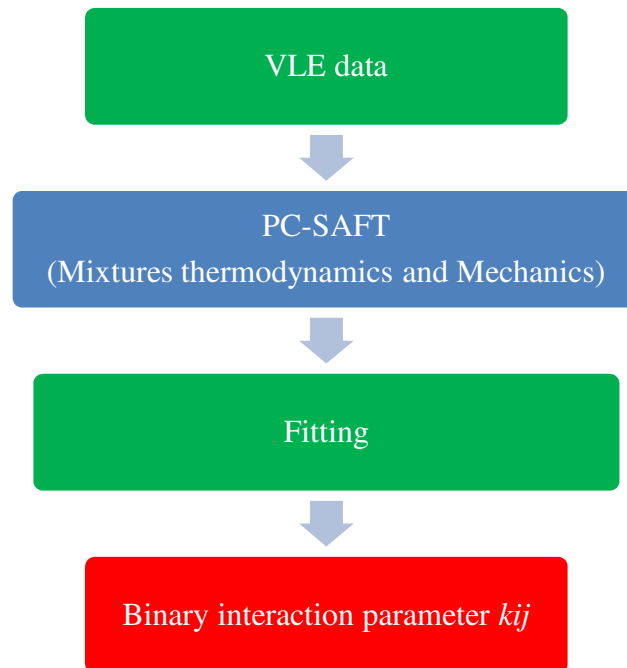


Figure 4.13 : Schematic procedure to calculate binary interaction parameter solvent-solvent

4.5.4.1 k_{ij} from sorption experiments

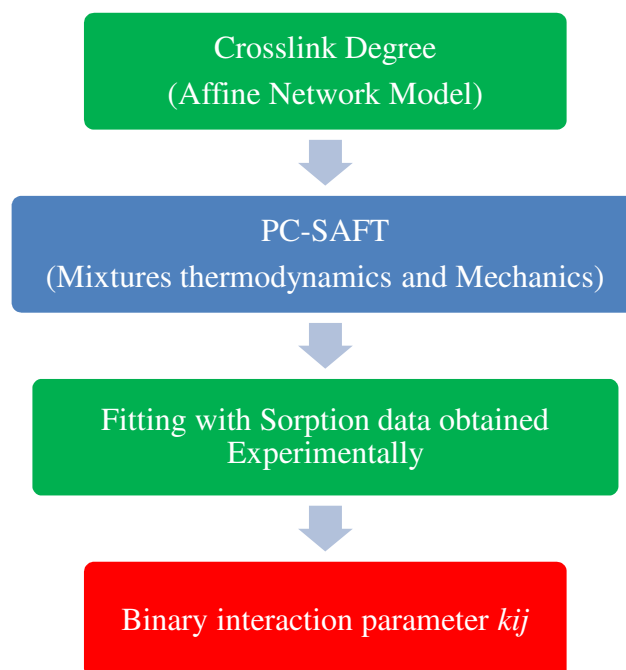


Figure 4.14: Schematic procedure to calculate binary interaction parameter from sorption experiments

The crosslink degree was evaluated setting equal to zero the binary interaction parameter between toluene and the membrane because from the tensile test the trend, but not the crosslink degree values were known.

For the alcohols from the knowledge of the crosslink degree and the sorption value obtained from the experiments described in the previous section of this chapter binary interaction parameters was obtained. The same procedure was followed for the n-hexane because the sorption values obtained experimentally was suffering from a high error.

Table 4.5 shows binary interaction parameters obtained with the procedure reported in Fig. 4.14.

		<i>kij</i> PDMS_1 and PDMS_2
PDMS	Toluene	0
	n-hexane	0.0210
	Ethanol	0.006
	Butanol	-0.070
	Dodecane	0.0210
	Docosane	0.0210

Table 4.5: Binary interaction parameters solvent/solute- membrane

The procedure illustrated in Fig. 4.14 is the same in case in which the solubility was obtained from the literature and not from the experiments.

4.5.4.2 k_{ij} fixed equal to zero

The binary interaction parameters between components and membrane can be placed equal to zero to simplify the problem or because solubility data are not available.

This is not an error because the specific interactions are taking into account in the PC-SAFT. For alcohol species (Fig. 4.3) the equation of state introduce two additional terms, ε^{AiBi} and k^{AiBi} , responsible for the hydrogen bonds.

4.5.5 Diffusion Coefficient or Conductance

4.5.5.1 Pure component

The diffusion coefficient of solvent in polymer $\mathcal{D}_{i,m}$ can be evaluated as illustrated in Fig. 15.

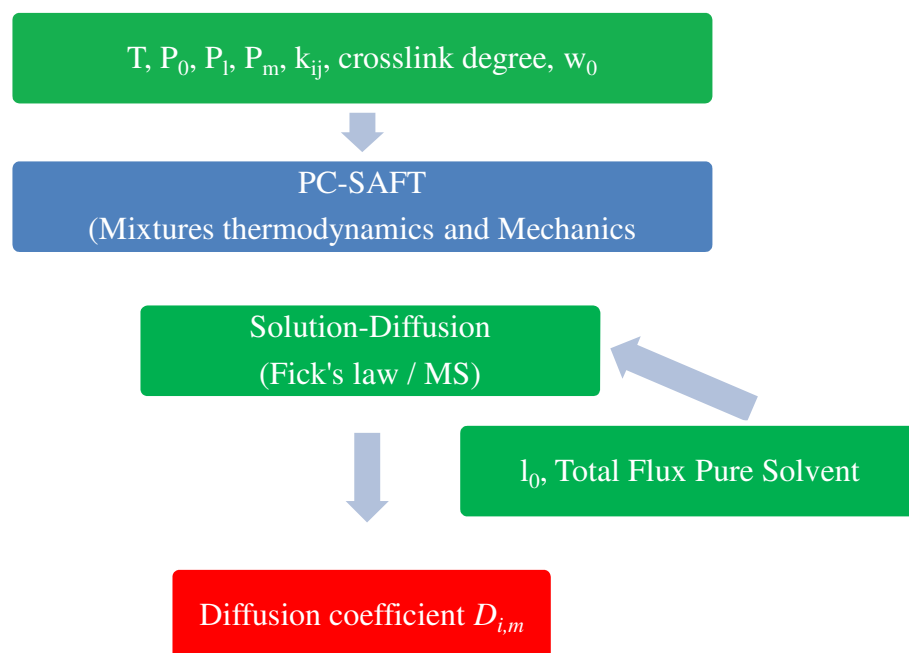


Figure 4.15: Schematic procedure to determine diffusion coefficient solvent-polymer

The information about operative condition such as temperature T and pressure in the feed side P_0 , inside the membrane P_m and in the permeate side P_l , binary interaction parameter and crosslink degree are used inside the PC-SAFT to determine the composition of component i in the membrane feed and permeate side.

For binary system (pure solvent and membrane) the solution-diffusion model is reduced to Eq. 4.9 using Fick's law or MS equation.

Compositions of component i previously determined, membrane thickness in dry conditions l_0 and total flux of pure solvent evaluated from the experiments are introduced in Eq. 4.9 to define the diffusion coefficient between solvent and membrane.

Unfortunately the membrane thickness in dry condition knowledge is not easy definable with these membranes because the active layer (PDMS) cannot be separate from the support one.

4.5.5.1.1 k_{ij} from experiments

The use of k_{ij} obtained from sorption experiments take to determine the diffusion coefficients show in Table 4.6 under the hypothesis that the membrane thickness in dry conditions is equal to $1,07 \mu\text{m}$ for PDMS_1 and $1 \mu\text{m}$ for PDMS_2.

	<i>Dim</i> (m ² /s) PDMS_1 and PDMS_2	<i>Dim</i> (m ² /s) Literature
Toluene	$2,5 \cdot 10^{-10}$	$1,9 \cdot 10^{-9}$ [79]
		$1,2 \cdot 10^{-10}$ [80]
n-hexane	$3,45 \cdot 10^{-10}$	$1,1 \cdot 10^{-10}$ [81]
		$9,0 \cdot 10^{-11}$ [62]
Ethanol	$1,03 \cdot 10^{-9}$	$5,2 \cdot 10^{-10}$ [82]
		$2,0 \cdot 10^{-10}$ [62]
Butanol	$5,87 \cdot 10^{-10}$	$6,0 \cdot 10^{-10}$ [80]
		$6,0 \cdot 10^{-11}$ [62]
		$3,0 \cdot 10^{-11}$ [62]

Table 4.6: Diffusion coefficients of solvent in the membrane

Due to the different values of diffusion coefficient found in literature and to the uncertain membrane thickness the use of binary interaction parameter from experiments was not undertaken.

4.5.5.1.2 k_{ij} fixed equal to zero

Overcoming the errors due to the uncertain membrane thickness and diffusion coefficient is possible by introducing the conductance, ratio between the diffusion coefficient and the thickness.

As said in the paragraph 4.5.4.2, the case of fixed binary interaction parameter equal to zero is not so dramatic because PC-SAFT takes into account the differences between molecules with or without hydrogen bonds.

Under this hypothesis composition of component i in the membrane feed and permeate side was evaluated and applying the transport mechanism equations conductance of component I was found.

In particular the procedure followed is illustrated in Fig.4.16.

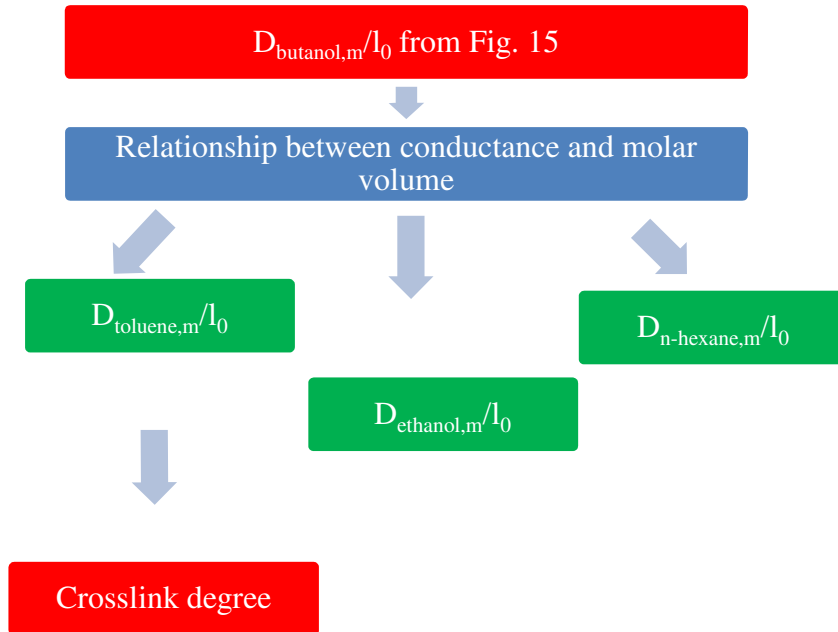


Figure 4.16: Schematic procedure to conductances and crosslink degree

Starting from the conductance value of butanol was possible to evaluate the other conductance applying the following relationship:

$$D_{j,m} = D_{i,m} \left(\frac{\tilde{v}_j}{\tilde{v}_i} \right)^{0,6} \quad (4.24)$$

The Eq. 4.24 [73] extracted from Wilke-Chang estimation method and is in essence an empirical modification of the Stokes-Einstein relationship:

$$D_{AB} = \frac{RT}{6\pi\eta_B r_A} \quad (4.25)$$

where η_B is the viscosity of the solvent and r_A is the radius of the spherical solute.

In the Eq. 4.24 $D_{i,m}$ and $D_{j,m}$ represent the diffusion coefficient of component i and j in the membrane m , while \tilde{v}_i and \tilde{v}_j are molar volume of solvent i and j at their normal boiling temperature.

Butanol was started as initial point because its conductance values is less affected by crosslink degree than the other species, while toluene was chosen to calculate the crosslink degree because the sensitiveness is higher than in other cases.

Table 4.7 displays the conductance of solvents in both membranes and the elastic modulus estimated from crosslink degree.

	D_{im}/l_0 (m/s)				E (MPa)
	Toluene	n-hexane	Ethanol	Butanol	
PDMS_1	$7,13 \cdot 10^{-5}$	$6,32 \cdot 10^{-5}$	$1,02 \cdot 10^{-4}$	$7,80 \cdot 10^{-5}$	0,03
PDMS_2	$1,01 \cdot 10^{-4}$	$8,92 \cdot 10^{-5}$	$1,44 \cdot 10^{-4}$	$1,10 \cdot 10^{-4}$	30,7

Table 4.7: Conductance of solvent in the membrane

The elastic modulus is lower for PDMS_1 where the experimental flux is higher.

5.5.5.2 Binary mixtures

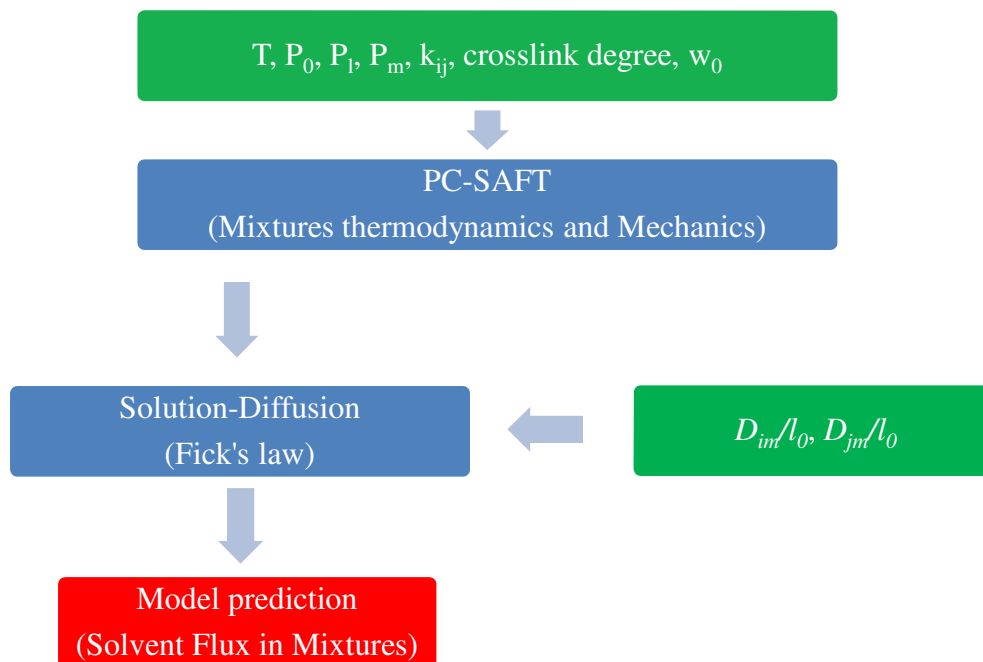


Figure 4.17: Schematic procedure: model prediction of solvent flux in binary mixtures (Fick's law)

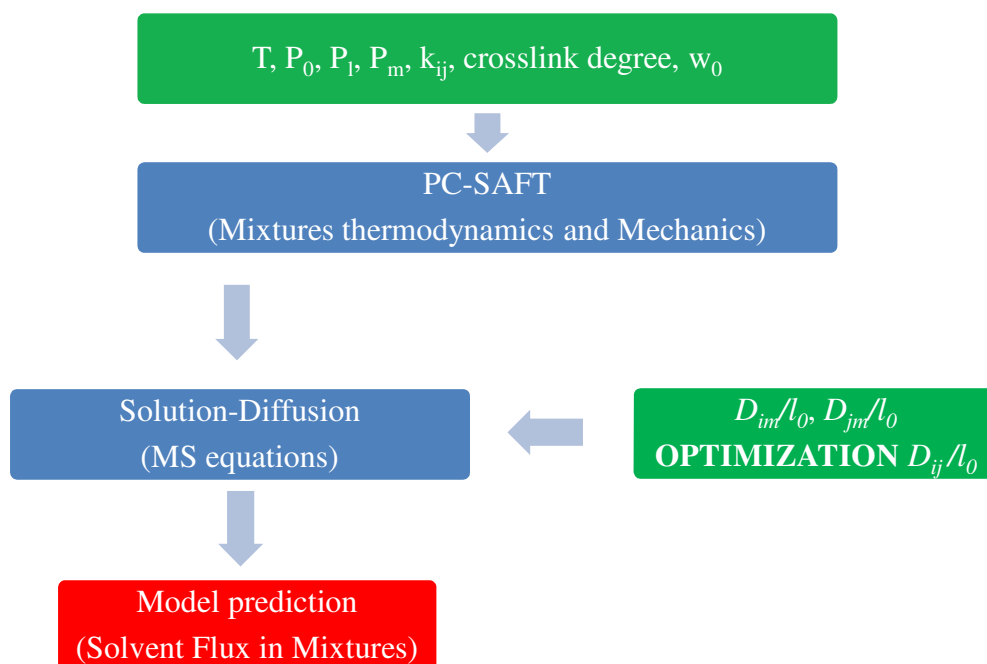


Figure 4.18: Schematic procedure: model prediction of solvent flux in binary mixtures (MS equations)

Fig. 4.17 and 4.18 represent the schematic procedure used to predict solvent flux in binary mixtures applying Fick's law or MS equations to describe transport mechanism.

MS equations, as reported in paragraph 4.5.1.2, differ from the Fick's law for the presence of the term D_{ij}/l_0 that symbolizes the conductance of component i in j . This conductance was determined by the optimization of the transport equation (MS) respect experimental values of flux obtained at different composition of binary mixture.

Table 4.8 reports D_{ij}/l_0 values obtained from the optimization.

	D_{ij}/l_0 (m/s)	
	PDMS_1	PDMS_2
Toluene-nhexane	$1 \cdot 10^{-2}$	$1 \cdot 10^{-2}$
Toluene-Ethanol	$7 \cdot 10^{-4}$	$5 \cdot 10^{-5}$
Toluene-Butanol	$2 \cdot 10^{-3}$	$5 \cdot 10^{-3}$
nhexane-Ethanol	$1 \cdot 10^{-4}$	$5 \cdot 10^{-5}$
nhexane-Butanol	$1 \cdot 10^{-4}$	$1 \cdot 10^{-2}$

Table 4.8: Conductance D_{ij}/l_0 in the membranes

4.5.5.3 Ternary mixtures

In presence of ternary mixtures, two solvents and 0,5 wt% of solute in the mixtures, the procedure become a little more difficult. The solute conductances were evaluated applying the Eq. 4.24, so event in this case the molecules are equate to a sphere.

	D_{km}/l_0 (m/s)	
	Dodecane	Docosane
PDMS_1	$4,53 \cdot 10^{-5}$	$4,37 \cdot 10^{-5}$
PDMS_2	$6,39 \cdot 10^{-5}$	$6,16 \cdot 10^{-5}$

Table 4.9: Conductance of solute k in the membrane

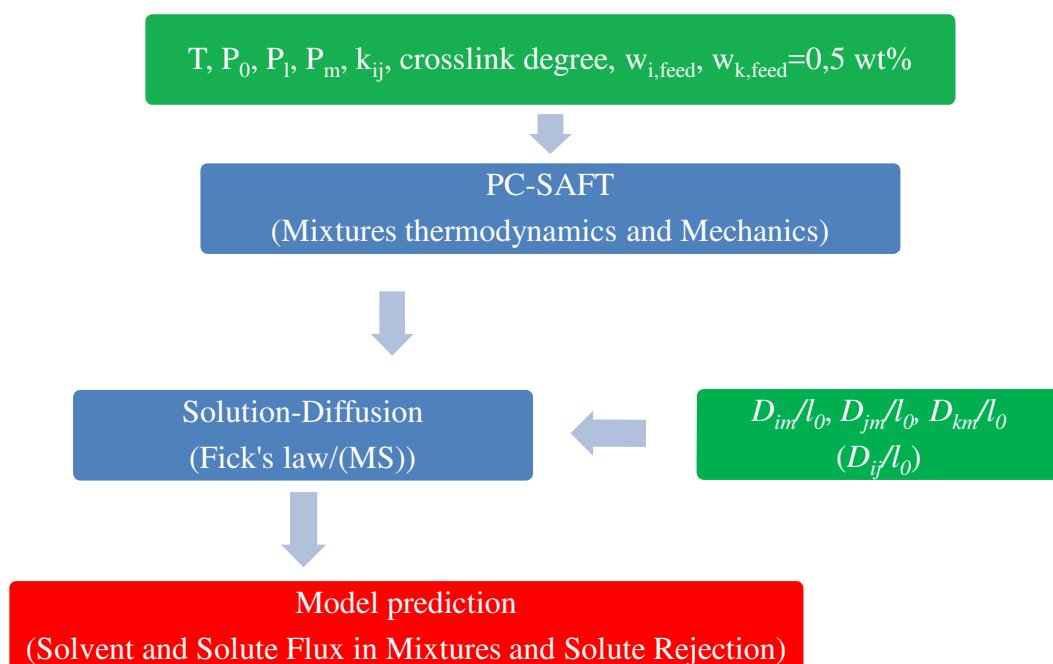


Figure 4.19: Schematic procedure: model prediction of solvent and solute flux and solute rejection in ternary mixtures

4.5.6 Calculation tools

A Fortran's code for the solution of phase equilibrium problems by means of , developed in the past at Memlab's laboratories, was revised to account for the elastic contribution to free energy and implemented with the mechanical characteristics for the membrane in this work and an excel sheet, was possible to describe phase equilibria and the mass transport.

In particular the Fortran's code is able to find the composition of the component i inside the membrane in the feed and permeate side, from the knowledge of the operative conditions such as temperature, upstream and downstream pressure and the weight fraction of component i in

the feed. The code uses the PC-SAFT equation of state, affine network theory to describe the mechanical terms (crosslink degree) and information such as:

- Molecular weight;
- PC-SAFT parameters;
- Interaction parameter solvent-solvent;
- Interaction parameter solvent-membrane;
- Crosslink degree.

These information are located inside Fortran's library.

Once the equation of state has been chosen, the first input required regards the number of solute components (solutes and solvents inside the mixtures) and it is possible to insert a number up to three. Successively it will be necessary to report the name or an acronym of the solvents, solutes and polymer present in the system. The name has to be equal to that present in the Fortran's library. Later the temperature is request with the information about the way in which the swelling due to the crosslink degree takes place. In particular the number that has to be insert are referred to the swelling in plane or out of plane. The value used will change the final output (fugacity and solubility of component i in the membrane). The last input parameter is related to the pressure in the reach-phase (membrane) and free-phase (feed or permeate).

The output data regards the activity coefficient, fugacity and solubility of component i in case of pure components or all solvents and solutes in case of mixture.

This step is important because the solubility output value will be the input inside the excel file. As said previously the excel sheet contains the balances, reported in chapter 4, in which the output will be:

- Diffusion or conductance;
- Flux and rejection.

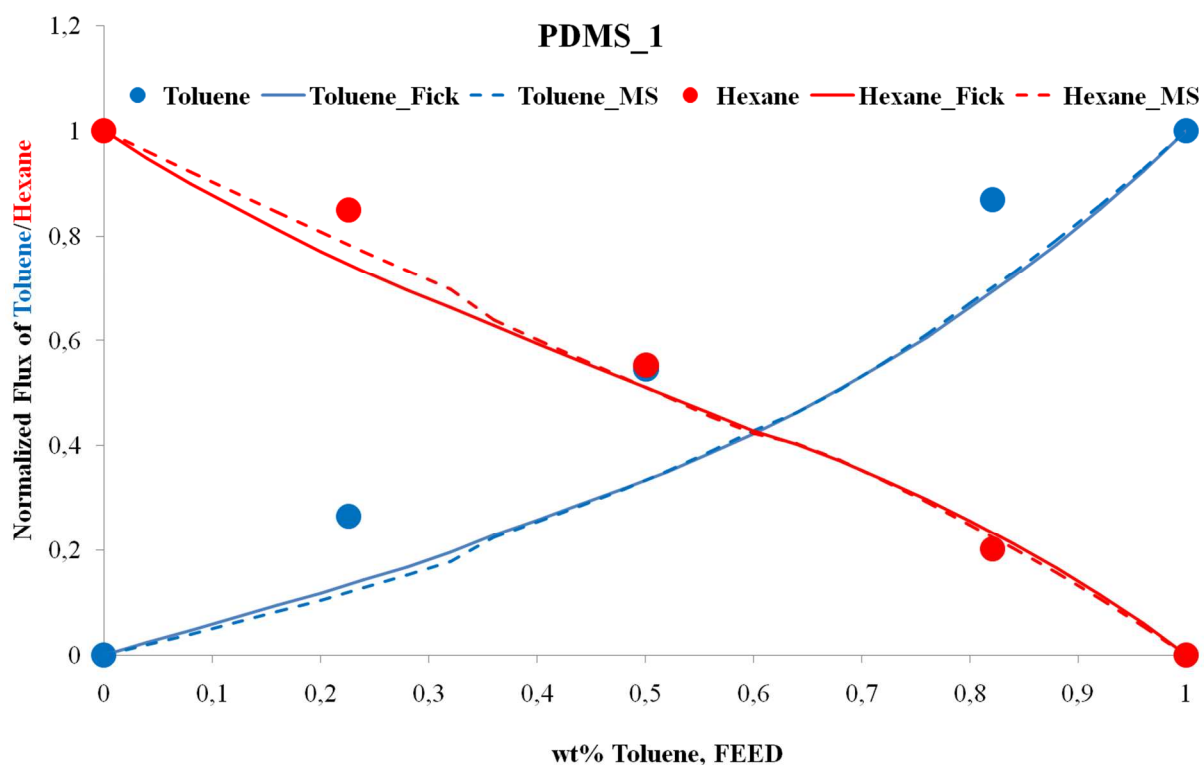
Inside the excel file the input data are the solubility values obtained with the code beforehand described at different composition, operative conditions and weight fraction of component i in the feed.

4.6 Results

4.6.1 Toluene-Hexane Mixtures

Figures 4.20 a,b report normalized flux prediction versus weight composition of component i in the feed side. The model developed is a prediction tool able to give account of the linear trend that is obtained working with similar solvent: toluene and n-hexane mixtures in this work.

Working with similar solvents inside the mixture (toluene-hexane) the model predicts a linear trend for both species and in particular increasing the composition of component i , normalized flux increases, as obtained experimentally. The differences between Fick's law or MS equations to describe transport mechanism are not so obvious.



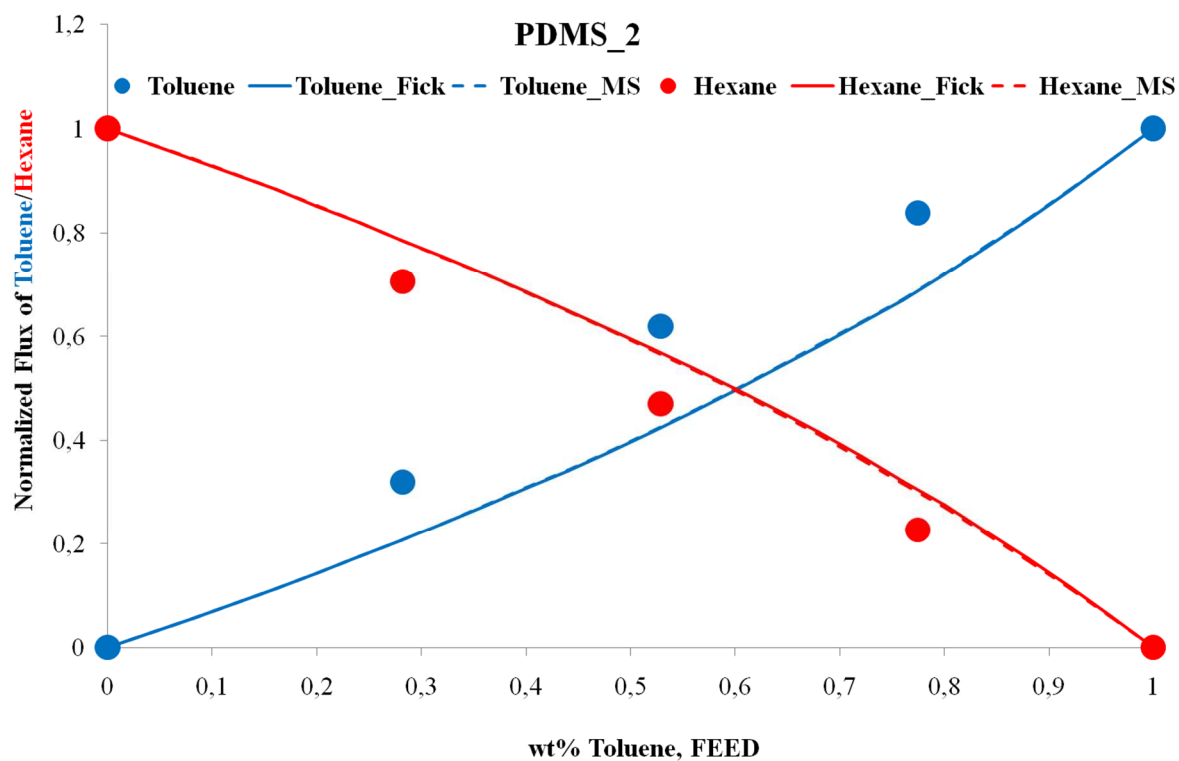


Figure 4.20 a,b: Normalized flux prediction of toluene and n-hexane vs toluene feed composition applying Fick's law and MS equations

Adding 0,5 wt% to this mixture, the rejection in terms of dodecane and docosane was obtained.

Figures 4.21 a,b show that the solute rejection does not change with the composition of the component *ias* as obtained experimentally. In both cases the model predict that the rejection for docosane is higher than dodecane.

Fig. 4.21 a report that MS equations are able to look alike to the experimental data, while Fig. 4.21 b shows the opposite.

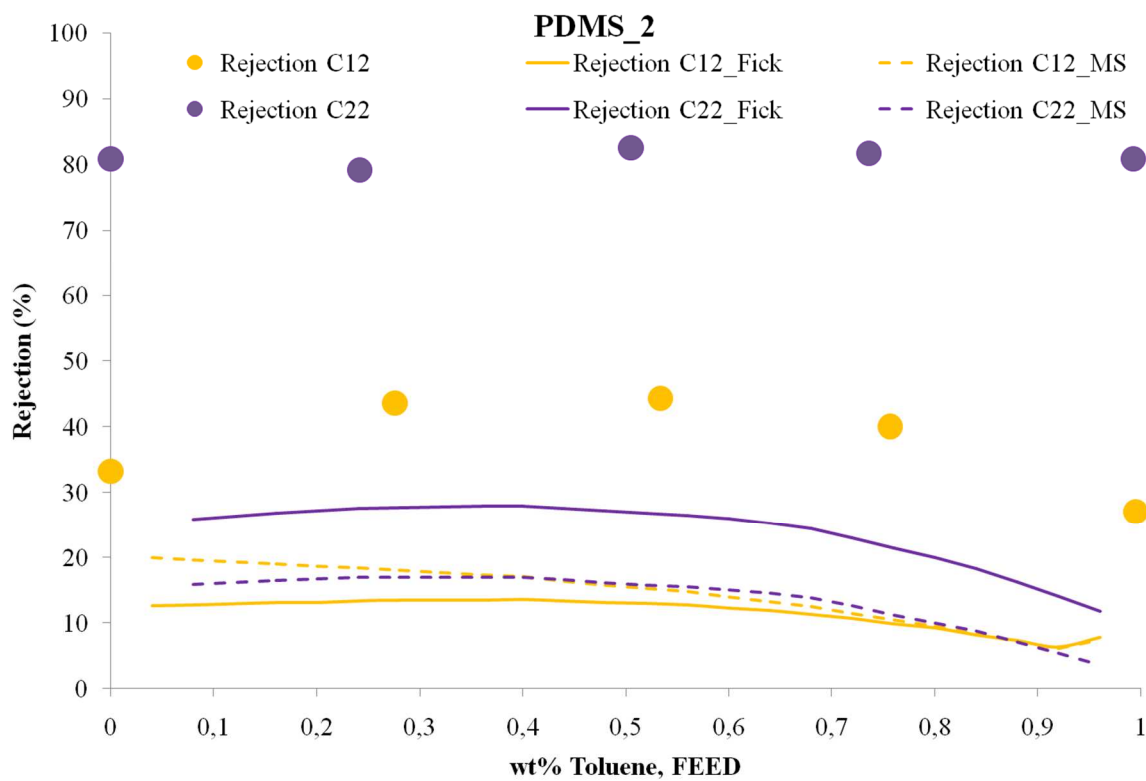
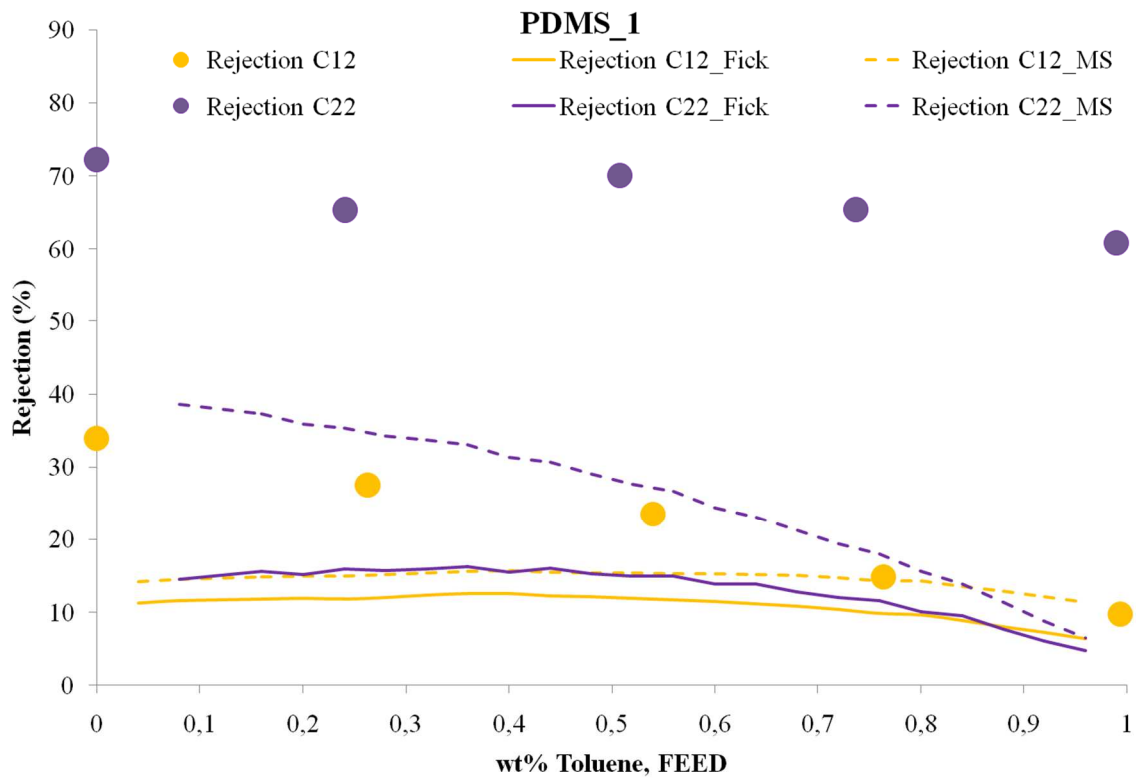


Figure 4.21 a,b: Rejection prediction of solutes vs toluene feed composition in toluene-hexane mixture applying Fick's law and MS equations

4.6.2 Hexane-Ethanol mixture

Figures 4.22 show normalized flux prediction versus weight composition of component i in the feed side.

The model is able to predict that the normalized flux trend is not linear as obtained experimentally. It is also able to describe that normalized flux of ethanol presents a maximum around 75% of alcohol inside the mixture. This phenomena is predominant for PDMS_1 than for PDMS_2 probably because the flux is higher.

Normalized flux for hexane is linear increasing alkane content in the mixture.

For both membranes the differences between Fick's law and MS equations are not so relevant as observed for toluene-hexane mixture.

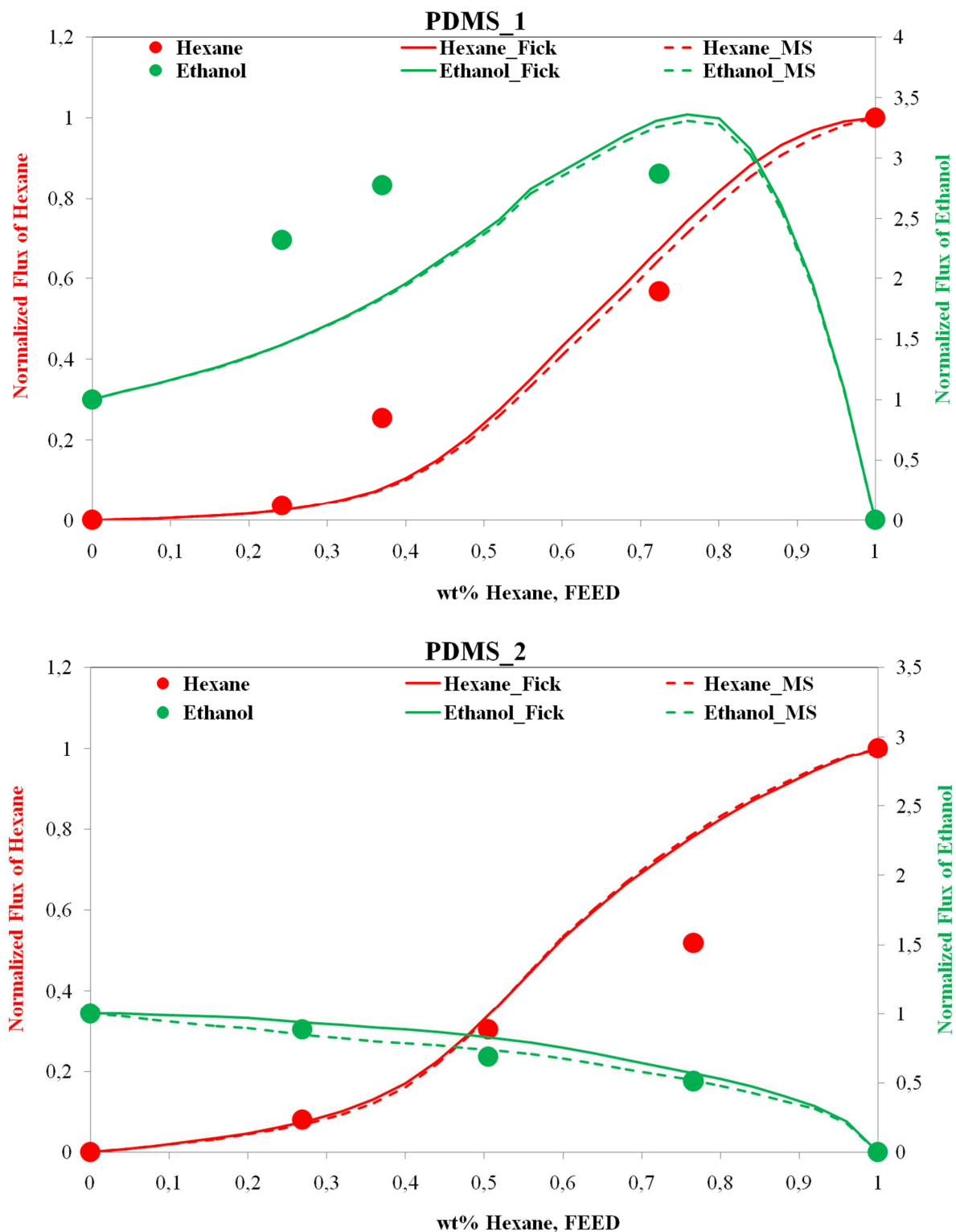


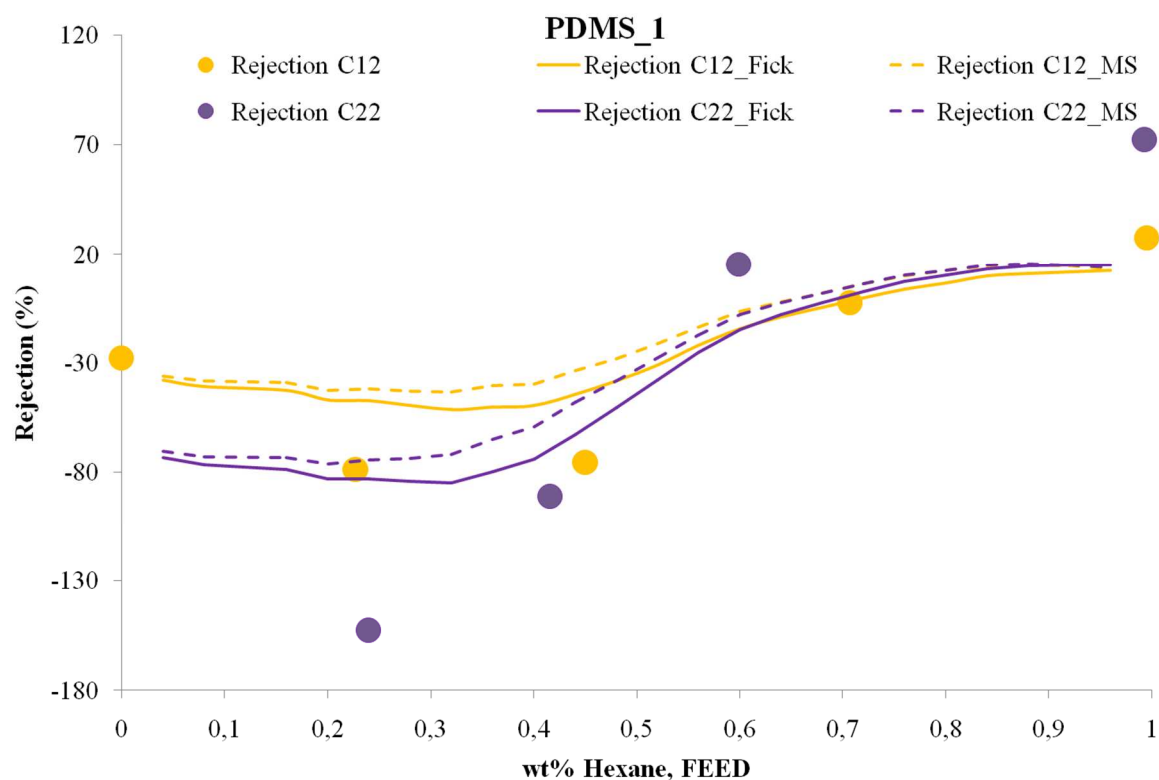
Figure 4.22 a,b: Normalized flux prediction of n-hexane and ethanol vs n-hexane feed composition applying Fick's law and MS equations

As in the previous case the rejection of solutes is obtained adding 0,5 wt% of dodecane and docosane to this mixture.

Figures 4.23 a,b show that the solute rejection change with the composition passing from negative to positive values.

The model is able to describe the trend of the alkanes rejection that changes from positive to negative values increasing the alcohol content. The predicted model is also able to discover the minimum of rejection close to 75% of alcohol in the mixture observed fro dodecane.

Fig. 4.23 b shows that MS equation represents worse the rejection of docosane.



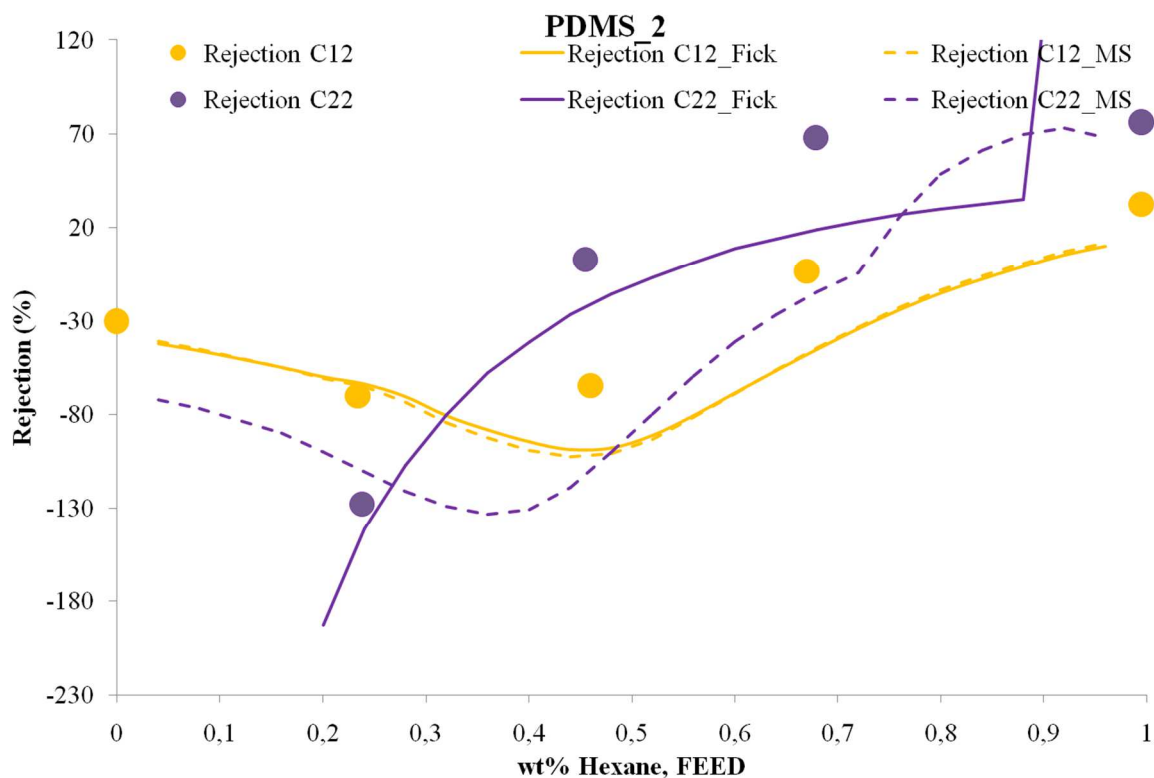


Figure 4.23 a,b: Rejection prediction of solutes vs n-hexane feed composition in hexane-ethanol mixture applying Fick's law and MS equations

In Appendix D, all the other binary and ternary mixtures results in terms of model prediction flux and alkanes rejection will be find.

4.7 Conclusions

Characterization of two commercial PDMS-based membranes was carried out with the purpose of develop a model able to explain flux and rejection behavior in binary and ternary mixtures. From the experimental characterization the membranes have shown similar nature but the results in terms of flux were different. Concerning the flux, PDMS_1 membrane exhibited towards alkanes three times higher flux than PDMS_2, but regarding alcohols the flux was higher for PDMS_2. Because the membrane nature is the same for both commercial membranes the reason for differences in terms of permeability need to be searched for around the crosslink degree.

The tests performed about solubility and elastic modulus have been used in a relative way because it was not possible to efficiently separate the PDMS layer from the support one. Solubility experiments were carried out using pure solvents at the temperature of 25°C, while tensile tests were performed with vapors of toluene and n-hexane at different fugacities. These experiments, although not directly used for the modeling, explained the crosslink effect on the performance results. The solubility is higher for PDMS_1 where the elastic modulus is lower.

To describe the experimental results a model based on the solution-diffusion model was developed using thermodynamic and mechanical properties.

Thermodynamic properties such as solubility of component i inside the membrane feed and permeate side were calculated with the help of the PC-SAFT equation of state. Binary interaction parameters between solvent and membrane were fixed equal to zero to simplify the model and because the absence of solubility results or reliable literature data, while binary interaction parameter between solvents were evaluated from VLE data found in literature.

Mechanical properties such as crosslink degree were considered in the model applying the affine network theory. The elastic pressure calculated with this theory is added to the pressure evaluated with the PC-SAFT.

Thermodynamics and Mechanical properties were introduced in the transport mechanism model. Fick's law and Maxwell-Stefan equations were used and compared as solution diffusion description.

Because it was not possible to estimated the active layer thickness, the conductance instead the diffusion coefficient was used in the model. The conductance was defined as the ratio between diffusion coefficient and thickness. The conductance of butanol was calculated from the flux of pure solvent obtained experimentally because its value is less affected by the crosslink degree. From its value the other conductance were calculated from a relationship between the conductance and molar volume. Crosslink degree was appreciated once the conductance of toluene was obtained.

Under these hypothesis conductances and elastic modulus were obtained and PDMS_2 shown 2 order higher elastic modulus than PDMS_1. The values evaluated were in agreement with the experimental results.

The model developed is a predict model and it was able to predict in a good way the experimental results in terms of flux. The flux trend is linear working with similar components inside the mixture and it is not linear with alcohol-alkane mixture. The model was able to identify the maximum of flux obtained experimentally increasing the amount of alcohol in the mixture.

The model was also able to predict the trend of the rejection of solutes obtained experimentally: no changes in rejection observed experimentally with alkanes mixtures and changes in rejection from positive to negative values observed for alcohol-alkane mixtures. Trends were satisfied, but not the absolute values probably because the relationship used to evaluate the solutes conductance is not completely right if the molecules are too long or heavy.

However the model can be improved evaluating diffusion coefficient and crosslink degree from independent tests such as solubility and tensile experiments.

Chapter 5

CONCLUSIONS

With aim to contribute to the analysis of coupled mechanical - mass transport problems in polymeric materials and to the development of tools for their characterization and modeling, two different cases were considered and approached in distinct activities in this work: characterization of in-plane stress induced by vapor sorption in polymer coatings and modeling of membrane transport in organic solvents nanofiltration systems.

The first problem was evaluated starting from a mechanical point of view. The in-plane stress arisen in polymer coating below the glass transition temperature as result of vapor sorption/desorption processes was evaluated in time. The in-plane stress was measured using bending beam cantilever technique at different temperature and using different fugacity of solvents inside the system. From the mechanical properties (stress state), knowing the material properties, the change in volume recorded during sorption/desorption process was derived. Through the use of non-equilibrium lattice fluid model (NELF) it was then possible to estimate vapor mass uptake/release in coating. Thermodynamic properties were evaluated at different speed rate of fugacity content with the help of mechanical properties. As a result of this specific activity, an apparatus suitable to the characterization of in-plane stress development and relaxation in coating films as induced by vapor sorption/desorption was developed and tested, which can be used in parallel with QCM technique to have independent information about stress and solute concentration in the system. Further efforts are needed to have additional independent information about volume swelling in the system, although the latter measurement is complicated by reduced thickness of coating films which need to be used in this kind of experiments in order to minimized diffusion time with respect to relaxation time. By performing an extensive experimental campaign which combines QCM and Bending Beam data for the same polymer-solute system, for the case of different operating conditions, the possibility is expected to define constitutive relations for stress relaxation/volume dilation and solubility evolution in time for an arbitrary process in which a glassy polymeric system is exposed to gases or vapor components.

The second problem was solved after performance characterization of two commercial PDMS-based membranes. From experimental results a predicting model was developed to explained flux and rejection values obtained. The model based on the solution-diffusion theory was applied using Fick's law and Maxwell-Stefan equations. The transport mechanism was evaluated with the support of thermodynamic and mechanical properties. Mixture thermodynamic was explained using the PC-SAFT equation of state while crosslink degree was estimated using affine network theory. The comparison between experimental results taken in wide range of feed conditions and predictions from the model here developed allows to conclude that most of complex features shown by separation performances of PDMS OSN

membranes can be satisfactorily described when a proper thermodynamic description is given which accounts for specific elastic properties of the polymeric material and for pertinent mechanical constraint exerted.

APPENDIX A

APPENDIX A: PERFORMANCE CHARACTERIZATION

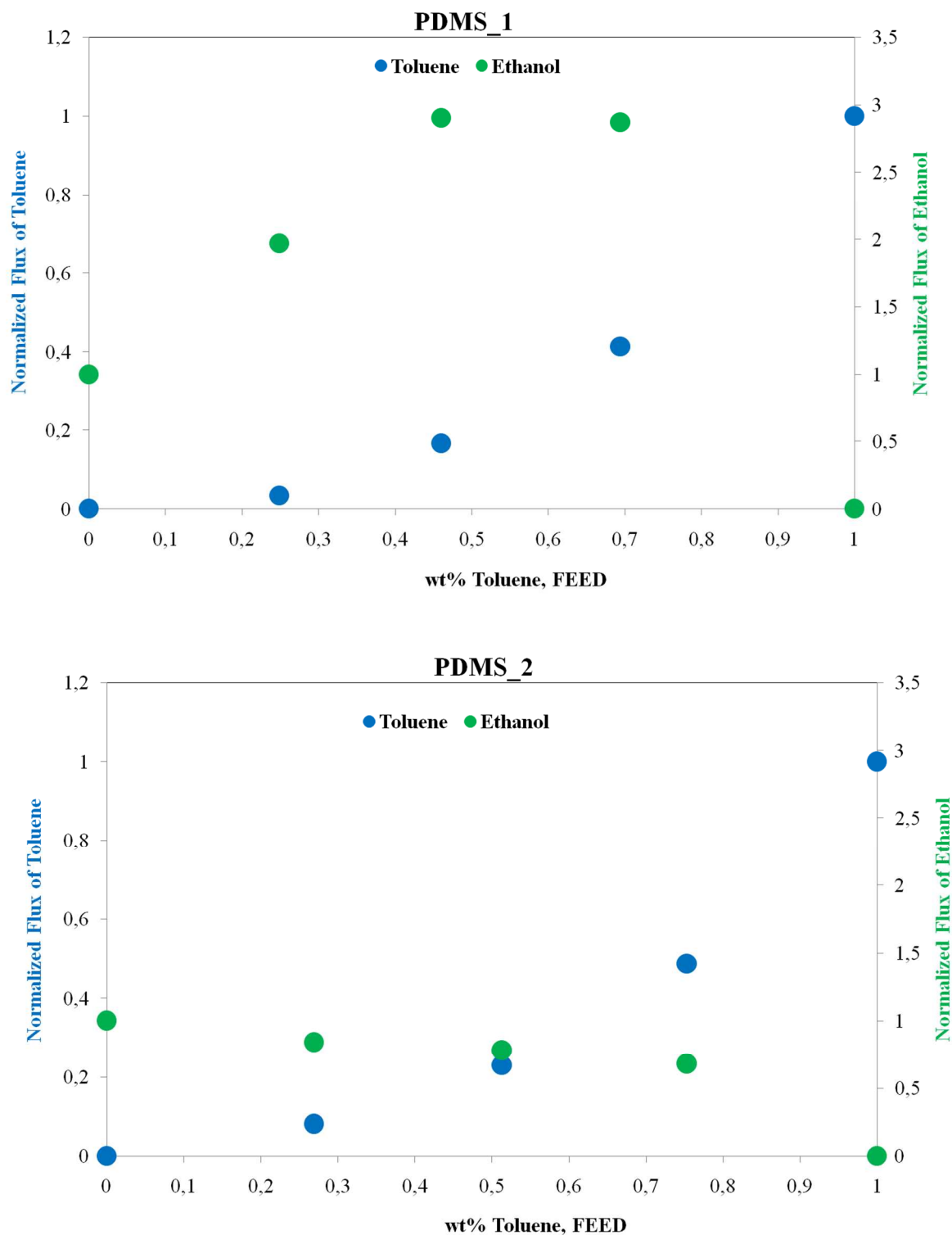


Figure A.1 a,b: Normalized flux of toluene and ethanol vs toluene feed composition in PDMS_1 and PDMS_2

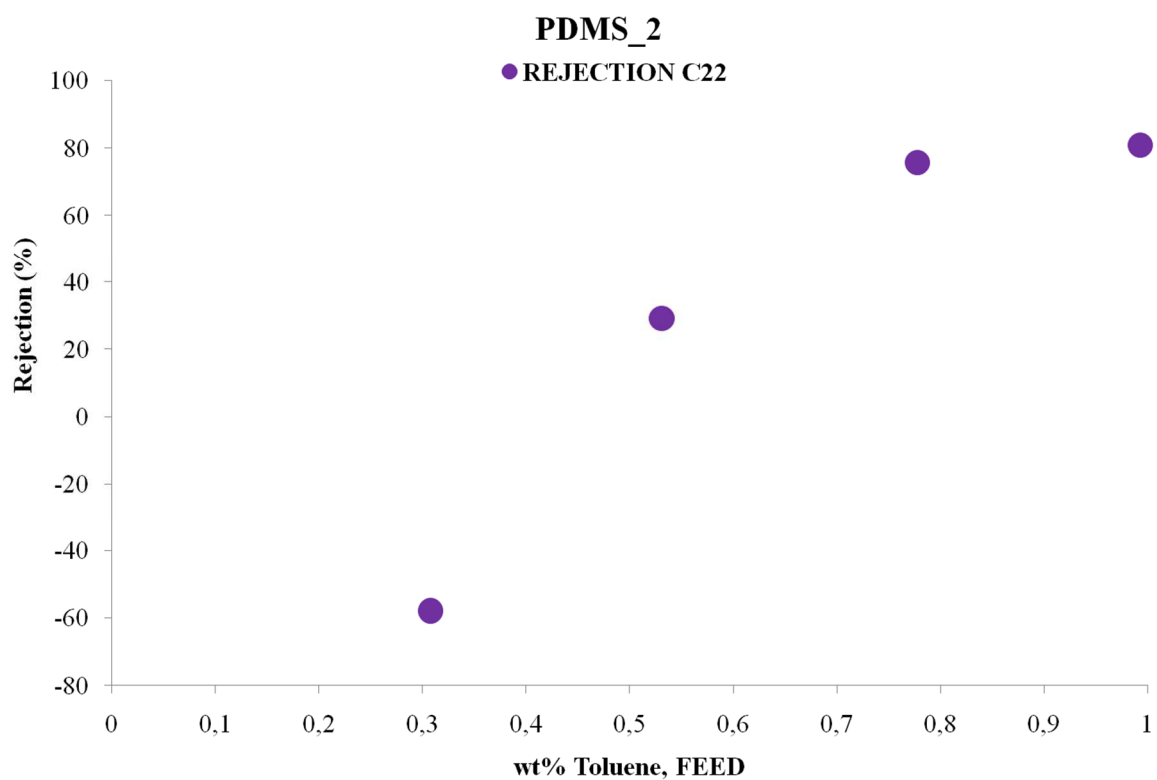
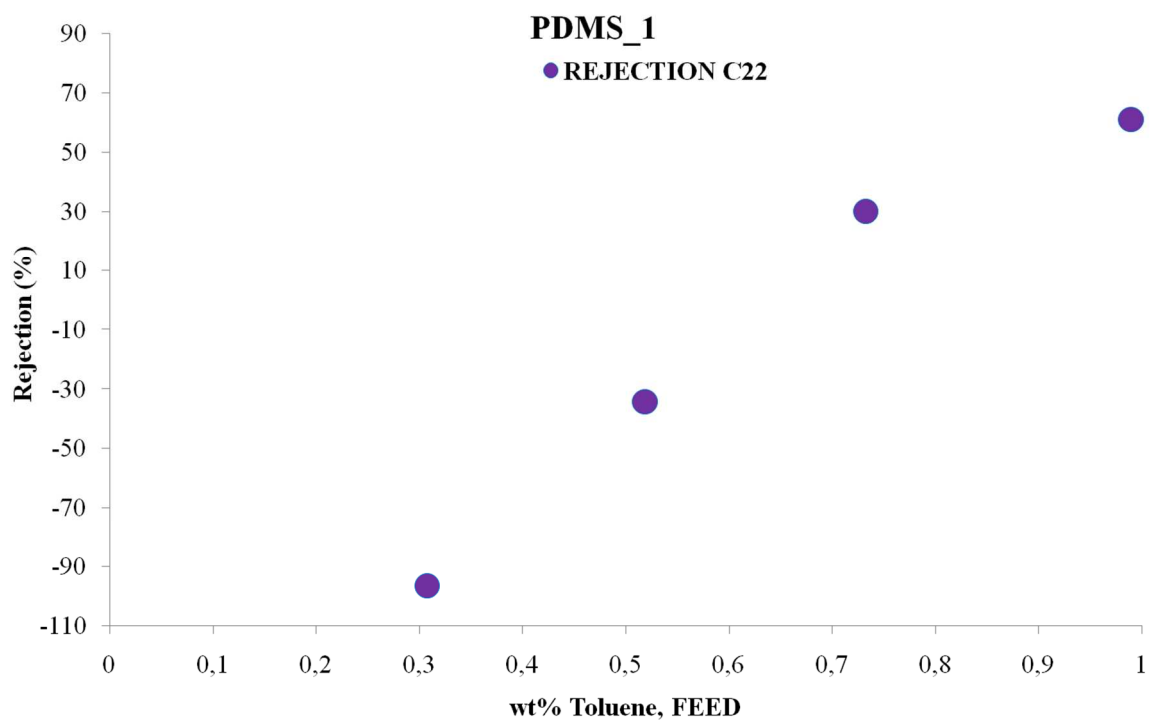


Figure A.2 a,b: Rejection of solutes vs toluene feed composition in toluene-ethanol mixture for PDMS_1 and PDMS_2

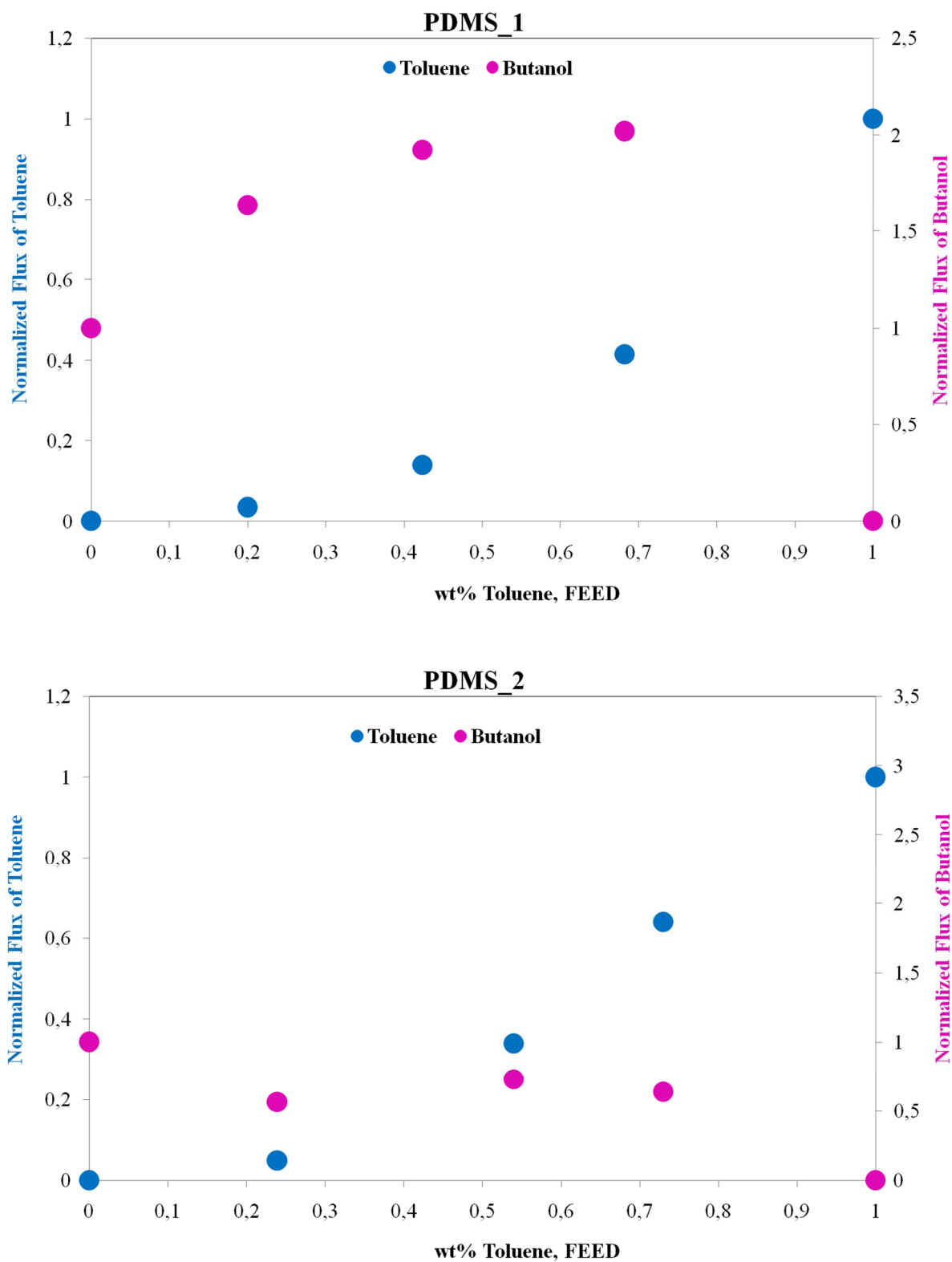


Figure A.3 a,b: Normalized flux of toluene and butanol vs toluene feed composition in PDMS_1 and PDMS_2

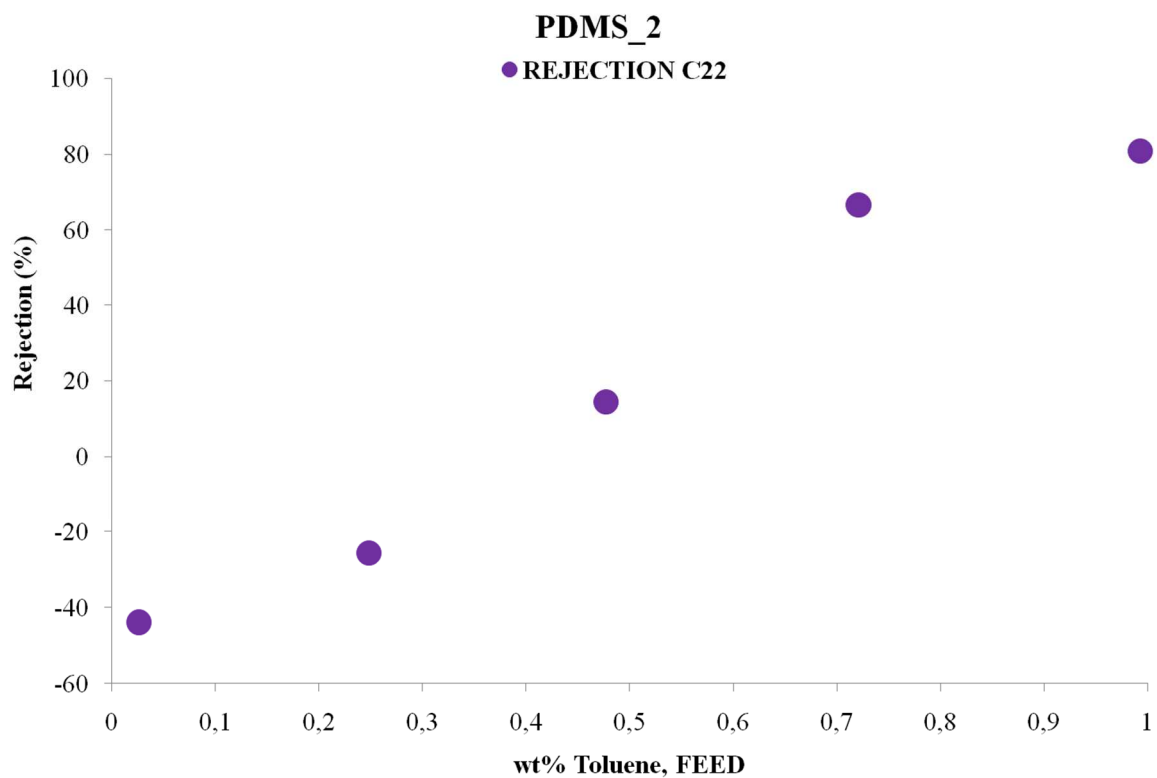
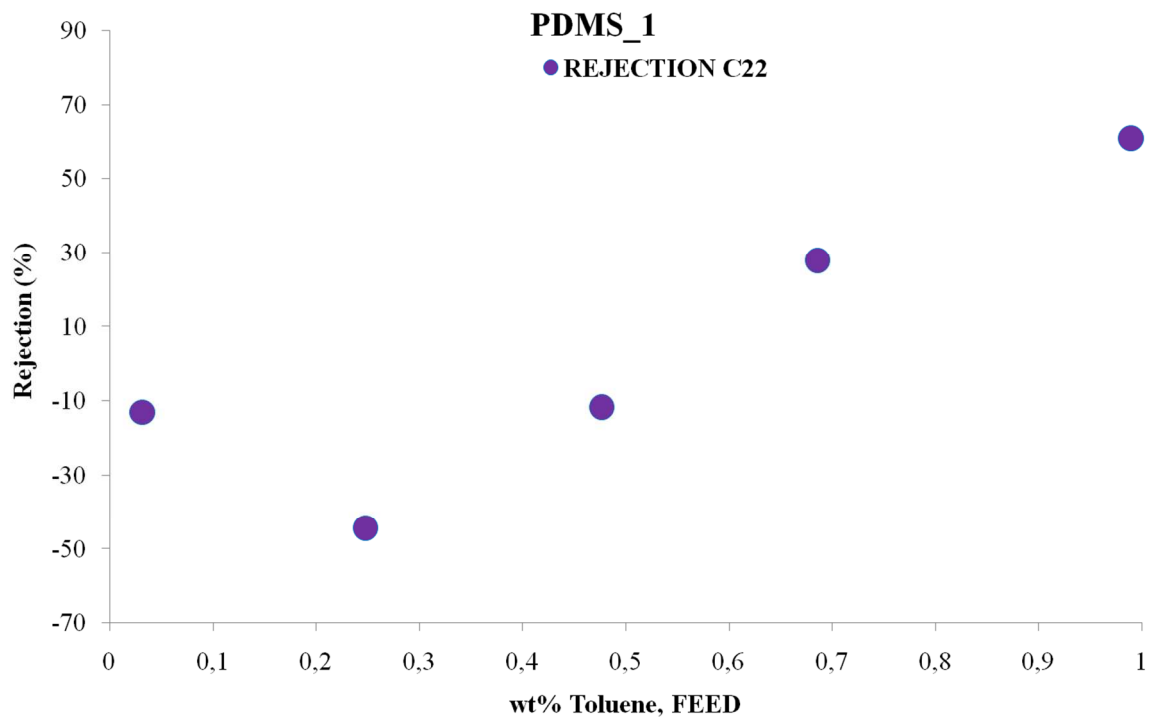


Figure A.4 a,b: Rejection of solutes vs toluene feed composition in toluene-butanol mixture for PDMS_1 and PDMS_2

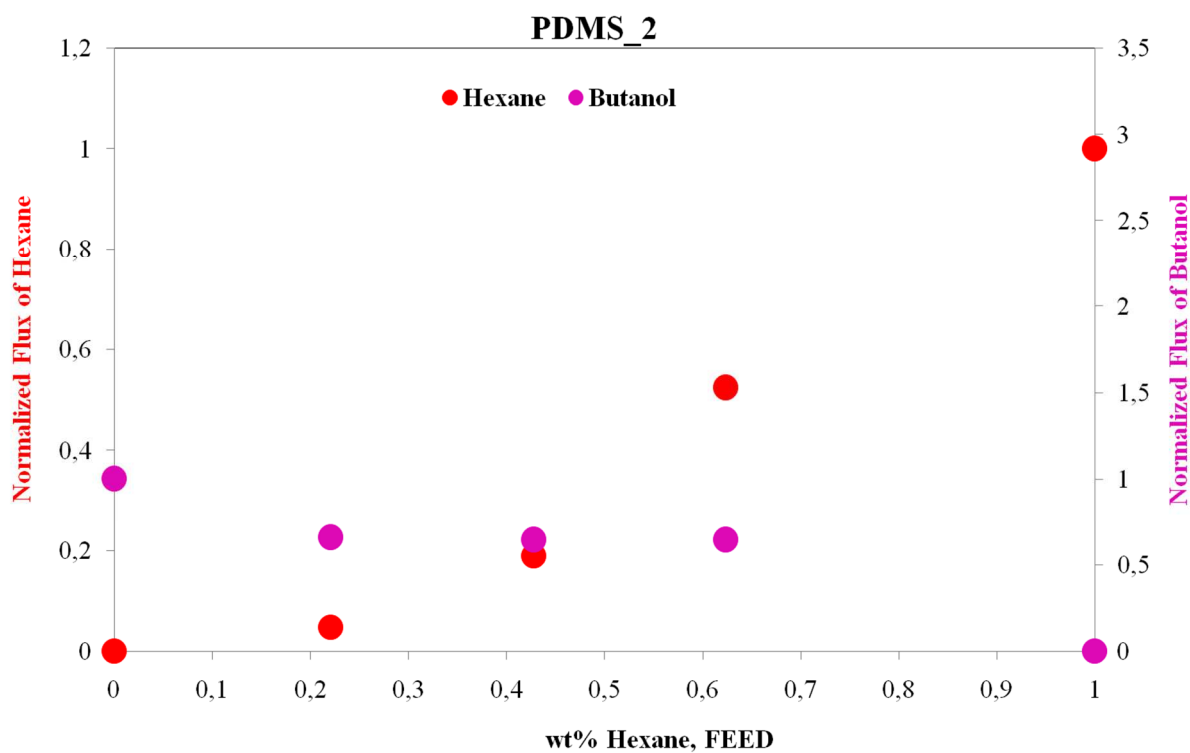
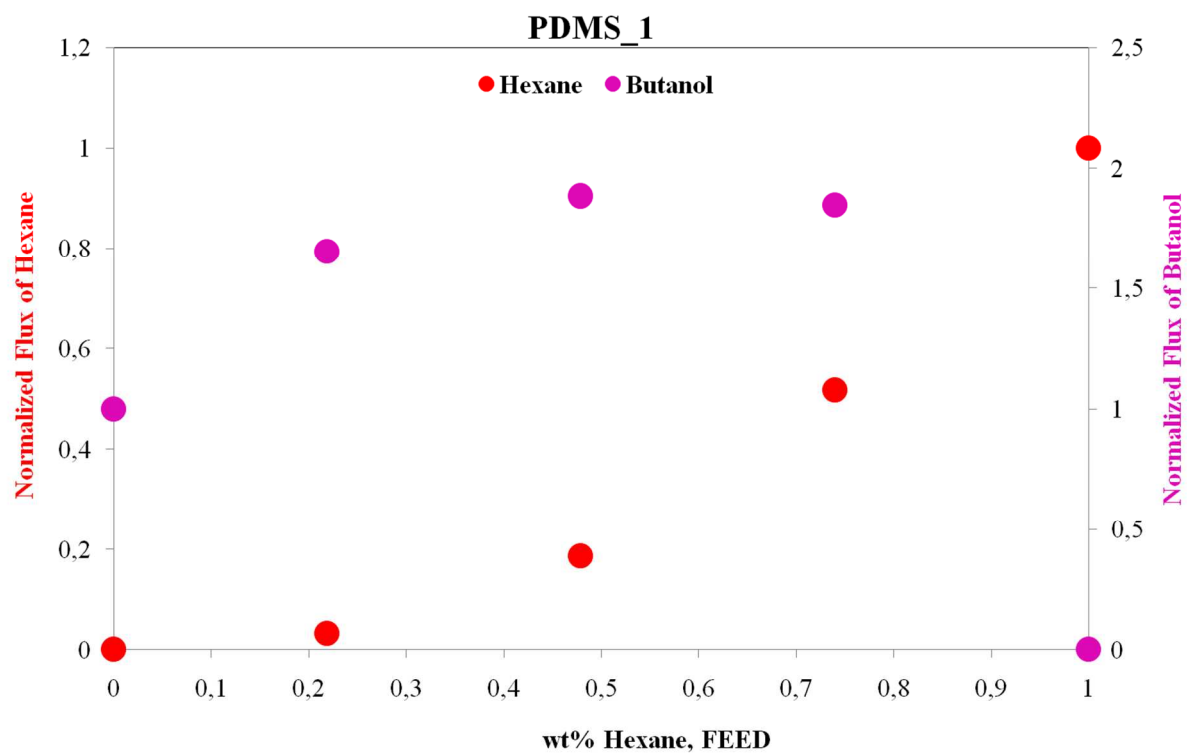


Figure A.5 a,b: Normalized flux of hexane and ethanol vs hexane feed composition in PDMS_1 and PDMS_2

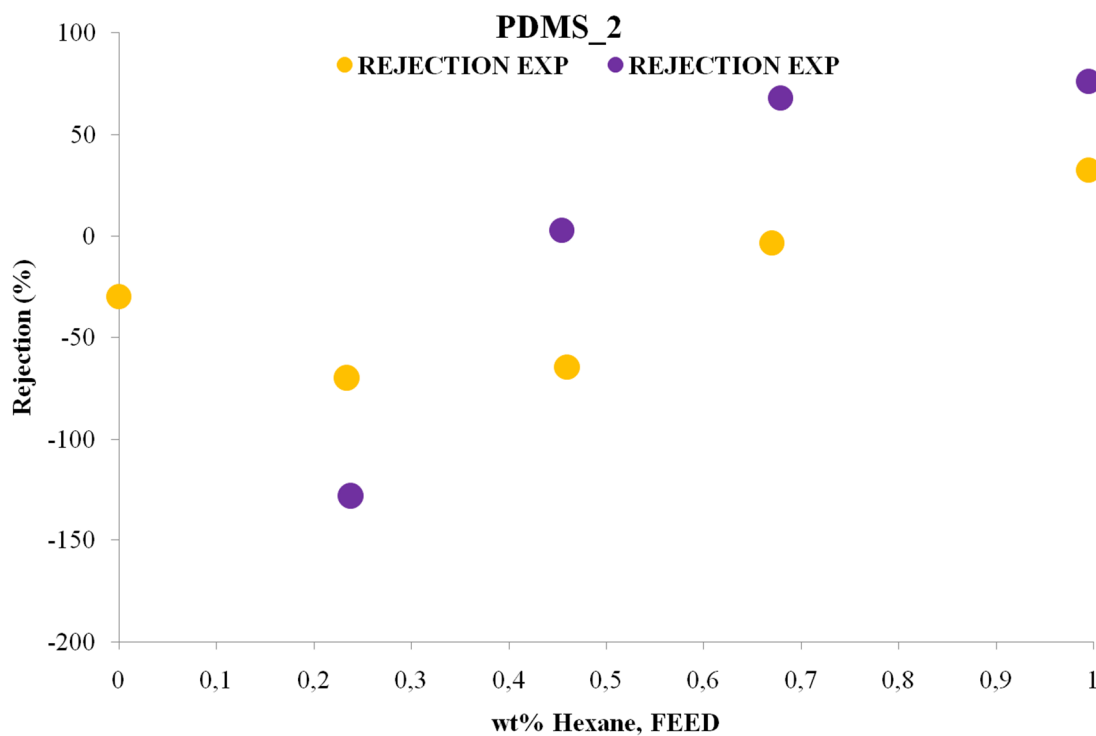
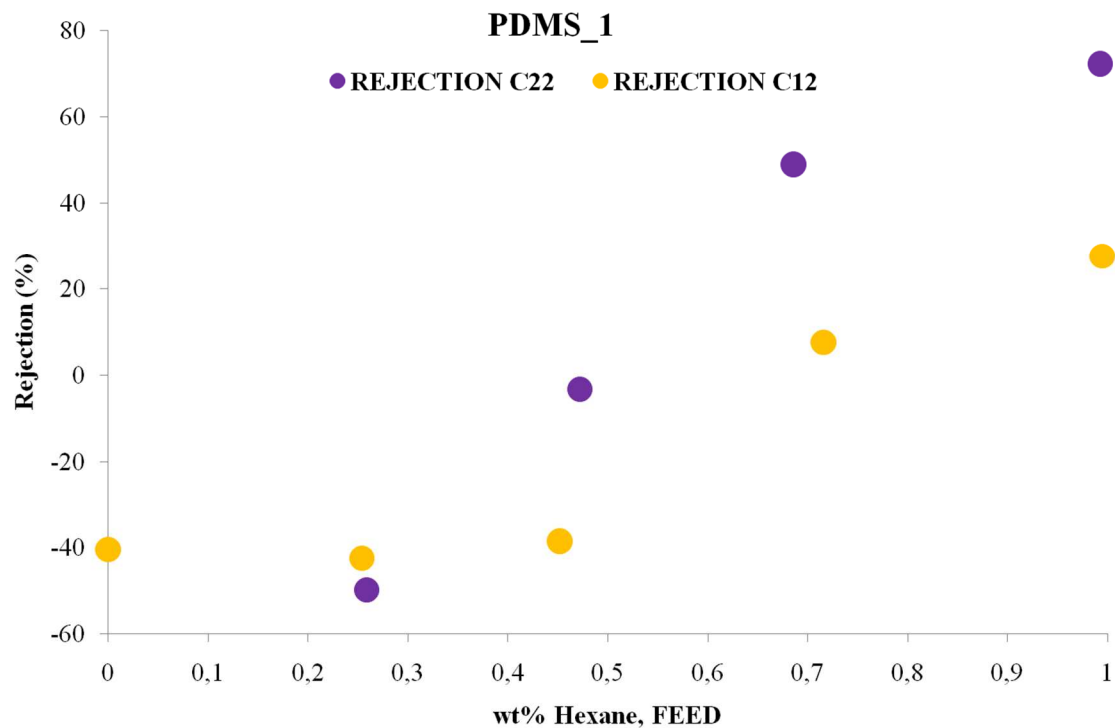


Figure A.6 a,b: Rejection of solutes vs toluene feed composition in hexane-butanol mixture for PDMS_1 and PDMS_2

APPENDIX B

APPENDIX B: FICK'S LAW ANALYSIS FOR TERNARY MIXTURES

Components i , j and k are the two solvents and one solute inside the ternary mixture.

$$n_i(1 - w_i) = (n_j + n_k)w_i - \rho D_{im} \frac{dw_i}{dz} \quad (\text{B.1})$$

$$n_j(1 - w_j) = (n_i + n_k)w_j - \rho D_{jm} \frac{dw_j}{dz} \quad (\text{B.2})$$

$$n_k(1 - w_z) = (n_i + n_j)n_k - \rho D_{km} \frac{dw_k}{dz} \quad (\text{B.3})$$

Replacing:

$$A = (1 - w_i)$$

$$B = (1 - w_j) \quad (\text{B.4})$$

$$C = (1 - w_z)$$

Eqs. (B.1), (B.2) and (B.3) become:

$$n_i A = (n_j + n_k)w_i - \rho D_{im} \frac{dw_i}{dz} \quad (\text{B.5})$$

$$n_j B = (n_i + n_k)w_j - \rho D_{jm} \frac{dw_j}{dz} \quad (\text{B.6})$$

$$n_k C = (n_i + n_j)n_k - \rho D_{km} \frac{dw_k}{dz} \quad (\text{B.7})$$

Substituting Eq. (B.6) in (B.5):

$$n_i A = \left(\frac{(n_j + n_k)w_j - \rho D_{jm} \frac{dw_j}{dz}}{B} + n_z \right) w_i - \rho D_{im} \frac{dw_i}{dz} \quad (\text{B.8})$$

$$n_i D = \left(n_z w_i (w_j + B) - w_i \rho D_{jm} \frac{dw_j}{dz} \right) - B \rho D_{im} \frac{dw_i}{dz} \quad (\text{B.9})$$

$$\text{with } D = (AB - w_i w_j)$$

Substituting Eq. (B.6) in (B.7):

$$n_k C = \left(n_i + \frac{(n_i + n_k) w_j - \rho D_{jm} \frac{dw_j}{dz}}{B} \right) n_k - \rho D_{km} \frac{dw_k}{dz} \quad (\text{B.10})$$

$$n_k E = \left(n_i w_k (B + w_j) - w_k \rho D_{jm} \frac{dw_j}{dz} \right) - B \rho D_{km} \frac{dw_k}{dz} \quad (\text{B.11})$$

$$\text{with } E = (CB - w_j w_k)$$

Substituting Eq. (B.11) in (B.9):

$$n_i D = \left(\frac{n_i w_k (B + w_j) - w_k \rho D_{jm} \frac{dw_j}{dz} - B \rho D_{km} \frac{dw_k}{dz}}{E} \right) w_i (w_j + B) - w_i \rho D_{jm} \frac{dw_j}{dz} - B \rho D_{im} \frac{dw_i}{dz} \quad (\text{B.12})$$

$$n_i F = -B E \rho D_{im} \frac{dw_i}{dz} - w_i \rho D_{jm} \frac{dw_j}{dz} (w_j w_k + B w_k + E) - w_i B \rho D_{km} \frac{dw_k}{dz} (w_j + B) \quad (\text{B.13})$$

$$\text{with } F = (DE - w_i w_k (B + w_j)^2)$$

Placing $G = (w_i w_k + B w_k + E)$ and $H = (B + w_j)$

$$n_i = \frac{B E \rho D_{im} (w_{i,0} - w_{i,l}) + \rho D_{jm} w_i G (w_{j,0} - w_{j,l}) + \rho D_{km} w_i B H (w_{k,0} - w_{k,l})}{l F} \quad (\text{B.14})$$

Substituting (B.14) in (B.11)

$$n_k E F = -B E H w_k \rho D_{im} \frac{dw_i}{dz} - \rho D_{jm} w_k I \frac{dw_j}{dz} - \rho D_{km} B L \frac{dw_k}{dz} \quad (\text{B.15})$$

Placing $I = (w_i G H + F)$ and $L = (w_i w_k H^2 + F)$

$$n_k = \frac{B E H n_k \rho D_{im} (w_{i,0} - w_{i,l}) + w_k I \rho D_{jm} (w_{j,0} - w_{j,l}) + \rho D_{km} B L (w_{k,0} - w_{k,l})}{l E F} \quad (\text{B.16})$$

APPENDIX C

APPENDIX C: MAXWELL-STEFAN EQUATION FOR TERNARY MIXTURES

Components i, j and k are the two solvents and one solute inside the ternary mixture.

$$n_i + \left(\frac{\bar{w}_j n_i - \bar{w}_i n_j}{\bar{w}_m} \right) \varepsilon_1 + \left(\frac{\bar{w}_k n_i - \bar{w}_i n_k}{\bar{w}_m} \right) \varepsilon_2 = \frac{\rho D_{im}}{\bar{w}_m l} (w_{i0} - w_{jl}) \quad (\text{C.1})$$

$$n_j + \left(\frac{\bar{w}_i n_j - \bar{w}_j n_i}{\bar{w}_m} \right) \varepsilon_3 + \left(\frac{\bar{w}_k n_j - \bar{w}_j n_k}{\bar{w}_m} \right) \varepsilon_4 = \frac{\rho D_{jm}}{\bar{w}_m l} (w_{j0} - w_{jl}) \quad (\text{C.2})$$

$$n_k + \left(\frac{\bar{w}_i n_k - \bar{w}_k n_i}{\bar{w}_m} \right) \varepsilon_5 + \left(\frac{\bar{w}_j n_k - \bar{w}_k n_j}{\bar{w}_m} \right) \varepsilon_6 = \frac{\rho D_{km}}{\bar{w}_m l} (w_{k0} - w_{kl}) \quad (\text{C.3})$$

$$\varepsilon_1 = \frac{D_{im}}{D_{ij}} \quad (\text{C.4})$$

$$\varepsilon_2 = \frac{D_{im}}{D_{ik}} \quad (\text{C.5})$$

$$\varepsilon_3 = \frac{D_{jm} M_j}{D_{ij} M_i} \quad (\text{C.6})$$

$$\varepsilon_4 = \frac{D_{jm}}{D_{jk}} \quad (\text{C.7})$$

$$\varepsilon_5 = \frac{D_{km} M_k}{D_{ik} M_i} \quad (\text{C.8})$$

$$\varepsilon_6 = \frac{D_{km} M_k}{D_{jk} M_j} \quad (\text{C.9})$$

Developing the equations (C.1)-(C.3):

$$n_i \left(1 + \left(\frac{\bar{w}_j}{\bar{w}_m} \right) \varepsilon_1 + \left(\frac{\bar{w}_k}{\bar{w}_m} \right) \varepsilon_2 \right) = \frac{\rho D_{im}}{\bar{w}_m l} (w_{i0} - w_{il}) + \left(\frac{\bar{w}_i n_j}{\bar{w}_m} \right) \varepsilon_1 + \left(\frac{\bar{w}_i n_k}{\bar{w}_m} \right) \varepsilon_2 \quad (\text{C.10})$$

$$n_j \left(1 + \left(\frac{\bar{w}_i}{\bar{w}_m} \right) \varepsilon_3 + \left(\frac{\bar{w}_k}{\bar{w}_m} \right) \varepsilon_4 \right) = \frac{\rho D_{jm}}{\bar{w}_m l} (w_{j0} - w_{jl}) + \left(\frac{\bar{w}_j n_i}{\bar{w}_m} \right) \varepsilon_3 + \left(\frac{\bar{w}_j n_k}{\bar{w}_m} \right) \varepsilon_4 \quad (\text{C.11})$$

$$n_k \left(1 + \left(\frac{\bar{w}_l}{\bar{w}_m} \right) \varepsilon_5 + \left(\frac{\bar{w}_j}{\bar{w}_m} \right) \varepsilon_6 \right) = \frac{\rho D_{3m}}{\bar{w}_m l} (w_{k0} - w_{kl}) + \left(\frac{\bar{w}_k n_i}{\bar{w}_m} \right) \varepsilon_5 + \left(\frac{\bar{w}_k n_j}{\bar{w}_m} \right) \varepsilon_6 \quad (\text{C.12})$$

To simplify the equations:

$$A = \left(1 + \left(\frac{\bar{w}_j}{\bar{w}_m} \right) \varepsilon_1 + \left(\frac{\bar{w}_k}{\bar{w}_m} \right) \varepsilon_2 \right)$$

$$B = \left(1 + \left(\frac{\bar{w}_l}{\bar{w}_m} \right) \varepsilon_3 + \left(\frac{\bar{w}_k}{\bar{w}_m} \right) \varepsilon_4 \right)$$

$$C = \left(1 + \left(\frac{\bar{w}_l}{\bar{w}_m} \right) \varepsilon_5 + \left(\frac{\bar{w}_j}{\bar{w}_m} \right) \varepsilon_6 \right)$$

Replacing in the Eqs. (C.10)-(C.12):

$$n_i A = \frac{\rho D_{im}}{\bar{w}_m l} (w_{i0} - w_{il}) + \left(\frac{\bar{w}_l n_j}{\bar{w}_m} \right) \varepsilon_1 + \left(\frac{\bar{w}_l n_k}{\bar{w}_m} \right) \varepsilon_2 \quad (\text{C.13})$$

$$n_j B = \frac{\rho D_{jm}}{\bar{w}_m l} (w_{j0} - w_{jl}) + \left(\frac{\bar{w}_j n_i}{\bar{w}_m} \right) \varepsilon_3 + \left(\frac{\bar{w}_j n_k}{\bar{w}_m} \right) \varepsilon_4 \quad (\text{C.14})$$

$$n_k C = \frac{\rho D_{km}}{\bar{w}_m l} (w_{k0} - w_{kl}) + \left(\frac{\bar{w}_k n_i}{\bar{w}_m} \right) \varepsilon_5 + \left(\frac{\bar{w}_k n_j}{\bar{w}_m} \right) \varepsilon_6 \quad (\text{C.15})$$

Substituting (C.15) in (B.14):

$$n_j D = \frac{\rho D_{jm}}{\bar{w}_m l} C (w_{j0} - w_{jl}) + \frac{\rho D_{km}}{\bar{w}_m l} \left(\frac{\bar{w}_j}{\bar{w}_m} \right) \varepsilon_4 (w_{k0} - w_{kl}) + \left(\frac{\bar{w}_j}{\bar{w}_m} \right) n_i E \quad (\text{C.16})$$

$$\text{With } D = BC - \left(\frac{\bar{w}_k}{\bar{w}_m} \right) \left(\frac{\bar{w}_j}{\bar{w}_m} \right) \varepsilon_4 \varepsilon_6$$

$$E = \left(C \varepsilon_3 + \left(\frac{\bar{w}_k}{\bar{w}_m} \right) \varepsilon_4 \varepsilon_5 \right)$$

Substituting (C.15) in (C.13):

$$n_i F = \frac{\rho D_{im}}{\bar{w}_m l} C (w_{i0} - w_{il}) + \frac{\rho D_{km}}{\bar{w}_m l} \left(\frac{\bar{w}_l}{\bar{w}_m} \right) \varepsilon_2 (w_{k0} - w_{kl}) + \left(\frac{\bar{w}_l n_j}{\bar{w}_m} \right) G \quad (\text{C.17})$$

$$\text{With } F = AC - \left(\frac{\bar{w}_k}{\bar{w}_m} \right) \left(\frac{\bar{w}_l}{\bar{w}_m} \right) \varepsilon_2 \varepsilon_5$$

$$G = \left(C \varepsilon_1 + \left(\frac{\bar{w}_k}{\bar{w}_m} \right) \varepsilon_2 \varepsilon_6 \right)$$

Substituting (C.16) in (C.17):

$$n_i = \left(\frac{\rho D_{im}}{\bar{w}_m l} CD (w_{i0} - w_{il}) + \frac{\rho D_{jm}}{\bar{w}_m l} CG \left(\frac{\bar{w}_l}{\bar{w}_m} \right) (w_{j0} - w_{jl}) + \frac{\rho D_{km}}{\bar{w}_m l} \left(\frac{\bar{w}_l}{\bar{w}_m} \right) I (w_{k0} - w_{kl}) \right) \frac{1}{H} \quad (\text{C.18})$$

$$\text{With } H = FD - \left(\frac{\bar{w}_l}{\bar{w}_m} \right) \left(\frac{\bar{w}_j}{\bar{w}_m} \right) GE$$

$$I = \left(\left(\frac{\bar{w}_j}{\bar{w}_m} \right) G \varepsilon_4 + D \varepsilon_2 \right)$$

Substituting (C.18) in (C.16):

$$n_j = \left(\frac{\rho D_{im}}{\bar{w}_m l} \frac{CE}{H} \left(\frac{\bar{w}_j}{\bar{w}_m} \right) (w_{i0} - w_{il}) + \frac{\rho D_{jm}}{\bar{w}_m l} \frac{C}{DH} J (w_{j0} - w_{jl}) + \frac{\rho D_{km}}{\bar{w}_m l} \frac{K}{DH} (w_{k0} - w_{kl}) \right) \quad (\text{C.19})$$

$$\text{With } J = \left(H + \left(\frac{\bar{w}_l}{\bar{w}_m} \right) \left(\frac{\bar{w}_j}{\bar{w}_m} \right) EG \right)$$

$$K = \left(\left(\frac{\bar{w}_j}{\bar{w}_m} \right) H \varepsilon_4 + \left(\frac{\bar{w}_l}{\bar{w}_m} \right) \left(\frac{\bar{w}_j}{\bar{w}_m} \right) EI \right)$$

Substituting Eqs. (C.18)-(C.19) in (C.15):

$$n_k = \left(\frac{\rho D_{im}}{\bar{w}_m l} \left(\frac{\bar{w}_k}{\bar{w}_m} \right) \frac{L}{H} (w_{i0} - w_{il}) + \frac{\rho D_{jm}}{\bar{w}_m l} \frac{M}{H} (w_{j0} - w_{jl}) + \frac{\rho D_{km}}{\bar{w}_k l} \frac{N}{C} (w_{k0} - w_{kl}) \right) \quad (\text{C.20})$$

$$\text{With } L = \left(\varepsilon_5 D - \left(\frac{\bar{w}_j}{\bar{w}_m} \right) \varepsilon_6 E \right)$$

$$M = \left(\left(\frac{\bar{w}_l}{\bar{w}_m} \right) \left(\frac{\bar{w}_k}{\bar{w}_m} \right) \varepsilon_5 G - \frac{J}{D} \right)$$

$$N = 1 + \left(\frac{\bar{w}_l}{\bar{w}_m} \right) \frac{1}{H} + \frac{K}{DH}$$

APPENDIX D

APPENDIX D: MODELING PREDICTION

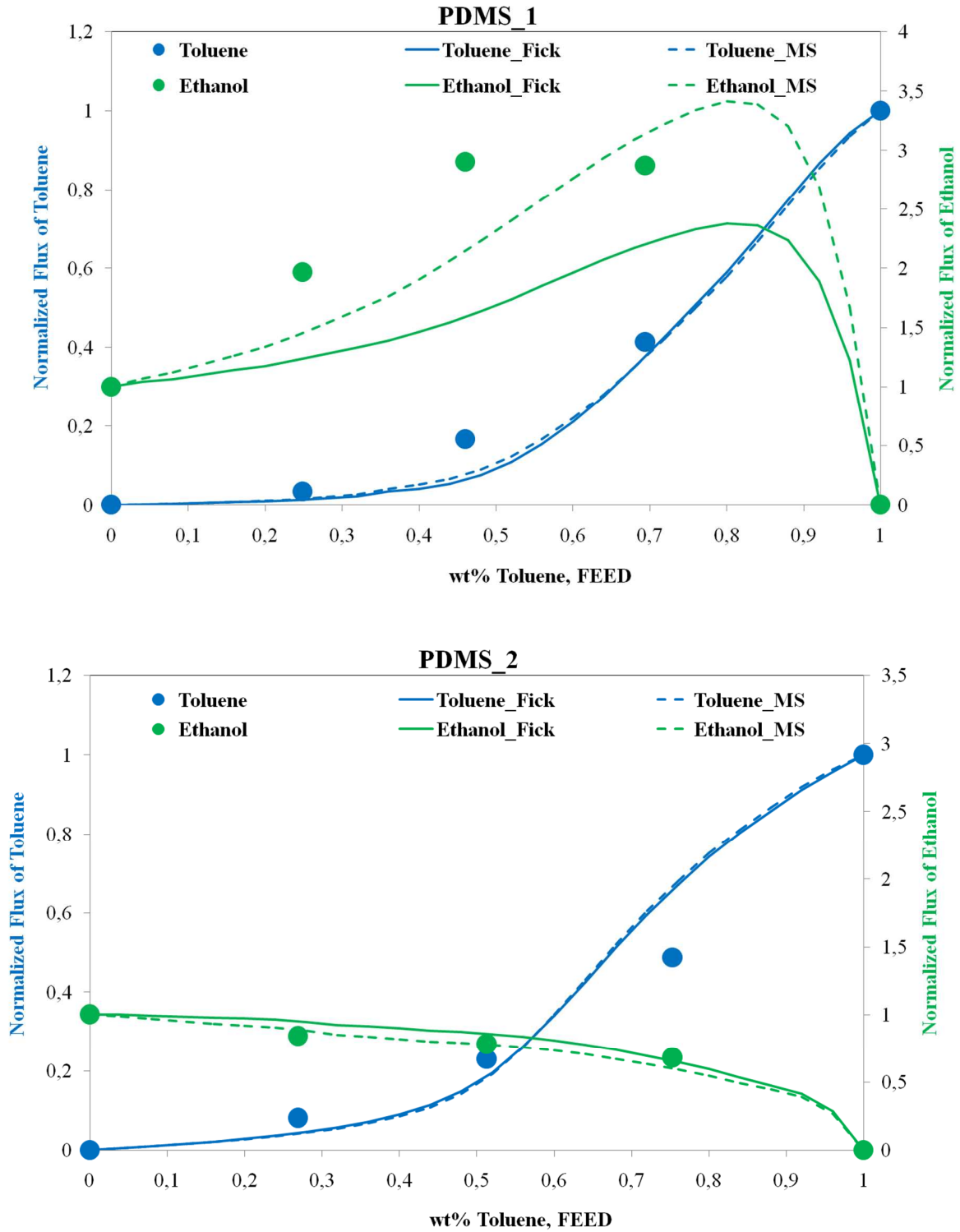


Figure D.1 a,b: Normalized flux prediction of toluene and ethanol vs toluene feed composition in PDMS_1 and PDMS_2 applying Fick's law and MS equations

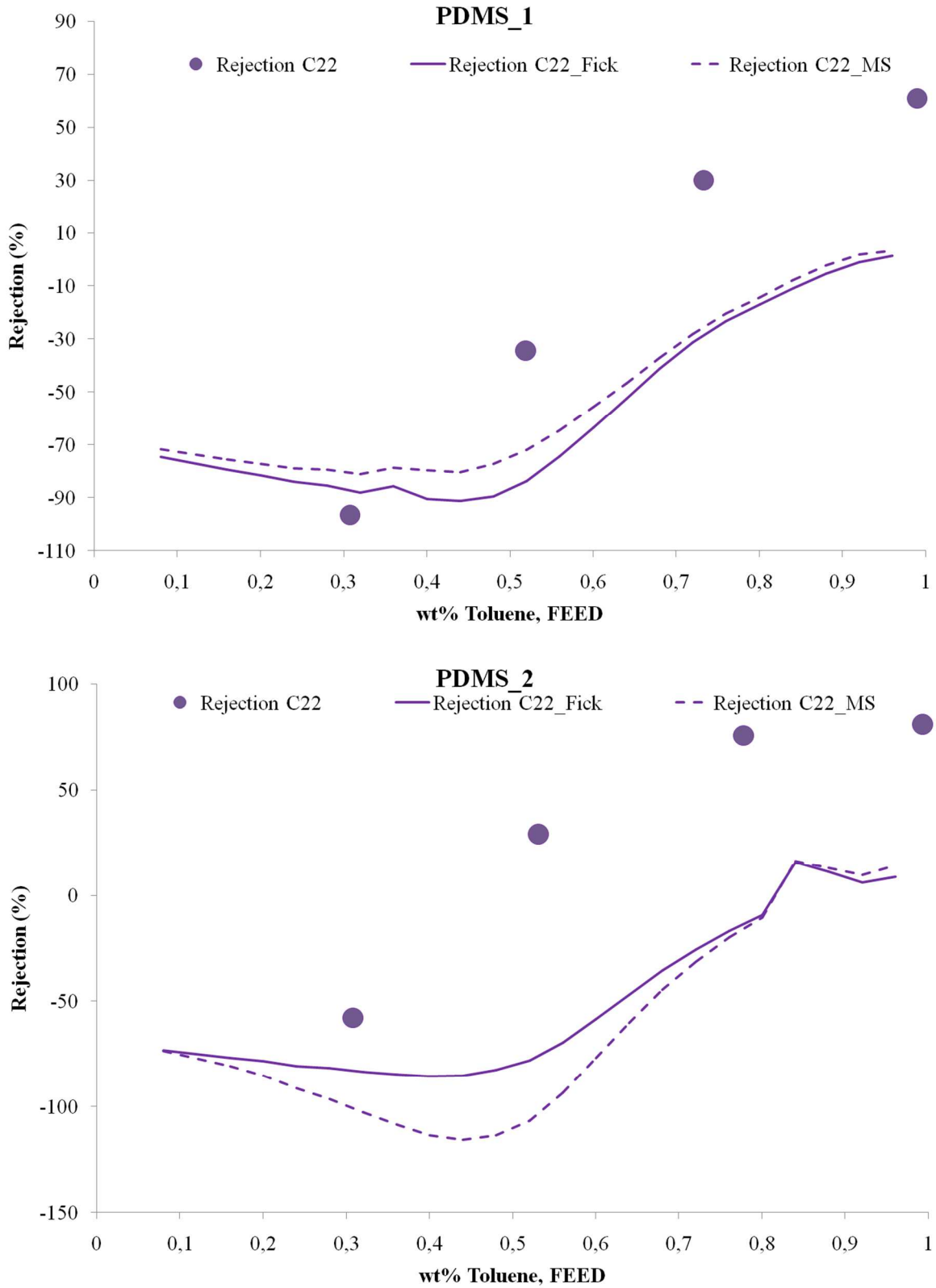


Figure D.2 a,b: Rejection prediction of solute vs toluene feed composition in toluene-ethanol mixture for PDMS_1 and PDMS_2 applying Fick's law and MS equations

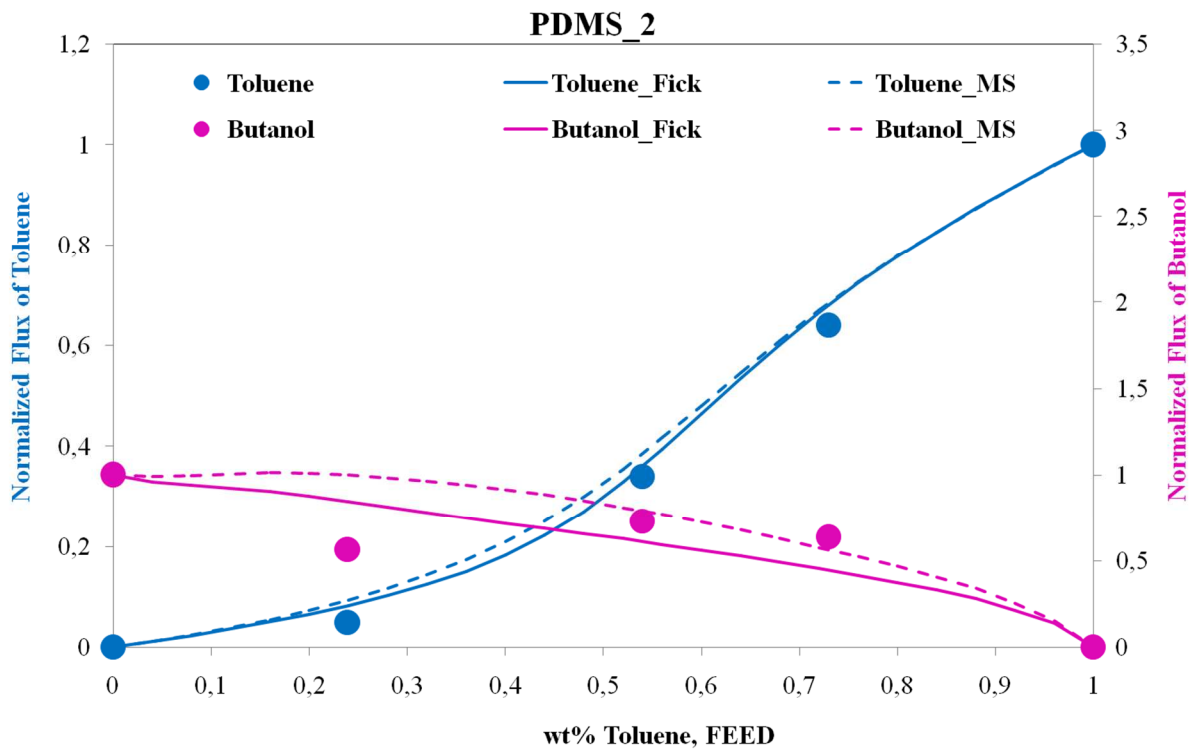
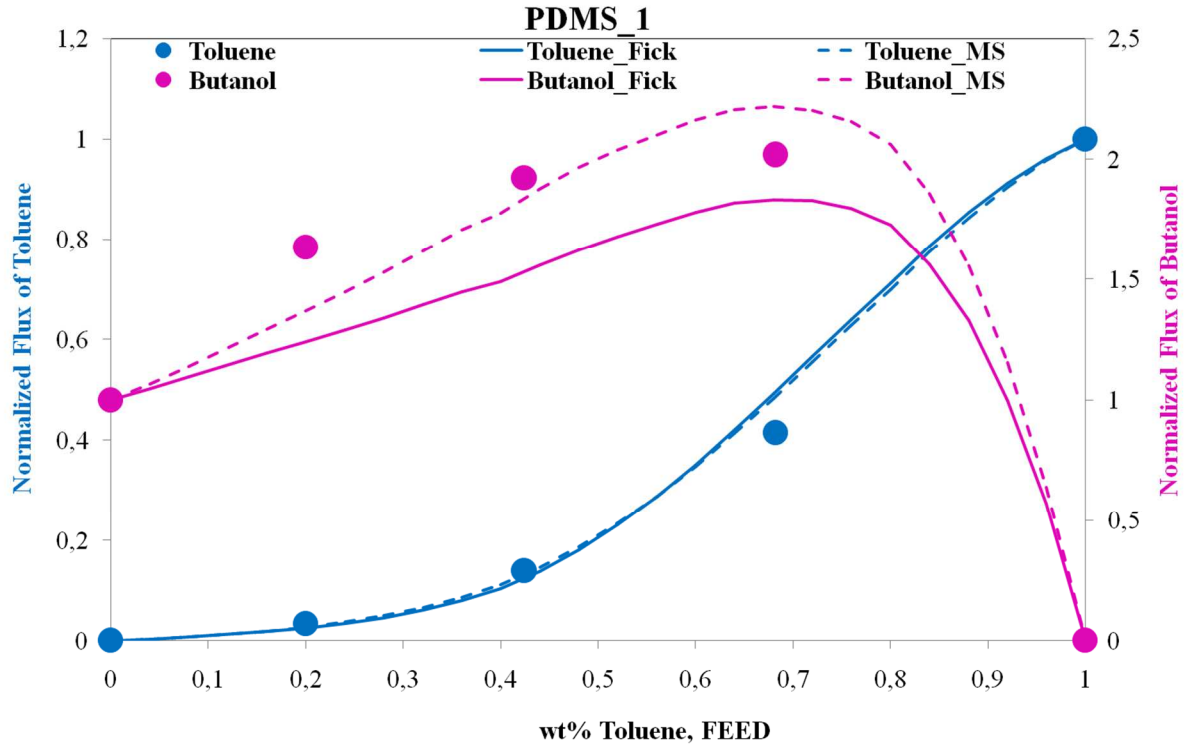


Figure D.3 a,b: Normalized flux prediction of toluene and butanol vs toluene feed composition in PDMS_1 and PDMS_2 applying Fick's law and MS equations

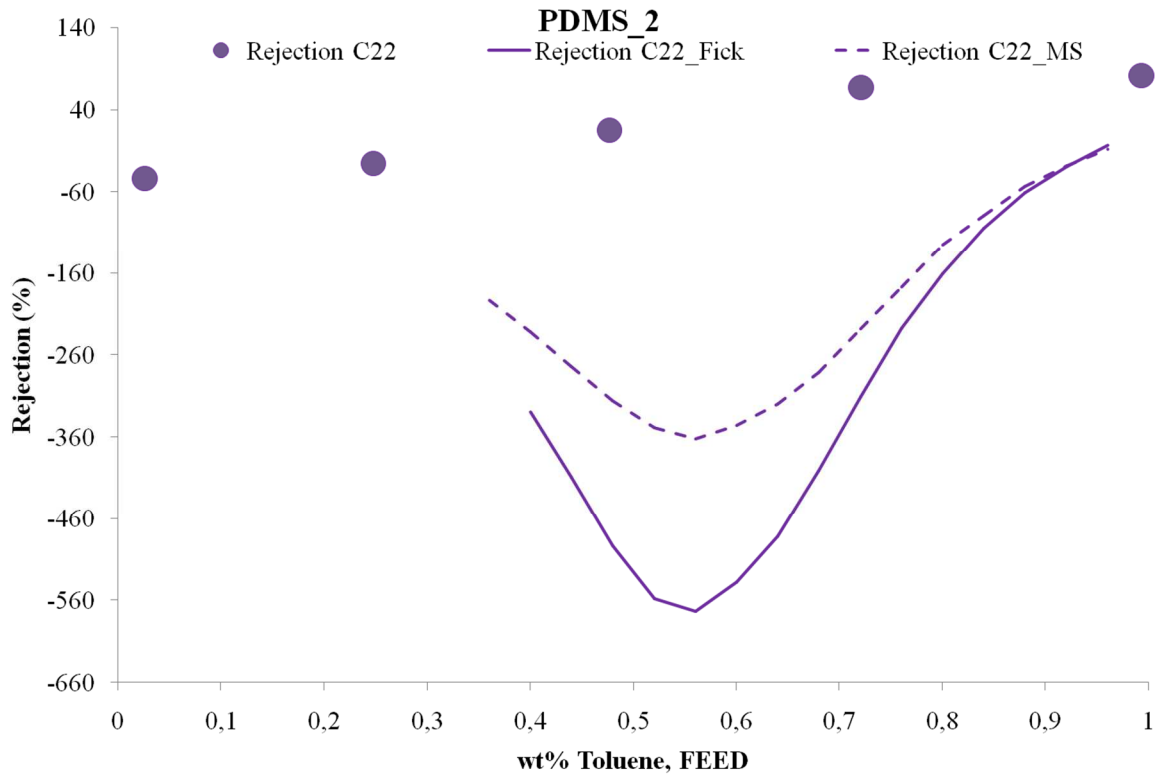
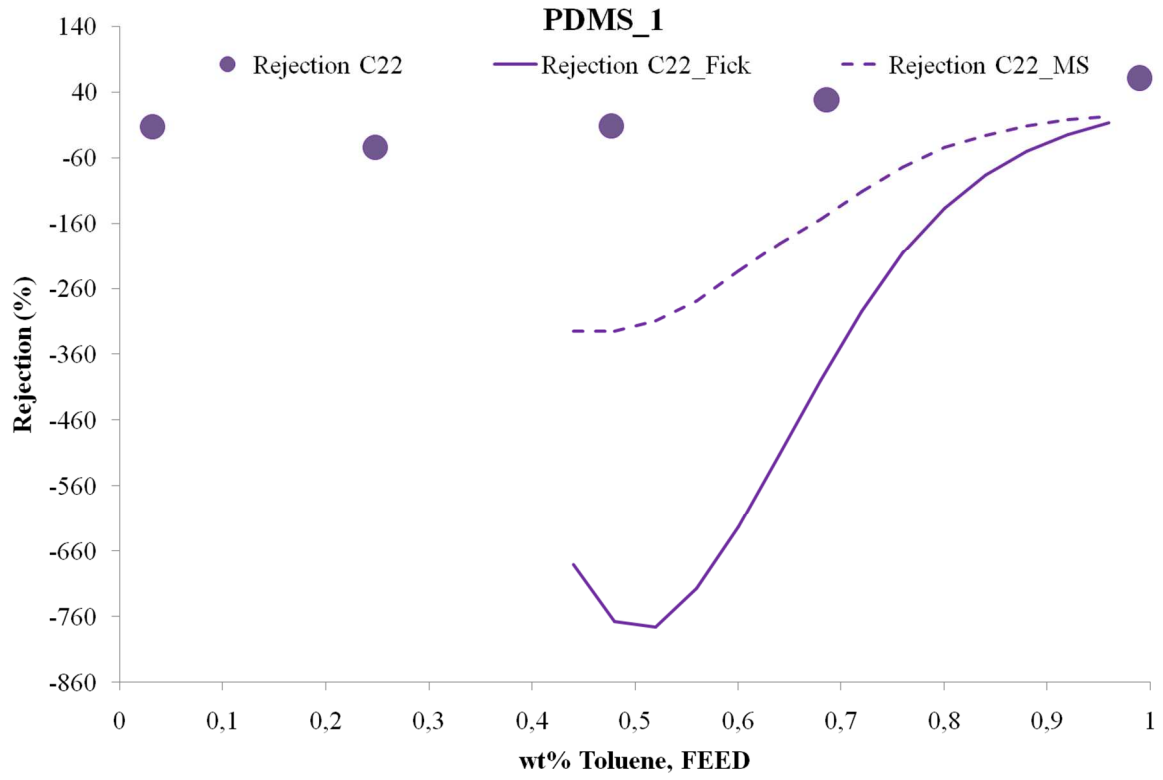


Figure D.4 a,b: Rejection prediction of solutes vs toluene feed composition in toluene-butanol mixture for PDMS_1 and PDMS_2 applying Fick's law and MS equations

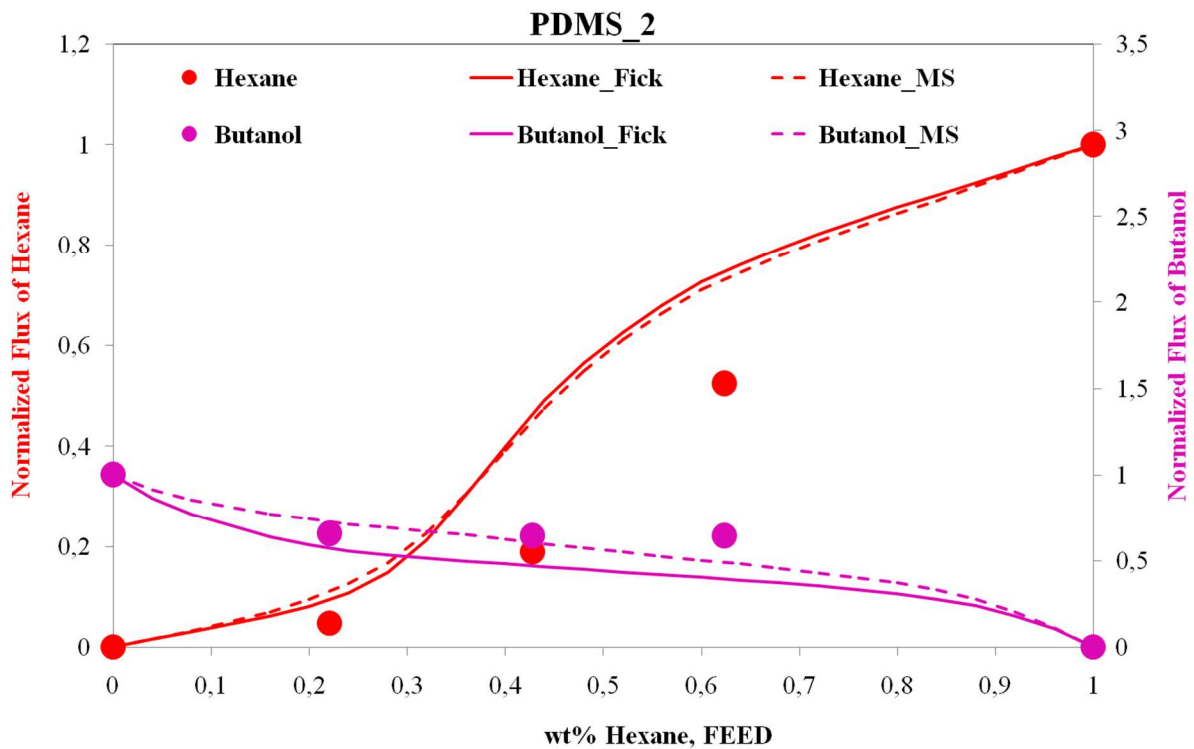
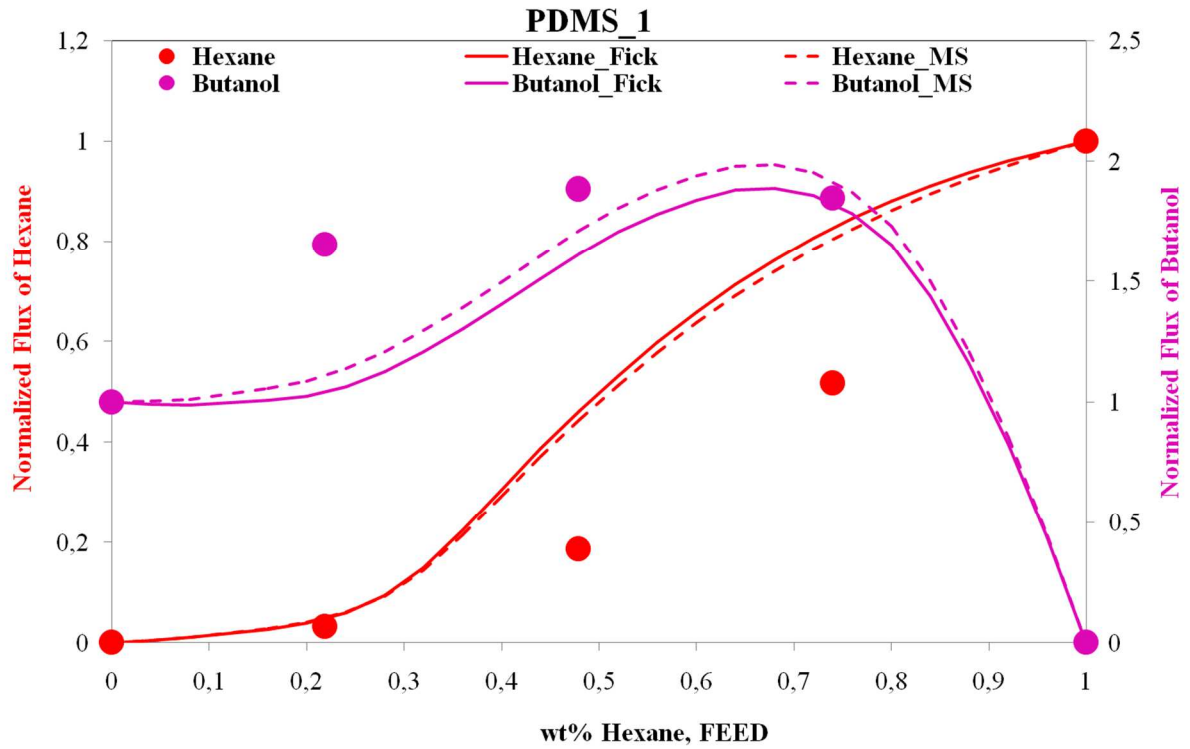


Figure D.5 a,b: Normalized flux prediction of hexane and ethanol vs hexane feed composition in PDMS_1 and PDMS_2 applying Fick's law and MS equations

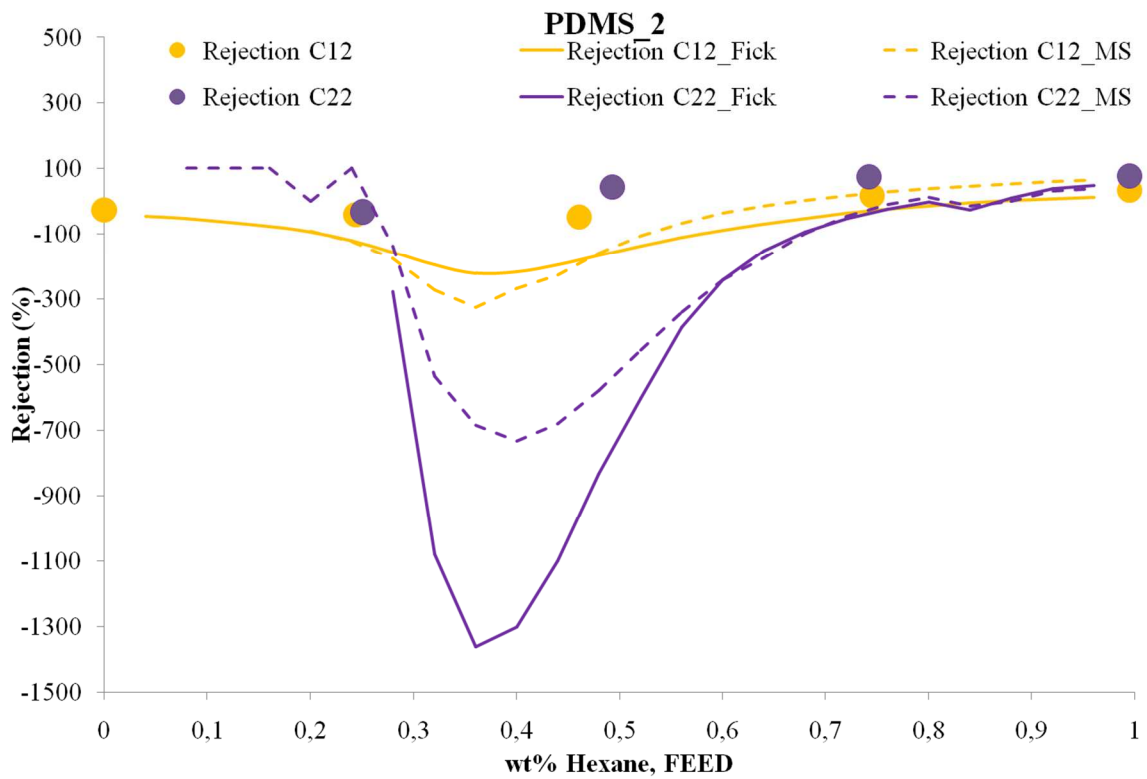
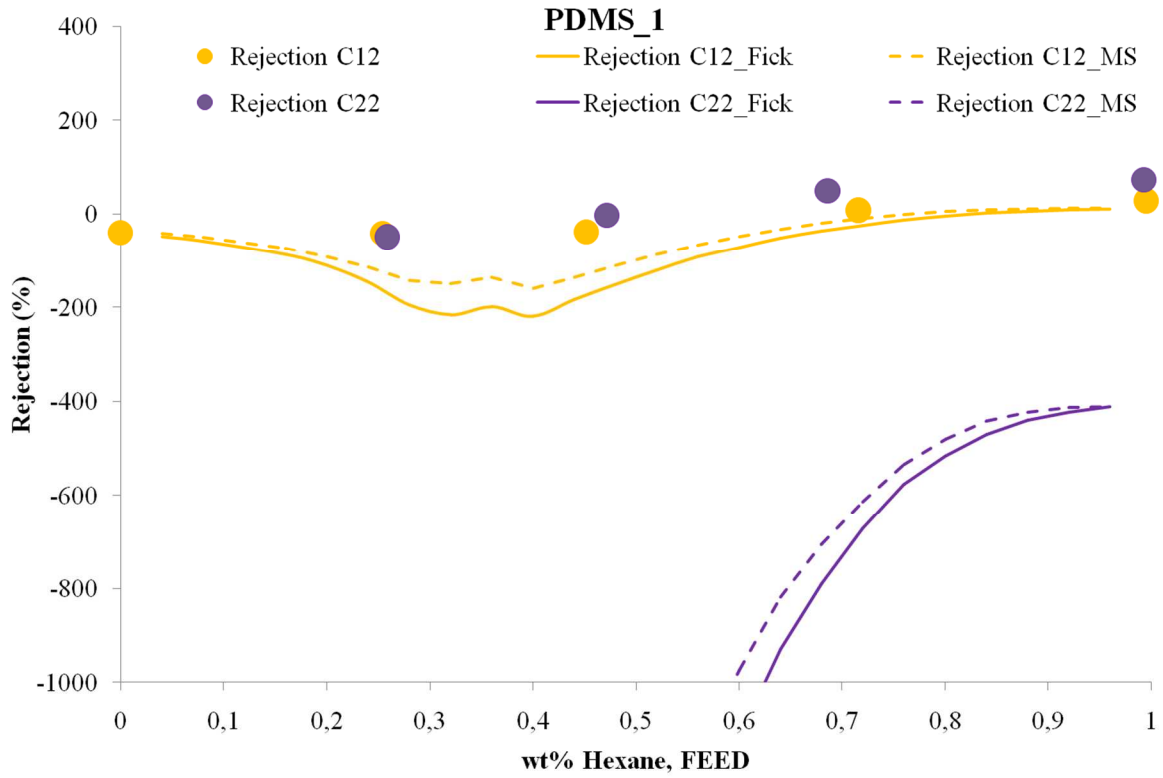


Figure D.6 a,b: Rejection prediction of solutes vs toluene feed composition in hexane-butanol mixture for PDMS_1 and PDMS_2 applying Fick's law and MS equations

Bibliography

- [1] B. Flacommeche M.H. Klopffer, "Transport properties of gases in polymers: Bibliografic review," *Oil and gas Science and Thecnology*, vol. 56, pp. 223-244, 2001.
- [2] GC Sarti F. Doghieri, "Mass Transport and Mechanical Properties of Solid Polymers," *Makromolekulare Chemie, Macromolecular Symposia*, vol. 68, pp. 257-275, 1993.
- [3] PY Furlan NE Schottler, "A review of Small Molecule Diffusion in Polyolefins," *Polymers*, vol. 33, pp. 3323-3342, 1992.
- [4] T. Savvas, CT Kelly BJ Briscoe, "Explosive decompression failure of rubbers - a review of the origins of pneumatic stress-induced repture in elastomer," *Rubber Chemistry and Technology*, vol. 67, pp. 384-416, 1994.
- [5] JM Caruthers, NA Peppas SR Lusting, "ContinuumThermodynamics and Transport Theory for Polymer Fluid Mixtures," *Chem. Eng. Scie.*, vol. 47, pp. 3037-3057, 1992.
- [6] PP Roussis, JH Petropoulos M. Sanopoulou, "A detailed Study of the Viscoelastic Nature of Vapor Sorption and Transport in a Cellulosic Polymer. 1. Origin and Phisical Implications ofDeviations form Fickian Sorption Kinetics," *Journal of Polymer Science part B- Polymer Physics*, vol. 33, pp. 993-1005, 1995.
- [7] R.H. Lacombe I.C. Sanchez, "An Elementary Molecular Theory of Classical Fluids. Pure Fluids," *J. Phys. Chem.*, vol. 80, p. 2352, 1976.
- [8] R.H. Lacombe I.C. Sanchez, "An elementary equation of state for polymer liquids," *J. Polym. Sci.*, vol. 80, p. 2568, 1976.
- [9] R.J. Sadus Y.S. Wei, "Equations of State for the Calculation of Fluid-Phase Equilibria," *AiChE J.*, vol. 46, p. 169, 200.
- [10] G. Jackson, K.E. Gubbins W. Chapman, "Phase equilibria of associating fluids. Chain molecules with multiple bonding sites," *Mol. Phys.*, vol. 65, p. 1057, 1988.
- [11] K.E. Gubbins, G. Jackson, M. Radosz W.G. Chapman, "New Reference Equation of state for Associating Liquids," *Ind. eng. Chem. Res.*, vol. 29, p. 1709, 1990.
- [12] G. Sadowski J. Gross, "Perturbed-chain SAFT: An equation of state based on a pertirbation theory for chain molecules," *Ind. Eng. Chem. Res.*, vol. 40, pp. 1244-1260, 2001.
- [13] P.J. Flory, *Principles of Chemistry*. Itacha: Cornell University Press, 1953.
- [14] J.L. Ellenson, B.E. Eichinger P.J. Flory, "Thermodynamics of Mixing of n-Alkanes with Polyisobutylene," *Macromolecules*, vol. 1, p. 279, 1968.

- [15] P.J. Flory, "Statistical Thermodynamics of Liquid Mixtures," *J. Am. Chem. Soc.*, vol. 87, p. 1833, 1965.
- [16] P.J. Flory, "Thermodynamics of High Polymer Solutions," *J. Chem. Phys.*, vol. 9, p. 660, 1941.
- [17] J.H. Vera C. Panayiotou, "Statistical Thermodynamic of r-mer Fluids and their Mixtures," *Polym. J.*, vol. 14, p. 681, 1982.
- [18] J.H. Vera C. Panayiotou, "Local Composition and Local Surface Area Fractions: A Theoretical Discussion," *Can. J. Chem. Eng.*, vol. 59, p. 501, 1981.
- [19] R.H. Lacombe I.C. Sanchez, "Statistical Thermodynamics of Fluid Mixtures," *J. Phys. Chem.*, vol. 80, p. 2568.
- [20] R.H. Lacombe I.C. Sanchez, "Statistical Thermodynamics of Polymer Solutions," *Macromolecules*, vol. 11, p. 1145, 1978.
- [21] T.C. Merkel, V.I. Bondar, B.D. freeman, F. Doghieri, G.C. Sarti M.G. De Angelis, "Hydrocarbon and Fluorocarbon Solubility and Dilatation in Poly(dimethylsiloxane): Comparison of Experimental Data with Predictions of the Sanchez-Lacombe Equation of State," *J. Polym. Sci. Part B: Polym. Phys.*, vol. 37, p. 3011, 1999.
- [22] D. Henderson J.A. Barker, "Perturbation Theory and Equation of Satte for Fluids: The Square-Well Potential," *J. Chem. Phys.*, p. 2856, 1967.
- [23] D. Henderson J.A. Barker, "Perturbation Theory and Equation of Satete for Fluids. II. A Successful Theory of Liquids.," *J. Chem. Phys.*, p. 4714, 1967.
- [24] Josef Chmelar. <http://www.kosekgroup.cz>.
- [25] S.I. Sandler J.P. Wolbach, "Using molecular orbital calculations to describe the phase behavior of crossassociating mixtures," *Ind. Eng. Chem. Res.*, vol. 37, pp. 2917-2928, 1998.
- [26] G.C. Sarti F. Doghieri, "Non-equilibrium Lattice Fluids: A predictive Model for the Solubility in Glassy Polymers," *Macromolecules*, vol. 29, pp. 2568-2580, 1996.
- [27] F. Doghieri, G.C. Sarti M. Giacinti Baschetti, "Solubility in Glassy Polymers: Correlations through the Nonequilibrium Lattice Fluid Model," *Ind. Eng. Chem. Res.*, vol. 40, p. 3027, 2001.
- [28] G.C Sarti F. Doghieri, "Predicting the Low-Pressure Solubility of Gases and Vapors in Glassy Polymers by the NELF model," *J. Membr. Sci.*, vol. 147, pp. 73-86, 1998.

- [29] Piccinini E., Studio delle Proprietà Volumetriche di Membrane Polimeriche nel Trasporto di Materia, 2003, Tesi di Dottorato, Università di Bologna.
- [30] Campbell D.S., "Handbook of Thin Film Technology," in *Mechanical Properties of Thin Films*. New York, NY: McGraw-Hill, 1969.
- [31] Saenger K.L. Tong H.M, "New Characterization Techniques for Thin Polymer Films," in *Bending-Beam Characterization of Thin Polymer Films*. New York, NY: Wiley Interscience, 1990.
- [32] Campbell D.S. Wilcox J.D., "A Sensitive Bending-Beam Apparatus for Measuring the Stress in Evaporated Thin Films," *Thin Solid Films*, vol. 3, p. 3, 1969.
- [33] Hoffman R.W., "Mechanical Properties of Non-metallic Thin Films," in *Physics of Nonmetallic Thin Films*. New York, NY: Plenum, 1976.
- [34] Hu C.K., Feger C., Ho P. Tong H.M, "Stress Development in Supported Polymer Films During Thermal Cycling," *Polym. Eng. Sci.*, vol. 26, p. 1213, 1986.
- [35] Hwang J., Hofer D.C. Jou J.H., "In Situ Measurement of Temperature Dependence of Internal Residual Stress in Polyimide Film Coated on Silicon Substrate," IBM Research Report, RJ 5984, 1987.
- [36] Tong H.M., Saenger K. L., Gryte C.C Han B., "Mechanical Property Determination for Supported Polymer Films Using Double Bending-Beams," *Mat. Res. Soc. Symp. Proc.*, vol. 76, p. 123, 1987.
- [37] Pritchett W.C. Berry B.S, "Elastic and Viscoelastic Behavior of a Magnetic Recording Tape," *IBM J. Res. Develop.*, vol. 32, p. 682, 1988.
- [38] Yang C.H., Faupel F., Ho P. Chen S.T., "Stress Relaxation During Thermal Cycling in Metal/Polyimide Layered Films," *J. Appl. Phys.*, vol. 64, p. 6690, 1988.
- [39] Sarti G.C. Astarita G., "Class of Mathematical Models for Sorption of Swelling Solvents in Glassy Polymers," *Polym. Eng. Sci.*, vol. 18, p. 388, 1978.
- [40] Pritchett W.C. Berry B.S., "Bending Cantilever Method for the Study of Moisture Swelling in Polymers," *IBM J. Res. Develop.*, vol. 28, p. 662, 1984.
- [41] Saenger K.L. Tong H.M., "Bending-Beam Study of Water Sorption by Thin Poly(methyl Methacrylate) Films," *J. Appl. Polym. Sci.*, vol. 38, p. 937, 1989.
- [42] Durning C.J., Tong H.M. Fu T.Z., "Simple Model for Swelling-Induced Stresses in a Supported Polymer Thin Film," *J. Appl. Polym. Sci.*, vol. 43, p. 709, 1991.

- [43] Hoffman R.W. Rottmayer R.E., "Boundary Conditions for Stress Measurement Using a Cantilevered Beam," *J. Vac. Sci. Tech.*, vol. 7, p. 461, 1970.
- [44] Klokholm E., "A Sensitive Device for Measuring Residual Stresses in Thin Films," IBM Research Report, RC 1352, 1965.
- [45] Seo M. Lång G.G., "On the Electrochemical Applications of the Bending-Beam Method," *J. Electroan. Chem.*, vol. 490, p. 98, 2000.
- [46] http://www.echeguru.com/html_data_files/Wagner_Constants.html.
- [47] Frisch H.L., "The time lag diffusion," *Journal of Physical Chemistry*, vol. 61, pp. 93-95, 1957.
- [48] J.D.Ferry, *Viscoelastic Properties of Polymers*, 3rd ed. New York: Wiley, 1980.
- [49] O. Pfohl, R. Dohm, G. Sadowski KM Kruger, "Phase equilibria and diffusion coefficients in the poly(dimethylsiloxane) + n-pentane system," *Fluid phase Equilibria*, vol. 241, pp. 138-146, 2006.
- [50] F. Doghieri G.C. Sarti, "Predictions of the Solubility of Gases in Glassy Polymers Based on the NELF Model," *Chem. Eng. Sci.*, vol. 53, pp. 3435-3447, 1998.
- [51] T. Gregor, H. Hajova, A. Nistor, J. Kosek J. Chmelar, "Experimental study and PC-SAFT simulations of sorption equilibria in polystyrene," *Polymer*, vol. 52, pp. 3082-3091, 2011.
- [52] R.H. Holley, V. Stannett H.B. Hopfenberg, "The effect of penetrant activity and temperature on the anomalous diffusion of hydrocarbons and solvent crazing in polystyrene part I: Biaxially oriented polystyrene," *Polym. Eng. & Sci.*, vol. 9, pp. 242-249, 1969.
- [53] M.F. Jimenez Solomon, G. Szekely, A.G. Livingston P. Marchetti, "Molecular Separation with Organic solvent Nanofiltration: A critical Review," *Chemical Reviews*, vol. 114, pp. 10735-10806, 2014.
- [54] G.A. Korneeva, G.F. Tereshchenko A.V. Volkov, "Organic solvent nanofiltration: prospects and application," *Russian Chem. Rev.*, vol. 77, pp. 983-993, 2008.
- [55] Y.H. Ma, T. Shimidzu W.J. Koros, "Terminology for gas membranes and membrane processes (IUPAC Recommendations 1996)," *J. Membr. Sci.*, vol. 120, pp. 149-159, 1996.
- [56] J.D. Ferry, *Properties of Polymers*. New York: John Wiley & Sons Inc., 1980.

- [57] C. Park, G.M. Whitesides J.N. Lee, "Solvent Compatibility of Poly(dimethylsiloxane)-Based Microfluidic Devices," *Anal. Chem.*, vol. 75, pp. 6544-6554, 2003.
- [58] K.V. Peinemann, N. Scharnagel, K. Friese, R. Schubert M. Schmidt, DE Patent 19,507,584 A1, 1996.
- [59] A.F.M. Barton, *CRC Handbook of Solubility Parameters and Other Cohesion Parameter*, Boca Raton, Ed.: CRC Press, 1983.
- [60] I.M. Smallwood, *Handbook of Organic Solvent Properties*. Oxford: Arnold, 1996.
- [61] B. Heuwers, F. Katzenberg, J.C. Tiller, G. Sadowski F. Mueller, "Tensile creep measurement of glassy VOC-loaded polymers," *Macromolecules*, vol. 43, pp. 8997-9003, 2010.
- [62] M.G. De Angelis, F. Doghieri G. Cocchi, "Solubility and diffusivity of liquids for food and pharmaceutical applications in crosslinked polydimethylsiloxane (PDMS) films: I. Experimental data on pure organic components and vegetable oil," *J. Membr. Sci.*, vol. 492, pp. 600-611, 2015.
- [63] H.K. Lonsdale E.A. Mason, "Statistical-mechanical theory of membrane transport," *J. Membr. Sci.*, vol. 51, pp. 1-81, 1990.
- [64] "J. Wang, D.S. Dlamini, A.K. Mishra, M.T.M. Pendergast, M. C.Y. Wong, B.B. Mamba, V. Freger, A.R.D Verliefe, E.M.V. Hoek," *J. Membr. Sci.*, vol. 454, pp. 516-537, 2014.
- [65] B.C. Baltiz, K.K. Sirkar J.A. Whu, "Nanofiltration studies of larger organic microsolute in methanol solutions," *J. Membr. Sci.*, vol. 170, pp. 159-172, 2000.
- [66] U. Merten, R.L. Riley H.K. Lonsdale, "Transport properties of cellulose acetate osmotic membranes," *J. Appl. Polym. Sci.*, vol. 9, pp. 1341-1362, 1965.
- [67] R.W. Baker J.G. Wijmans, "The solution-diffusion model: a review," *J. Membr. Sci.*, vol. 107, pp. 1-21, 1995.
- [68] J.S. Welfoot W.R. Bowen, "Modelling of membrane nanofiltration-pore size distribution effects," *Chem. Eng. Sci.*, vol. 57, pp. 1393-1407, 2002.
- [69] A.E. Yaroshchuk, "Solution-diffusion-imperfection model revised," *J. Membr. Sci.*, vol. 101, pp. 83-87, 1995.
- [70] U. Marten, R.L. Riley H.K. Lonsdale, "Transport properties of cellulose acetate osmotic membranes," *J. Appl. Polym. Sci.*, vol. 9, no. 1341-1362, 1965.
- [71] W.J. Koros H.D. Kammarudin, "Some observation about the application of Fick's first law for membrane separation of multicomponent mixtures," *J. Membr. Sci.*, vol. 135, pp.

- 147-159, 1997.
- [72] E.N. Lightfoot, R.N. Bird W.E. Stewart, *Transport Phenomena*. New York: John Wiley, 2002.
- [73] C.F. Curtiss R.B. Bird, "Multicomponent diffusion," *Ind. Eng. Chem. Res.*, vol. 38, pp. 2515-2522, 1999.
- [74] D.R. Paul, "Reformulation of solution-diffusion theory of reverse osmosis," *J. of Memb. Sci.*, vol. 241, no. 371-386, 2004.
- [75] F. Ruether G. Sadowski, "Modeling the Solubility of Pharmaceuticals in Pure Solvent Mixtures for Drug Process Design," *J. Pharm. Sci.*, pp. 4205-4215, 2009.
- [76] N. Von Solms G.M. Kontogeorais, "Computational and Physical Performance of a Modified PC-SAFT EoS for Highly Asymmetric and Ass. Mixtures," *Ind. Eng. Chem. Res.*, pp. 2057-2064, 1999.
- [77] R. Dohm, G. Sadowski, K.M.Kruger O. Pfohl, "Phase equilibria and diffusion coefficients in the poly(dimethylsiloxane) + n-pentane system," *Fluid phase Equilibria*, vol. 241, pp. 138-146, 2006.
- [78] S. Wessel, T. Keil, P. Eiselt, M. Wessling S. Postel, "Multicomponent mass transport in organic solvent nanofiltration with solvent mixtures," *J. Memb. Sci.*, vol. 466, pp. 361-369, 2014.
- [79] A.T. Boam, A.G. Livingston, D.C. Stuckey S.D. Doing, "Mass transfer of hydrophobic solutes in solvent swollen silicone rubber membranes," *J. Mem. Sci.*, vol. 154, pp. 127-140, 1999.
- [80] P.M. Demoustier, F. Charbit, J.L. Fanlo, P. Moulin F. Heymes, "Treatment of gas containing hydrophobic VOCs by a hybrid absorption-pervaporation process: The case of toluene," *Chem. Eng. Sci.*, vol. 62, pp. 2576-2589, 2007.
- [81] Z. Ding, L. Liu, R. Ma D. Lin, "Experimental study of vapor permeation of C5-C7 alkane through PDMS membrane," *Chemical Engineering Research and Design*, vol. 90, pp. 2023-2033, 2012.
- [82] P.J. Akoto-Ampaw, M. Elbaccouch, M.L. Hurrey, S.L. Wallen, C.S. Grant Y.T. Wu, "Quartz srystal microbalance (QCM) in high-pressure carbon dioxide (CO₂): experimental aspect of QCM theory and CO₂ adsorption," *Langmuir*, vol. 20, pp. 3665-3673, 2004.
- [83] W.E. Stewart, E.N. Lightfoot R.B. Bird, *Transport Phenomena*. New York: John Wiley, 2002.

- [84] R.B. Bird C.F. Curtiss, "Multicomponent diffusion," *Ind. Eng. Chem. Res.*, vol. 38, no. 2515-2522, 1999.
- [85] G.Sadowski J.Gross, "SAFT Perturbed-chain, an equation of state based on a perturbation theory for chain molecules," *Ind. Eng. Chem. Res.*, vol. 40, pp. 1244-1260, 2001.
- [86] G.Sadowski J.Gross, "Modeling polymer systems using the perturbed-chain statistical associating fluid theory equation of state," *Ind. Eng. Chem. Res.*, vol. 41, pp. 1084-1093, 2002.
- [87] G.Sadowski J.Gross, "Application of the perturbed-chain SAFT equation of state to associating system," *Ind. Eng. Chem. Res.*, vol. 41, pp. 5510-5515, 2002.
- [88] G.Sadowski F.Ruether, "Modeling the Solubility of Pharmaceuticals in Pure Solvent Mixtures for Drug Process Design," *J. Pharm. Sci.*, pp. 4205-4215, 2009.
- [89] G.M. Kontogeorais N. von Solms, "Computational and Physical Performance of a Modified PC-SAFT EoS for Highly Asymmetric and Ass. Mixtures," *Ind. Eng. Chem Res.*, pp. 2057-2064, 1999.
- [90] R.W. Baker J.G. Wijmans, "The solution-diffusion model: a review," *J. Membr. Sci.*, vol. 107, no. 1-21, 1995.
- [91] H. Tanaka, K. Nakanishi Y. Tamai, "Molecular Simulation of Penetration of Small Penetrants through Membranes. 1. Diffusion Coefficients," *Macromolecules*, vol. 27, 1994.
- [92] J.M. Prausnitz, B.E. Poling R.C. Reid, *The properties of gases and liquids*. New York: McGraw-Hill, 1987.